MODELING CONTAMINANT SPREAD AND MITIGATION IN THE INDOOR ENVIRONMENT

BY

LINGJUN MENG

DISSERTATION

Submitted in partial fulfillment of the requirements
for the degree of Doctor of Philosophy in Mechanical Engineering
in the Graduate College of the
University of Illinois at Urbana-Champaign, 2014

Urbana, Illinois

Doctoral Committee:

Professor Anthony M. Jacobi, Chair, Director of Research
Professor Clark W. Bullard
Professor Predrag S. Hrnjak
Associate Professor Xinlei Wang

ABSTRACT

Experimental and modeling efforts, using a pilot-scale testbed and multizone modeling, are undertaken to develop filtration and ventilation strategies aimed at improving indoor air quality (IAQ). As part of this effort, a model is developed to effectively estimate crack areas of the multizone testbed. The model is divided into two sub-approaches: one approach is to assume the same crack area for the same type of opening and determine them by minimizing the sum of the squares of relative error between the calculated and experimental ventilation rates for the whole facility; the other is to assume that the crack areas are independent of each other and a similar least-squares minimization is applied to determine these crack areas zone by zone. A comparison of the two approaches shows that both can provide satisfactory results, and the latter approach is preferred, because it provides more flexibility and detail.

Ventilation systems are explored using multizone simulations. The model results suggest a distributed unbalanced ventilation system is preferred for maintaining IAQ, because 1) it can provide positive pressure difference across the building envelope to prevent exterior contaminant infiltration; and 2) some contaminated indoor zones can be "isolated" from adjacent ones by adjusting the relative pressure differences. Realistic particle distributions typical to a particular contamination threat of interest are considered, and an acoustically enhanced impaction (AEI) filtration device is investigated together with other filters. The protection factor (PF, a ratio of concentration integrated over time in the ambient to that indoors) is chosen as a performance metric. A PF-oriented evaluation framework has been established such that ventilation system/strategy (or filter) comparison in terms of IAQ enhancement is straightforward. For instance, 16 filtration schemes are compared to identify preferred ventilation and filtration strategies. For the indoor environment, a highly efficient outside air (OA) filter is recommended, but a recirculated air (RA) filter is relatively much less effective. For vestibule protection, a stand-alone balanced system with 100% RA filtration is recommended. The AEI device can be an alternative to a HEPA filter when the ambient contamination level is low to moderate.

Extension of an existing analytical steady-state PF model is undertaken to demonstrate the advantages of pressurization protection of buildings over non-pressurization protection. The analytical PF model can be used to determine the ventilation flow rate and filter efficiency at a specific PF level and guide the vestibule door operation. It is found that the minimum closing period of the vestibule interior door typically should be 20 minutes to protect the room.

To my parents and my wife

ACKNOWLEDGEMENTS

This work was sponsored by Construction Engineering Research Laboratory (CERL). I am grateful to my academic advisor, Prof./Dr. Anthony Jacobi, for his guidance and support all these years. I appreciate the constructive suggestions and comments from my dissertation committee: Dr. Clark Bullard, Dr. Predrag Hrnjak and Dr. Xinlei Wang and from the CERL project team: Mark D. Ginsberg, Andrew Nelson, Alexander Bui and K. James Hay. I also want to extend my appreciation to my colleagues and friends in the Air Conditioning and Refrigeration Center for the support and the valuable memories.

I want to thank my parents for everything I've achieved. Mom and Dad, this is for you. I want to thank my wife for all the support and happiness I can ever imagine. The world is a much better place with you in my life.

TABLE OF CONTENTS

LIST OF FIGURES

LIST OF TABLES

LIST OF SYMBOLS

English Symbols

A_{crack}	leakage area	(m^2)
A_L	equivalent leakage area or ELA	(m^2)
b	regression intercept	
C	flow coefficient for crack flow in "blower-door" test	($m^3/(s \cdot Pa^n)$)
c_f	steady-state contaminant concentration	(mg/m^3 or $\#/cm^3$)
c_i	contaminant concentration in the indoor room	(mg/m^3 or $\#/cm^3$)
c_V	contaminant concentration in the vestibule	(mg/m^3 or $\#/cm^3$)
C_D	discharge coefficient	($m/(s \cdot (Pa \cdot m^3/kg)^{1/2})$)
C^*	flow coefficient in modified crack flow equations	($m/(s \cdot Pa^n)$)
d_p	particle average diameter	(μm)
f_o	outdoor (make-up) air fraction, OA/SA	
f_{RA}	recirculated air fraction indoors, RA/SA	
Factor	penalty factor	
FB	fractional bias	
FS	fractional bias of variance	
HEPA	highly efficient particulate air (filter)	
L_i	contaminant intake into a human lung	
m	regression slope	
N	row(s) of experimental data (N=1, 2, 3, 4)	
n	crack flow exponent or zone number	
n_i	particle bin i number density	($\#/cm^3$)
NMSE	normalized mean square error	
p_n	(zone n) absolute pressure	(Pa)
Δp	differential pressure	(Pa)
PF_i	indoor protection factor	
PF_V	vestibule protection factor	
Q	volume flow rate	(m^3/s)
q	unit air infiltration through exterior door	($L/(s \cdot m^2$ of door area))

r	correlation coefficient	
R	ventilation flow rate indoors	(m^3/s)
R_V	ventilation flow rate in the vestibule	(m^3/s)
R_{IV}	inter-zone leakage rate from the room to the vestibule	(m^3/s)
$SSRE$	summed squares of relative error	
$SSRE^*$	modified summed squares of relative error	
t_0	time both the vestibule doors are opened	(second or minute)
t_1	time particles are deposited in the vestibule (t_1=62 seconds in this study)	(second or minute)
t_2	the period of outdoor contamination (t_2=5 hours in this study)	(minute or hour)
Δt	door opening time	(second or minute)
T_0	period of the source deposition	(second or minute)
T_{IA}	transmittance of recirculated air filter indoors	
T_{OA}	transmittance of outdoor air filter indoors	
T_V	transmittance of recirculated air filter in the vestibule	
V_I	volume of indoor room	(m^3)
V_n	volume of zone n	(m^3)
V_V	volume of vestibule	(m^3)
X	a specific MERV rating level	

Greek Symbols

α	air exchange volume (m^3) when vestibule interior door is opened or constant air exchange rate (m^3/s)	
β	air exchange volume (m^3) when vestibule interior door is opened or constant air exchange rate (m^3/s)	
η	filtration efficiency	
Θ	respiratory rate	(kg/m^3)
ρ	air density	(kg/m^3)
μ	geometrical mean diameter	(μm)
σ	geometrical standard deviation	

Subscripts

3nda (or 3da)	(crack area) of zone 3 north door
3nwa	(crack area) of zone 3 north window
3swa	(crack area) of zone 3 south window
3sdampera	(crack area) of zone 3 damper
5la	(crack area) of zone 5 left window
5ra	(crack area) of zone 5 right window
AEI(off)	AEI device with power turned off
AEI(on)	AEI device with power turned on
cal	calculated
exp	experimental
in	indoor
l	large crack
L	leakage
max	maximum
na	(crack area) between zone *n* and the ambient environment
nm	(crack area) between zone *n* and zone *m*
OA	outdoor air
out	ambient environment
r	reference
RA	recirculated air
s	small crack
SA	supply air
vd	vestibule door

LIST OF ACRONYMS

AEI	acoustically enhanced impaction
AEIFS	acoustically enhanced impaction filtration system
AHU	air handling unit
ASHRAE	American Society of Heating, Refrigerating and Air-Conditioning Engineers
ARA	Applied Research Associates
CUBVS	central unbalanced ventilation system
DBVS	distributed balanced ventilation system
DOE	department of energy
DUBVS	distributed unbalanced ventilation system
EA	exhaust air
ELA	equivalent leakage area
EPA	Environmental Protection Agency
HEPA	high-efficiency particulate air
IAQ	indoor air quality
IC	initial condition
LD_{50}	median lethal dose (abbreviation for “lethal dose, 50%”)
LSM	least-squares minimization
MERV	minimum efficiency reporting value
NIST	National Institute of Standards and Technology
OA	outdoor air
PF	protection factor
PM	particulate matter
RA	recirculated air
SA	supply air
TEP	triethyl phosphate
UVGI	ultraviolet germicidal irradiation
WHO	World Health Organization

CHAPTER 1-INTRODUCTION

1.1 Introduction

Although clean air is widely recognized as a basic requirement for human health, a World Health Organization (WHO) assessment indicates that the effects of urban outdoor and indoor air pollution still cause over 2 million premature deaths each year. More than half of this burden is born by the populations of developing countries (WHO, 2005). The mortality in cities with high levels of pollution exceeds that observed in relatively cleaner cities by 15–20%. Even in the European Union, average life expectancy is 8.6 months lower due to exposure to particulate matter smaller than 2.5 μm ($PM_{2.5}$) produced by human activities (WHO Regional Office for Europe, 2013). According to the U.S. Environmental Protection Agency (EPA) studies of human exposure to air pollutants, the typical indoor levels of pollutants may be two to five times higher than those in the outdoor environment. These indoor air pollutant levels are of particular concern because most people, especially in developed countries, spend about 90% of their time indoors.

The association of morbidity and mortality with air pollution has motivated advances in ensuring indoor air quality (IAQ). Persily (2004) pointed out that one of the common approaches to reducing the indoor particulate matter (PM) is to utilize ventilation and filtration systems in buildings. Prior research has shown that this approach works effectively, but due to the addition of the complex duct systems and especially the filters, the flow resistance in these ventilation systems can be large, thus the accompanying power consumption of these systems can be significant. To be specific, buildings consume roughly 40% of the nation's primary energy in United States, and this usage is steadily growing (U.S. Energy Information Administration, 2012). Ventilation alone consumes 6% of the U.S. commercial sector primary energy consumption (Office of Energy Efficiency & Renewable Energy, 2012), a significant amount of which is spent on filtration.

Prioritizing IAQ enhancement and noting the energy-intense status quo of "ventilation+filtration" systems, it is of interest in the present study to evaluate filtration alternatives which might not incur a high pressure drop but still provide high particle filtration efficiency for ensuring the IAQ. In this study, an acoustically enhanced impaction (AEI) device with low pressure drop is evaluated in the application of building protection. Here *building protection* means maintaining a safe indoor environment during an outdoor particulate

contamination event, mainly by reducing contaminant levels. In order to quantify the safety level of indoor environment, the *protection factor* (PF) is adopted. The protection factor is the ratio of the ambient contaminant concentration to the indoor contaminant concentration integrated over time. Studied scenarios include but are not limited to protecting a building by protecting its vestibule, through which people may enter or exit the building. In this scenario, it is of interest to know the effect of building leakage level, suitable ventilation system configurations, filtration methods and the time needed to clear a threat. Evaluations will use multizone modeling and CONTAM, a multizone indoor air quality and ventilation analysis software package developed by the National Institute of Standards and Technology (NIST).

Particle transport involves a number of complicated phenomena and processes. In the present study, the particles of interest are assumed to be suspended in the air. They may be biologically active but chemically inert. Phenomena such as coagulation, phase change, deposition and resuspension are not considered. The covered processes are filtration, exfiltration and/or infiltration. The present study is focused on protecting a building against exterior particulate matter such as biological agents by protecting its vestibule(s), including but not limited to: 1) estimating crack areas in a multizone building based on supply air flow rates and pressure differences across the building shell; 2) exploring ventilation and filtration strategies to select the best ventilation system and filtration schemes using CONTAM; and 3) evaluating the vestibule characteristics in terms of protection factor at given ventilation flow rates and filtration efficiencies. A literature review is presented and representative earlier work in the above three categories is reviewed, highlighting the developments in each of the areas, with more emphasis on recent work. The review is followed by a statement of the objectives.

1.2 Literature Review

1.2.1 Building Leakage Estimation

Building leakage information, as an indicator of the building airtightness, is important for the estimation of air/contaminant infiltration and exfiltration, evaluation of indoor air quality and building energy performance, and exploration of mitigation/ventilation strategies. An early study touching on building leakage was presented by Shaw (1907) who used a fully turbulent orifice flow for ventilation modeling. In more recent work, Etheridge (1977) and Baker *et al*. (1987) obtained detailed and fairly accurate leakage area measurements for each opening in their testing

facility. Their approaches were time consuming and sometimes inadequate, especially in light of the randomness of crack shape and size distribution. Nowadays, a common practice is the so-called "blower-door" test, which was first developed in Sweden around 1977 and significantly improved by Sherman in the US around 1987 (Sherman, 1995). Prior to the work of Sherman, "blower-door" test results could not be used to determine real-time air exchange in buildings under natural conditions, or even to determine average annual air exchange levels. Sherman made the first attempt at doing this to assist Kronvall and Persily, who estimated annual average air exchange as 5% of air changes per hour at a 50 Pa positive pressure difference across the building shell. In this test, all the interior openings are normally kept open to yield a relatively uniform pressure within the building, and leakage flow rate and pressure difference are measured. The problem with this method is that no detailed inter-zone leakage information can be obtained. It is not realistic to measure every single inter-zone leakage flow rate in a complex multizone building. Thus, a fast and reasonably accurate estimation method for predicting the interior and exterior leakage is highly desirable. CONTAM has been utilized to predict ventilation flow rate and contaminant concentration (ASHRAE, 2009). However, further empirical and/or inter-model comparisons are needed to fully demonstrate the validity and reliability of CONTAM (ASHRAE, 2009).

1.2.2 Contaminant Mitigation

In order to mitigate indoor contamination, it is important to know the building leakage for any pressure difference across the building envelope, because air infiltration rate or ventilation flow rate is directly impacted by the building airtightness.

In the case when the building is under negative pressures, ambient air infiltration and particle penetration occur. A few researchers such as Liu and Nazaroff (2001) and Chen and Zhao (2011) pointed out, based on their modeling and/or experimental work, that the ambient particle penetration coefficient across building envelopes is mainly influenced by the pressure difference, the crack dimensions (especially crack height and length), and particle properties (especially the size). Their work indicated that the best way to protect a non-pressurized building is to tighten the envelope, but particle penetration will still occur. What this means is that installing a balanced ventilation system in a building is not the best approach to protecting the building from any possible particulate contamination because this system cannot pressurize the

building to prevent air infiltration and particle penetration. Here the *balanced* means that the outdoor air (OA) flow rate is equal to the exhaust air (EA) flow rate.

In the case when the building is under positive pressures, at least one unbalanced ventilation system is necessary to pressurize the building. Here the *unbalanced* means that the OA flow rate is larger than the EA flow rate, such that the superfluous flow will pressurize and eventually exfiltrate the building. Persily (2004) pointed out the benefit of enhancing the IAQ by maintaining positive pressures in airtight buildings. In this study, development of ventilation strategies will be focused on unbalanced systems.

1.2.2.1 Ventilation

For the unbalanced system, Zhao and Wu (2009) identified four factors that impact the IAQ: 1) OA flow rate, 2) filter efficiency, 3), ventilation mode, and 4) duct type. In this case, ambient air infiltration and particle penetration cannot occur due to sufficient building pressurization, thus the only contamination source is considered as the supply air filtered by imperfect filters. For the first two factors, increasing the OA fraction and lowering the filter efficiency both mean reducing the indoor protection factor. The ventilation mode in their paper means the position or the angle at which supply air is delivered to the room. The duct type in their context means duct roughness, which impacts the particle deposition velocity. The authors found that the ventilation mode had very little impact on indoor contaminant of outdoor origin due to its negligible effect on the particle concentration at the supply air duct outlet. The effect of duct roughness on particle deposition is out of scope of the current work. Thus, in the present study, only the first two factors will be investigated. It can be seen that for the pressurized buildings, design of ventilation systems requires building leakage information because ventilation flow rate is directly related to it.

There have been many prior studies exploring the effect of ventilation system and ventilation strategies on the IAQ. For instance, Persily (1998) and Persily and Martin (2000) simulated many conditions for forced-air and local exhaust systems for buildings to get more insight into: 1) the effect of duct leakage, local exhaust fans, and ventilation inlets on ventilation flow rates, air movement patterns and building pressures; 2) energy impacts; and/or 3) effectiveness of different systems in terms of indoor contaminant control. It is worth noting that the authors incorporated many complexities and approximations in their models in order to make

their models more realistic, but these complexities obfuscated some of the fundamental relationships between building leakage, ventilation flow rate, OA fraction, ventilation strategies and filtration schemes.

1.2.2.2 Filtration

Filters are usually utilized to achieve particle filtration. Minimum efficiency reporting value, commonly known as MERV rating, is a measurement scale designed in 1987 by the American Society of Heating, Refrigerating and Air-Conditioning Engineers (ASHRAE) to rate the effectiveness of air filters. A filter is required to meet filtration efficiency requirements in three different particle ranges (0.3-1.0 μm, 1.0-3.0 μm and 3.0-10.0 μm) in order to be considered a specific MERV rating. For instance, a MERV rating of 16 means that a filter is capable of removing 95% of particles in the size ranges of 0.3-1.0 μm, 1.0-3.0 μm and 3.0-10.0 μm, respectively. For ease of notation, a filter with a specific MERV rating *X* is hereafter noted as a "MERV *X* filter." Among all kinds of filtration equipment for providing clean indoor air, a High-Efficiency Particulate Air (HEPA) filters is considered one of the most effective types. In United States, a HEPA filter must meet stringent standards set by the Department of Energy (DOE). To be specific, DOE-STD-3020 (DOE, 1997) states that the HEPA filter must remove 99.97% of all airborne particles as small as 0.3 μm in diameter. As a comparison, ASHRAE Standard 52.2 (ASHRAE, 2007) only states that the MERV 16 filter must remove 95% of all airborne particles as small as 0.3 μm in diameter. Even though the relation between HEPA rating and MERV rating is not clearly defined, it is estimated that a HEPA filter is equivalent to a MERV 16+ filter.

There have been extensive experimental and modeling activities regarding MERV filter efficiency such as representative work of Kowalski *et al*. (1999) and Kowalski and Bahnfleth (2002) for MERV 6-16 filters. Pressure drop data for MERV filters are commonly reported by manufacturers. Novick *et al*. (1992) conducted representative work in measuring and modeling the effect of solid particle loading on pressure drop of HEPA filters, and they derived a linear relationship between the pressure drop and the flow rate that was consistent with some earlier work such as that reported by Rudnick and First (1978). The filter efficiency model developed by Kowalski *et al*. (1999) covered the HEPA filter.

For some cases where there were exterior threats, HEPA filters were confirmed to be effective in controlling bacteria- and/or fungi-carrying particles in many places where the IAQ was a top concern, such as hospitals (Barnes and Rogers, 1989; Withington *et al*., 1998). In these situations, normally the HEPA filters were targeted at filtering the spores in the OA and the rooms involved were pressurized. It is noteworthy that the accompanying energy cost associated with using HEPA filters is an issue due to the high pressure drop commonly required to operate this type of filter.

Acoustic aerosol agglomeration has recently emerged as a method to enhance the efficiency of the current filtration techniques to retain fine particles (Riera and Gallego-Juarez, 1986). The working mechanism is that a sound field transverse to the airflow can induce particle drift and enhance aerosol agglomeration. Using this technology, Meegan and Gallia (2008) designed and tested prototypes of a kind of acoustically enhanced impaction (AEI) device stacked in arrays with some coarse fiber media stuffed in the rectangular flow channels. The intensified particle motion caused by the sound field will increase the probability of particle impaction on coarse filter media. One of the advantages of this AEI device is that it does not incur a high pressure drop.

Nelson (2011) used the same AEI device array in his research, focusing on evaluating this novel AEI air purification technology as a potential alternative to HEPA filtration in building protection applications. His results were compared to pressure drop and particle removal efficiency of conventional HEPA filters based on available data in the literature. A cost analysis was performed to compare annualized operational cost of the first-generation AEI device to a commercially available HEPA filter. He found out that the projected power budget of the AEI devices was at least an order of magnitude lower than that of HEPA filters. This result suggests that the AEI devices could be a promising alternative to the HEPA filters.

Considering the energy consumption by existing building ventilation and air cleaning systems, there is tremendous potential for savings by low-pressure-drop filtration schemes. There are some existing low-pressure drop filtration technologies/products such as ultraviolet germicidal irradiation (UVGI) systems, electrostatic precipitators and electrostatic filters composed of polarized fibers. The UVGI is a disinfection method that uses ultraviolet light at a sufficiently short wavelength to kill microorganisms, and it must be combined with filters for air filtration purposes. There have been extensive studies regarding UVGI technology since 1909

(Kowalski and Bahnfleth, 2000). An electrostatic precipitator is a particulate collection device that removes particles from a flowing gas using the force induced by electrostatic charge. A negative side-effect of electrostatic precipitation devices is the potential production of toxic ozone and NO_x. Electrostatic filters may lose their collection efficiency over time or when exposed to certain chemicals, aerosols, or high relative humidity. Unlike its counterparts, the AEI device is an emerging low-pressure drop technology that is without the above problems/drawbacks. The AEI device is still in prototype phase and needs more research/exploration regarding its application.

1.2.3 IAQ Performance Metric

There are mainly three parameters to assess the relationship between indoor and outdoor particles: indoor/outdoor (I/O) ratio, infiltration factor, and penetration factor. I/O ratio is the ratio of indoor to outdoor particle concentrations. The penetration factor is the fraction of particles in the infiltration air that penetrates the building shell. The infiltration factor is a factor related to air exchange rate due to infiltration, penetration factor, particle deposition rate and indoor particle concentration contributed by indoor sources. Infiltration and ambient particle penetration are prevented by pressurization protection of buildings. Thus, the infiltration factor and penetration factor are not applicable to the present study.

Chen and Zhao (2011) reviewed 77 studies over 4000 homes and concluded that the I/O ratios varied considerably across all the studies. Thus, it was difficult to draw uniform conclusions, which made "I/O ratio hardly helpful for understanding the indoor/outdoor relationship" (Chen and Zhao, 2011).

An appropriate IAQ performance metric is necessary for producing meaningful results. Ginsberg and Bui (2013) proposed a model to evaluate indoor air quality at neutral pressures, in which they connected the protection factor to the ventilation flow rate, filter efficiency, inter-zone flow exchange rate and zone volume. Their definition of the protection factor was "the asymptotic ratio of outdoor to indoor air concentration of particulate matter." Using Laplace transforms of a state space equation, the authors found the relationships between the protection factor, ventilation and inter-zone flow rates, filtration efficiencies and room volume at neutral pressures.

1.2.4 Vestibule Characterization

Vestibule requirements are just briefly covered in ASHRAE Standard 90.1-2010 (ASHRAE, 2010b) and International Energy Conservation Code C402.4.7 (ICC, 2012). The only specific geometry requirement is that the vestibule interior and exterior doors must be at least 7 ft (2.13 m) away from each other in closed position (ASHRAE, 2010b). No operation requirement or ventilation/filtration requirement is available at the current stage.

Sellers *et al*. (2004) performed pressurization tests to investigate the effect of turning off the return fans and closing the relief dampers. They were aware of the fact that minimizing building leakage was important, even though building-leakage-related operational problems can be managed through adjusting existing HVAC systems in their system. They recommended providing vestibules on lobbies, arranged with an air lock between the interior and exterior of the building under normal operating traffic flow rates. The authors did not continue to characterize the vestibule.

1.2.5 Multizone Simulation

The demand for improving IAQ and reducing energy costs has motivated significant research on the modeling of infiltration and indoor air flow in buildings. For typical multizone buildings, some simulation methods are time consuming, such as a CFD modeling in which a room is divided into a fine grid. Some other methods give indication of airflow and temperature distributions such as a zonal method in which a room is divided into a few sub-zones and complimentary information and models are needed to define flows (Megri and Haghighat, 2007). As a comparison, multizone models are able to predict the air flow rates across the envelopes, between the rooms, and through the mechanical ventilation system as well as the transient contaminant concentration without getting into much detail, because of the so-called "well-mixed" assumption. The well-mixed assumption is that air temperature and contaminant concentrations are assumed uniform in each zone, and air momentum effects are neglected. Most multizone models consider the multizone building as a complicated interconnecting system of flow paths, and take into account other factors such as mechanical ventilation, tightness of the envelope, and terrain effects, shielding and climate conditions. The difficulties in developing and applying such a model include the determination of extensive information about flow characteristics, leakage, ambient wind pressure distribution, and model validation (Li, 1993).

Many multizone models were developed (Liddament and Allen, 1983; Feustel and Kendon, 1985) since Jackman (1970) published the first one, LEAK. There are currently two well-known and publically accessible multizone simulation tools. The first one is called CONTAM, which is developed in and Conjunction of Multi-zone Infiltration Specialists (COMIS). Lorenzetti (2002a) assessed both tools, and he cautioned against their use for novel ventilation control systems, duct system design, or natural or hybrid ventilation after identifying the limitations of the two. Lorenzetti (2002b) also investigated computational aspects of multizone airflow systems, and found that CONTAM and COMIS were better programmed, following a series of underlying assumptions to guarantee a symmetric positive-definite Jacobian matrix for an airflow network such that a unique solution was obtainable. As a comparison, at least one of the underlying assumptions was omitted in other competing codes. Wang and Chen (2008) evaluated the validity of the "well-mixed" assumption for multizone simulation with a focus on displacement ventilation for situations with indoor sources. They suggested some criteria for examining the validity of uniform air temperature and uniform contaminant concentration assumptions. They also reasoned that the assumption of neglecting air momentum effect was reasonable when the jet momentum effect was dissipated before reaching an opening. It is noteworthy that their work was focused on displacement ventilation for situations with indoor sources; thus, the corresponding temperature variation would be noticeable, and indoor source effects and jet flow effects cannot be neglected. In the present study where there is either no indoor source or the zone with indoor source is heavily ventilated through a central HVAC system with the supply point fixed near the ceiling and some appropriate diffuser installed on the outlet, the above three issues will be less important and the well-mixed assumption is valid.

1.2.6 Summary of Literature Review

Through the above literature review, it is apparent there are gaps in the earlier work. One serious deficiency is that the common "blower-door" test for estimating leakage area for a multizone facility cannot provide information on interior leaks (Sherman, 1995).

Three parameters have been commonly used to interpret the indoor/outdoor particle concentration relationship, but they were either not applicable to the present study or not very meaningful (Chen and Zhao, 2011). The protection factor was shown in the literature (Ginsberg and Bui, 2013) to be an appropriate performance metric. However, Ginsberg and Bui (2013) did

not fully explain the meaning of the protection factor except deriving the relationship between the PF, ventilation/leakage flow rates, filtration efficiencies and room volume.

In prior research on ventilation and filtration, I/O ratios were typically obtained at specific ventilation flow rates, filtration efficiencies, and room volume. Due to limits in funding, time, and preparation, only a few ventilation flow rates and filters were tested. It can be expensive to answer this question experimentally: "Which minimum grade of the MERV filter is to be selected in order to maintain a specific indoor PF level?" The multizone simulation software CONTAM is a suitable tool for exploring such a question, provided that filter efficiency curves, ambient particle distribution, building leakage area, and ventilation flow rates are known.

Nelson (2011) suggested that the AEI device be considered as a candidate to substitute for the HEPA filter. This implies that any future comparisons between the AEI device and the HEPA and/or MERV filters need to be performed in the same framework (using the same metric). There are no previous studies in the open literature on the potential of the AEI device in enhancing building IAQ.

The current standards (ICC, 2012; ASHRAE, 2010b) treat the vestibule as a space for energy-saving purpose instead of for the IAQ enhancement purpose. No detailed requirement on the vestibule interior and exterior door operation is available at the current stage. The current lack of requirements for a vestibule implies a lack of understanding of vestibule characteristics.

1.3 Statement of Objectives

In order to address that gaps identified above, the objectives of this study are as follows:

1. Develop a general method to estimate building interior and exterior leakage areas simultaneously in one test, something not currently available.

2. Outline a framework of IAQ evaluation suitable for investigating the performance of filter combinations (AEI device/MERV filters/HEPA filters) for common ventilation schemes. This framework is expected to represent performance in terms of "Protection factor *vs*. Filtration power" using CONTAM, which is generalizable for any multizone IAQ evaluation using any ventilation/filtration system. Such an evaluation can be used to identify the best filtration scheme for pressurization-protection of multizone buildings and/or protection of vestibules.

3. Extend the model of Ginsberg and Bui (2013) for pressurization-protection scenarios to predict the protection factors and characterize the vestibule.

CHAPTER 2-LEAKAGE ESTIMATION

2.1 Overview

In light of the needs outlined above and the limitations of current practice, a new method capable of providing detailed leakage area information from experimental pressures and flow rate data has been developed. The method consists of two parts: 1) a model for estimation of leakage area using pressure differences and flow rates and 2) validation and evaluation of a CONTAM 3.0 model utilizing the estimated leakage areas against the experimental overpressure data.

2.2 Background

A facility representative of a typical office building (Figure 2.1(a)) was constructed in a well-sealed hangar and subjected to external contamination by triethyl phosphate (TEP). This facility was designed to assess the impact of common building configurations on overall IAQ. The test facility shown in Figure 2.1(a) is represented approximately as shown in Figures 2.1(b) and 2.1(c) in a CFD model and Figure 2.1 (d) in a CONTAM 3.0 model.

(a)

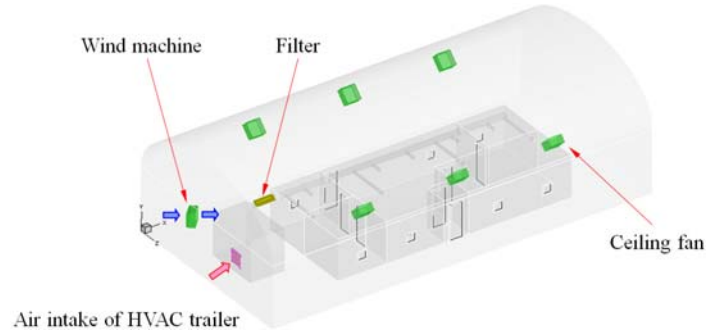

(b)

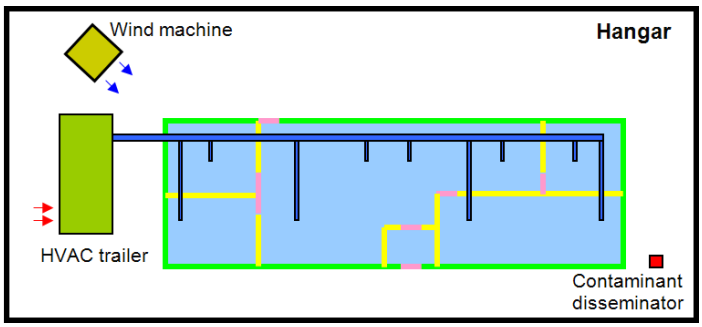

(c) Figure 2.1 (cont.)

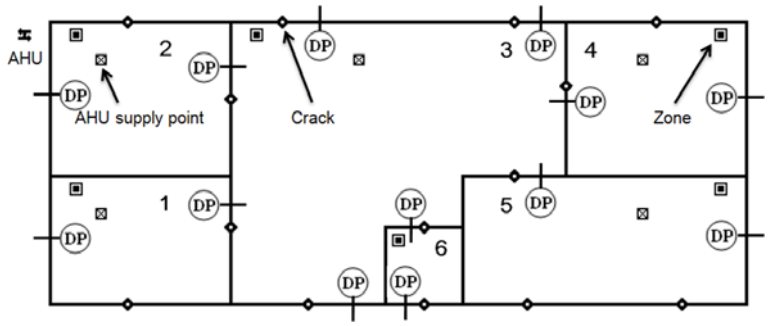

(d)

Figure 2.1 a) Photograph of the testbed (provided by M. Ginsberg), b) 3D representation of the testbed, c) 2D representation of the testbed, and d) 2D representation of the testbed in the CONTAM 3.0 interface. The 3D/2D models are drawn to our best estimate of the facility, as is the location of the contaminant source.

Experiments were performed over a range of wind speeds (0 – 11.18 m/s) and internal overpressures (0 – 155 Pa). In each trial, six fans were mounted above the facility to provide mixing, and a wind machine was used to provide a specific wind speed. An external trailer-mounted HVAC system was used to provide a specified internal overpressure. The trailer was fitted with a HEPA filter and granular activated carbon cartridge to mitigate TEP transport by the HVAC system. All doors and windows of the facility were closed and cracks around doors sealed with gaskets. After the internal overpressure was maintained near steady state for typically one hour, Miniature Infra-Red gas Analyzers (Foxboro MIRAN 1A CVF) and Miniature Chemical Agent Monitoring Systems (MINICAMS from OI Corporation) were used to measure background outdoor and indoor contaminant concentrations, respectively. After assessing background levels, a chemical contaminant disseminator was cycled on and off to maintain outdoor contaminant concentration near 200 mg/m^3 (varied from trial to trial within the range of 180 mg/m^3 to 250 mg/m^3). The outdoor TEP concentration was subsequently monitored by the MIRANs and indoor contaminant concentration monitored by the MINICAMS for 90 to 130 minutes. The experimental data collected through the above experiments included air volume flow rate through each air supply duct, pressure differences between different zones, and contaminant concentration in each zone.

2.3 Basis Data for Model Development

A testing matrix is presented in Table 2.1; the supply air flow rate in each zone is summarized in Table 2.2, but only the used trials are presented. As shown in Table 2.2, notation of each trial follows this rule: wind speed (unit: mph)-leakage level (Low, Moderate, High)-overpressure (unit: inch of water column gauge pressure or in wg). For instance, 0-L-0.00 in trial 19 means there is no wind speed, low leakage and no pressure difference across the building shell. The IP unit is kept only to ease the notation of the test conditions.

Table 2.1 The complete testing matrix

Wind (mph)			0	5	15	25	0	0	5	15
Wind (m/s)			0	2.24	6.71	11.18	0	0	2.24	6.71
Leakage			MED	MED	MED	MED	LOW	HIGH	HIGH	HIGH
Overpressure	in wg	Pa								
	0	0	20	21			19	23	24	22
	0.02	5	9	13						
	0.03	7.5			14					
	0.05	12.5	6	8	10	18				
	0.1	25	4	5	7	17				
	0.2	50	1	2	3	16				
	0.3	75				15				
	0.5	125	11	12						

used in determining leakage areas; outlier

not useful due to lack of test data or no pressure difference across the building shell

Not used due to wind effects; contaminant infiltration occurred

Table 2.2 Summary of the supply air volumetric flow rate in each zone

Trial	Test condition	Zone 1 (m^3/s)	Zone 2 (m^3/s)	Zone 3 (m^3/s)	Zone 4 (m^3/s)	Zone 5 (m^3/s)
4	0-M-0.1	0.023	0.133	0.531	0.097	0.202
6	0-M-0.05	0.000	0.087	0.275	0.092	0.185
11	0-M-0.5	0.252	0.368	1.446	0.347	0.677
12	0-M-0.5	0.334	0.361	1.276	0.326	0.116

Pressurization test data are needed to develop a leakage estimation model. As can be seen from Table 2.2, trials 19-24 are of little value due to the neutral pressures, and trials 14 and 18 are not selected due to contaminant infiltration. There is a lack of supply air flow rate in trials 13 and 23. For the trials at different wind speeds in the well-sealed hangar, the wind effect can only be estimated using case-by-case CFD simulations with large uncertainties due to the fluctuating nature of the wind. The large uncertainties of the ambient pressure data have a negative impact on the development of a crack area estimation method. Among the rest of the experimental trials, trials 1 and 9 are found to be outliers. Thus, only four trials at zero wind speed, namely: trials 4, 6, 11 and 12, are selected as a basis for model development, and they are called the "basis trials."

2.4 Leakage Estimation Model

2.4.1 Leakage Estimation

There has been a relatively quick and inexpensive fan pressurization testing method to evaluate envelope airtightness of multizone buildings, which requires the partitioning (internal walls and floors) to be kept open such that a relatively uniform pressure difference across the entire building shell can be achieved, and the effects of partitioning usually are insignificant. Then, the building effective air leakage area (ELA) A_L (m^2), as an indicator of building envelope airtightness, can be calculated following the ASHRAE handbook (2009).

From a "blower-door" test,

$$Q_r = C\left(\Delta p_r\right)^n \tag{2.1}$$

Then, the building A_L is the whole-building leakage area at a known pressure difference assuming a sharp-edged orifice.

$$Q_r = C_D\sqrt{\frac{2\Delta p_r}{\rho}}A_L \tag{2.2}$$

Thus, A_L can be determined,

$$A_L = Q_r\frac{\sqrt{\rho/2\Delta p_r}}{C_D} \tag{2.3}$$

Combining Equations (2.1) and (2.2),

$$C = \frac{C_D \sqrt{\frac{2\Delta p_r}{\rho}} A_L}{\Delta p_r^n} \tag{2.4}$$

Finally, the relationship for a crack flow at any pressure is obtained,

$$Q = C_D \sqrt{\frac{2\Delta p_r}{\rho}} \left(\frac{\Delta p}{\Delta p_r} \right)^n A_L \tag{2.5}$$

where ρ is the air density (taken to be 1.2 kg/m^3); Δp_r is a reference pressure difference (Pa), 50 or 75 Pa is often recommended; Q_r is the corresponding airflow through opening at $\Delta p_r = 4$ Pa (m^3/s); C_D is the so-called "discharge coefficient." It represents the flow resistance due to crack characteristics and C_D=1.0 at 4 Pa; C is the flow coefficient (m^3/(s·Pa^n)) normally curve fitted from experimental data; n is a dimensionless pressure exponent, typically between 0.6 and 0.7 for small cracks. In the present work, n is taken to be 0.65 for small cracks and 0.5 for large cracks.

With the above constants set, Equation (2.5) is reduced to:

$$Q = 1.05 \Delta p^{0.65} A_{L,s} \qquad (n = 0.65, \text{for small cracks}) \tag{2.6a}$$

$$Q = 1.29 \Delta p^{0.5} A_{L,l} \qquad (n = 0.5, \text{for large cracks}) \tag{2.6b}$$

It is possible to rewrite Equations (2.6a) and (2.6b) as:

$$Q = \Delta p^{0.65} A_{crack,s} \qquad (n = 0.65, \text{for small cracks}) \tag{2.7a}$$

$$Q = \Delta p^{0.5} A_{crack,l} \qquad (n = 0.5, \text{for large cracks}) \tag{2.7b}$$

and the conversion between $A_{crack,s}$ (or $A_{crack,l}$) and A_L is straightforward:

$$1.05 A_{L,s} = A_{crack,s} \qquad (n = 0.65, \text{for small cracks}) \tag{2.8a}$$

$$1.29 A_{L,l} = A_{crack,l} \qquad (n = 0.5, \text{for large cracks}) \tag{2.8b}$$

In the current study, the focus is contaminant mitigation in a multizone facility while each partition is fairly well sealed. It can be seen from above introduction that the "blower-door" testing method is not appropriate for recreating the current field test, because the interior partitions were kept closed during the field test. Thus, pressure distribution is not uniform within the building shell. Partitioning effects cannot be addressed by a "blower-door" test, because this method only evaluates the overall building envelope airtightness instead of detailed opening

leakage. In view of the limitations of this method, some modification is necessary to predict the pressure difference, airflow through each crack in each opening and contaminant concentration in each zone.

A steady-state crack estimation model has been developed for the sufficient-positive-pressure situation by Meng *et al*. (2010) based on the following considerations: 1) air mass conservation in each zone; 2) adoption of a modified leakage function $Q = \Delta p^n A_{crack}$ (n=0.65 for small cracks, n=0.5 for large cracks) to calculate the air flow between two zones driven by known pressure differences.

The air and contaminant flow direction in the testbed for the sufficient-positive-pressure trials (≥ 3 Pa, as observed from trials) is illustrated in Figure 2.2.

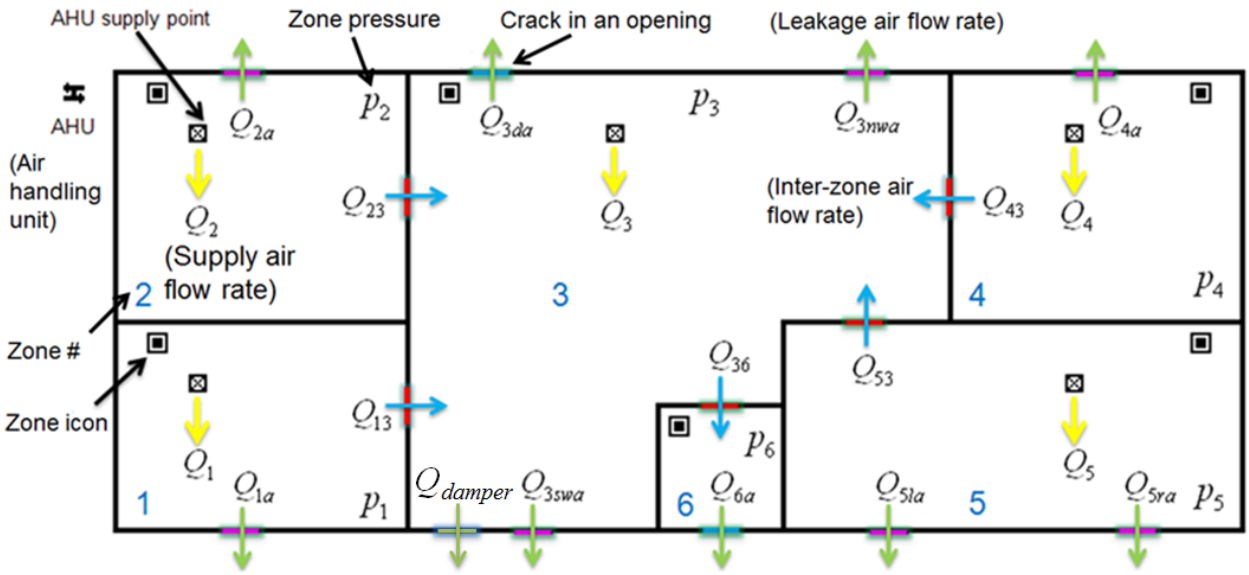

Figure 2.2 Illustration of the involved quantities and flow direction

With the above steady-state model, it is possible to solve crack areas in the testbed for each trial, as shown in Table 2.3 (see Appendix A). It is assumed that the seven windows are of the same crack area and the two exterior doors are of the same crack area. Clearly, the calculated crack areas vary significantly across trials. Thus, a uniform set of crack areas cannot be determined following this approach. An alternative is to determine the crack areas by least-squares minimization (LSM) based on trials 4, 6, 11 and 12.

Table 2.3 Summary of trial-by-trial calculated crack areas

Parameter	Trial 4	Trial 6	Trial 11	Trial 12
A_{window} (cm^2)	168.7	154.4	119.1	152.4
$A_{\text{exterior door}}$ (cm^2)	2.254	1.859	111.6	4.847
A_{13} (cm^2)	2201	1305	218.8	167.4
A_{23} (cm^2)	28.29	14.20	224.3	45.45
A_{43} (cm^2)	444.5	50.60	233.3	443.7
A_{53} (cm^2)	869.9	52.46	250.9	1005
A_{63} (cm^2)	2.750	2.375	348.7	9.571
A_{damper} (cm^2)	105.4	9.800×10^{-04}	321.6	4.338×10^{-04}

There are two ways to assume the crack areas: one is to assume the same crack area for the same type of opening and determine them by minimizing the summed squares of relative error between the calculated and experimental ventilation rates for the whole facility (hereafter referred to as the "whole-facility approach"); the other is to assume that crack areas of different types of openings and in different rooms (zones) are independent of each other. A similar least-squares minimization is applied to determine these crack areas zone by zone (hereafter referred to as the "zone-by-zone approach"). Regardless of which approach was taken, a least-squares minimization was performed using the genetic algorithm in Engineering Equation Solver (EES) software to determine the crack areas.

2.4.2 Approach 1: Whole-facility Crack Estimation Approach

In this whole-facility approach, it was assumed that the crack areas of all seven windows, two exterior doors, five interior doors and one damper were different constants. A modified summed squares of relative error (SSRE*) was minimized to determine the crack areas. A penalty factor (Factor) was set as a measure of maintaining the model quality as shown in Equations (2.9)-(2.11) where its value was somewhat arbitrarily chosen but sufficiently large to distinguish optimized results that satisfy the three imposed criteria from those that do not.

$$\text{Factor} = \begin{cases} 1 & \left(NMSE_Q \le NMSE_{\max,Q} \text{ and } FB_Q \le FB_{\max,Q} \text{ and } FS_Q \le FS_{\max,Q}\right) \\ 1000 & \left(NMSE_Q > NMSE_{\max,Q} \text{ or } FB_Q > FB_{\max,Q} \text{ or } FS_Q > FS_{\max,Q}\right) \end{cases} \tag{2.9}$$

$$SSRE = \sum_{N=1}^{4}\sum_{i=1}^{5}\left(Q_{iN,\exp} / Q_{iN,cal} - 1\right)^2 \tag{2.10}$$

$$SSRE^* = SSRE \times Factor \tag{2.11}$$

The "*N*" in the SSRE expression in Equation (2.10) refers to the *N* rows (trials) of experimental data, and the "5" refers to five volume-flow-rate data in each trial; the subscript "exp" denotes experimental volume flow rate, and "cal" denotes calculated volume flow rate (see Appendices B and C). The door area is assumed as 1×2 m^2; the window area is assumed as 1×1 m^2. Crack width was estimated to be uniform around each opening.

Table 2.4 Calculated leakage area in each opening

Parameter	Crack area (cm^2)	Estimated crack width (cm)
Window leakage	96.19	0.24
Exterior door leakage	4.6	0.008
Interior door leakage	104.75	0.175
Damper leakage	837.21	NA

A CONTAM 3.0 model was constructed using the calculated crack areas in Table 2.4, and the leakage type was set as "Leakage area data" in "One-way flow using power-law models." For all the cases, reference conditions were set as follows: leakage areas according to Table 2.5; discharge coefficient: 1; flow exponent: 0.65 and pressure difference: 4 Pa.

Simulated pressure differences (or called "overpressures") were compared to the experimental ones, as shown in Figure 2.3. In Figure 2.3, values in zones are experimental (or simulated) gauge pressures based on corresponding ambient wind pressure profiles.

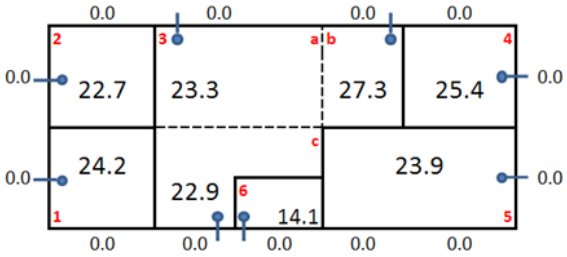

(a) Experimental overpressures (Pa) in trial 4

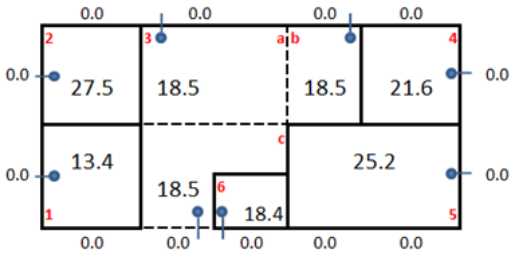

(b) Simulated overpressures (Pa) in trial 4

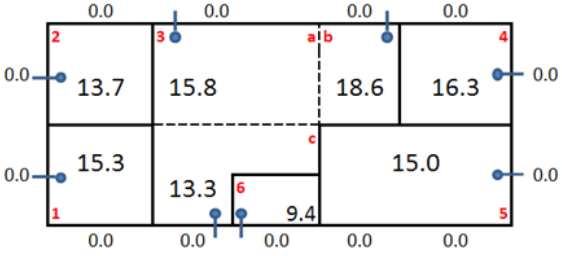

(c) Experimental overpressures (Pa) in trial 6

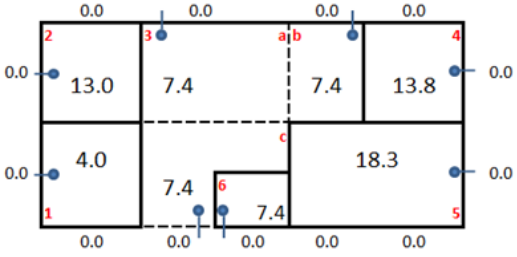

(d) Simulated overpressures (Pa) in trial 6

(Figure 2.3 (cont.))

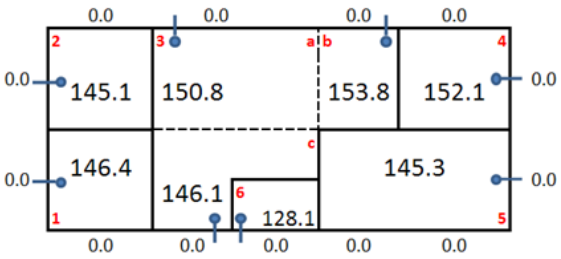

(e) Experimental overpressures (Pa) in trial 11

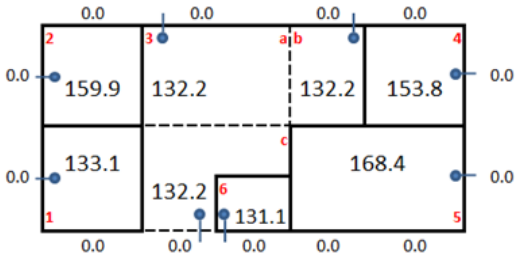

(f) Simulated overpressures (Pa) in trial 11

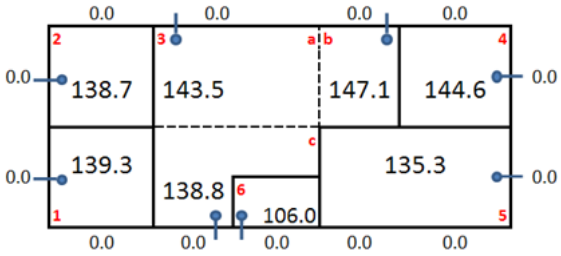

(g) Experimental overpressures (Pa) in trial 12

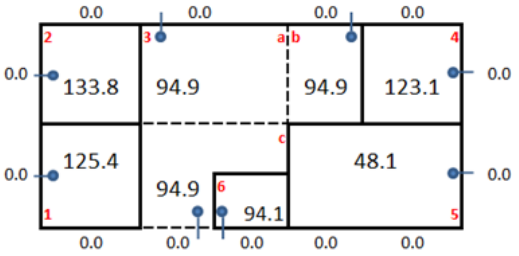

(h) Simulated overpressures (Pa) in trial 12

Figure 2.3 Empirical validation using calculated leakage areas in Table 2.4

The ASTM D5157-97 standard (ASTM, 2008) was introduced to evaluate the CONTAM model performance. Following this standard, six quantitative indicators are introduced in Table 2.4. Fractional Bias (FB) provides a normalized range of values between ± 2.0 and is very similar to percent difference for values between ± 25 %. FB values between ± 1.636 indicate that averages are within one order of magnitude of each other, and values between ± 1.960 are within two orders of magnitude of each other. It is noteworthy that the ASTM D5157-97 standard (ASTM, 2008) was developed for contaminant concentration, not exactly for overpressure yet. These indicators are only measures to ensure prediction quality, which means they can still be used in the present study.

Table 2.5 Six quantitative indicators in the ASTM D5157-97

Parameter	Range
Correlation coefficient, r	$r \geq 0.9$
Regression slope, m	$0.75 \leq m \leq 1.25$
Regression intercept, b	$b/\overline{Co} \leq 0.25$
Normalized mean square error, $NMSE$	$NMSE \leq 0.25$
Fractional bias, FB	$\lvert FB \rvert \leq 0.25$
Fractional bias of variance, FS	$\lvert FS \rvert \leq 0.50$

Following the ASTM D5157-97 standard (ASTM, 2008), Table 2.6 can be obtained based on Figure 2.3. It can be seen that 44 out of the 48 evaluation results are within specified ranges of the standard, which shows a good model performance.

Table 2.6 Model performance evaluation for the whole-facility crack estimation approach

Parameter	Range	Zone							
		1	2	3a	3b	3c	4	5	6
Correlation coefficient, r	$r \geq 0.9$	1.00	1.00	0.98	0.98	0.98	0.99	0.80	0.99
Regression slope, m	$0.75 \leq m \leq 1.25$	0.96	1.04	0.80	0.79	0.82	0.94	0.77	0.97
Regression intercept, b	$\lvert b/\bar{C}\,o \rvert \leq 0.25$	0.14	0.003	0.06	0.09	0.05	0.02	0.05	0.01
NMSE	$\lvert NMSE \rvert \leq 0.25$	0.035	0.013	0.165	0.191	0.133	0.022	0.479	0.014
FB	$\lvert FB \rvert \leq 0.25$	0.176	0.036	0.286	0.319	0.245	0.076	0.207	0.035
FS	$\lvert FS \rvert \leq 0.50$	0.083	0.087	0.411	0.432	0.365	0.106	0.078	0.041

2.4.3 Approach 2: Zone-by-zone Crack Estimation Approach

In this zone-by-zone approach, it was assumed that crack areas were not necessarily the same. Optimization was performed on a zone-by-zone basis, and the objective function was based on the volume flow rate in each zone only, as shown in Equations (2.12)-(2.14). To be specific, crack areas in zones 1, 2, 4 and 5 were first determined through the LSM then used to determine the zone-3 crack areas. The zone 3-6 interior-door crack area (A_{36}) was finally used to determine the zone-6 crack area (A_{6a}).

$$\text{Factor} = \begin{cases} 1 & \left(NMSE_{i,Q} \leq NMSE_{\max,i,Q} \text{ and } FB_{i,Q} \leq FB_{\max,i,Q} \text{ and } FS_{i,Q} \leq FS_{\max,i,Q}\right) \\ 1000 & \left(NMSE_{i,Q} > NMSE_{\max,i,Q} \text{ or } FB_{i,Q} > FB_{\max,i,Q} \text{ or } FS_{i,Q} > FS_{\max,i,Q}\right) \end{cases} \tag{2.12}$$

$$SSRE_i = \sum_{N=1}^{4}\left(Q_{iN,\exp} / Q_{iN,cal} - 1\right)^2 \tag{2.13}$$

$$SSRE_i^* = SSRE_i \times Factor \tag{2.14}$$

After all the crack areas were determined, $SSRE_i^*\left(i = 1,2,4,5\right)$ contours and 3D $SSRE_i^*\left(i = 1,2,4,5\right)$ plots were made for zones 1, 2, 4 and 5 as shown in Figure 2.4. Some points in these contour plots were obtained from solving mass conservation equations for any two of the 4 trials (trials 4, 6, 11 and 12) just to check if it was possible to obtain solutions that were close

to each other. If that was true, it indicated that the assumptions made in the current model were valid. Unfortunately these points exhibited significant scatter, which suggested that there was some discrepancy between the employed assumptions and reality. Some other points in the contour plots were gathered from EES optimization history file. They were the best candidate solutions at different instants of the optimization process. The path these best candidate solutions typically took was as follows: the first candidate was identified at a higher SSRE* value, then more and more candidates were found near the "valley" of the SSRE surface. In the present optimization work, it was observed that the best candidate points on the SSRE surface tended to be on the parameter boundaries, which meant that at least one crack area was zero. This was probably due to either the model assumptions (for instance, inappropriate guess of flow exponent *n*) or the experimental data quality, or due to both of the above reasons. In light of the above issue, three extra criteria were introduced to ensure the quality of the optimization results. With the addition of the three criteria, the model performance was constantly checked and penalty factor was used to constantly adjust the SSRE value into SSRE*. Once a candidate point was identified that satisfied the three extra criteria and gave a minimum SSRE* value (in this case, Factor=1, SSRE*=SSRE), what was typically observed was that the minimum of SSRE* was away from the boundaries. The EES optimization history file and the contour plots showed that the imposed three criteria actually enhanced the model performance by checking prediction quality and identifying a reasonable result away from the parameter boundaries. It was also seen that the EES genetic algorithm was not trapped by the parameter boundaries in this study.

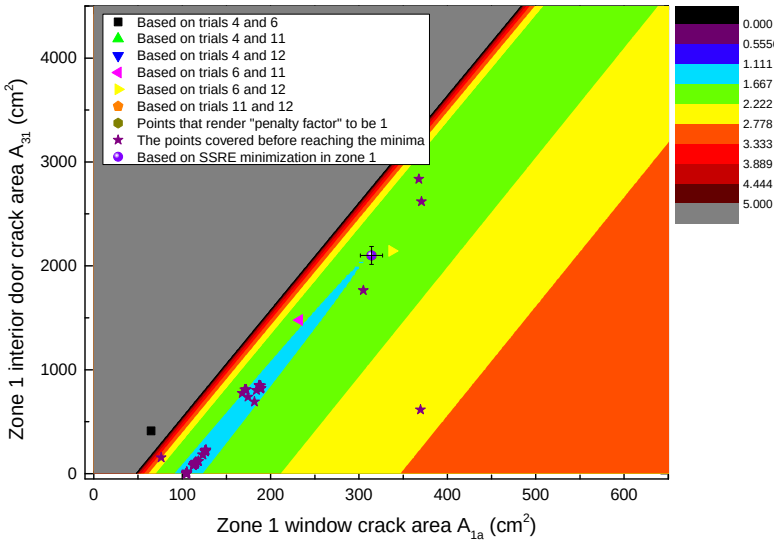

(a) $SSRE_1^*$ contours in zone 1 (Figure 2.4 (cont.))

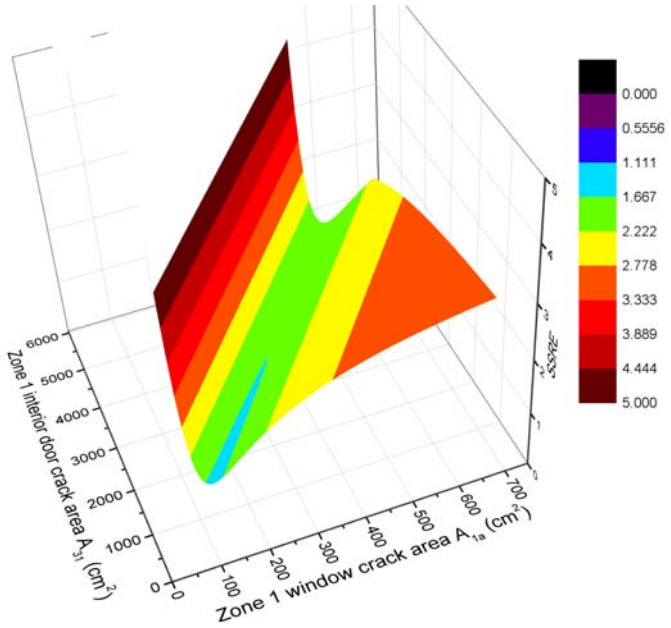

(b) 3D $SSRE_1^*$ plot in zone 1

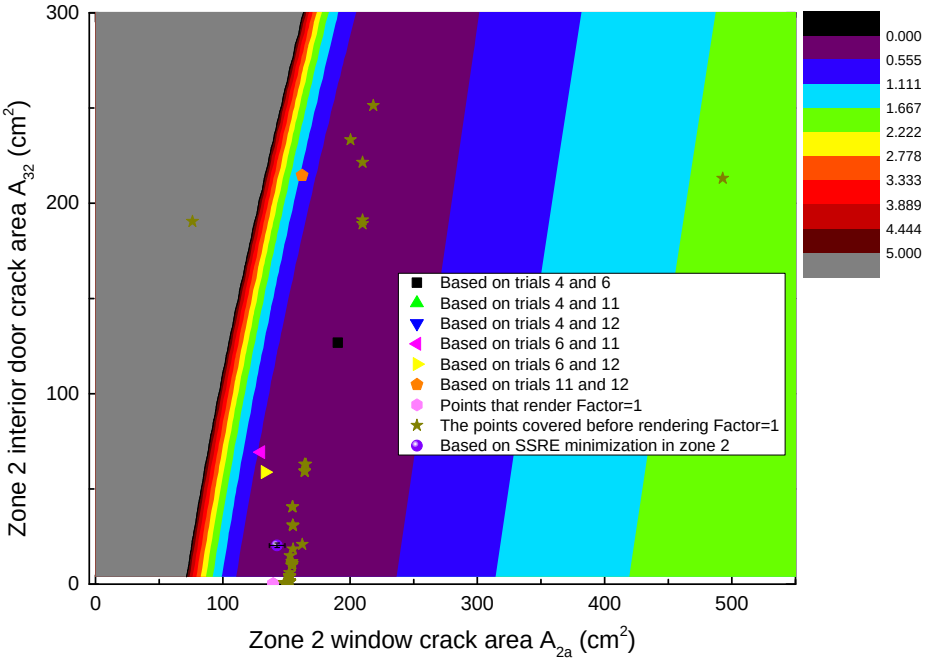

(c) $SSRE_2^*$ contours in zone 2 (Figure 2.4 (cont.))

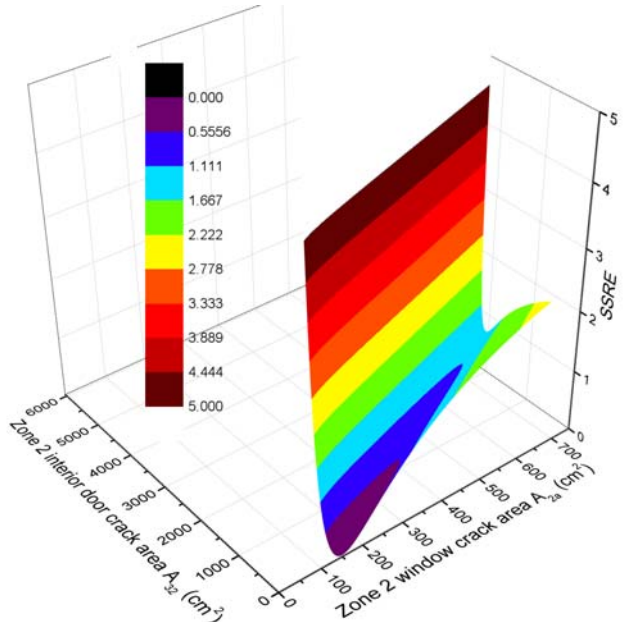

(d) 3D $SSRE_2^*$ plot in zone 2

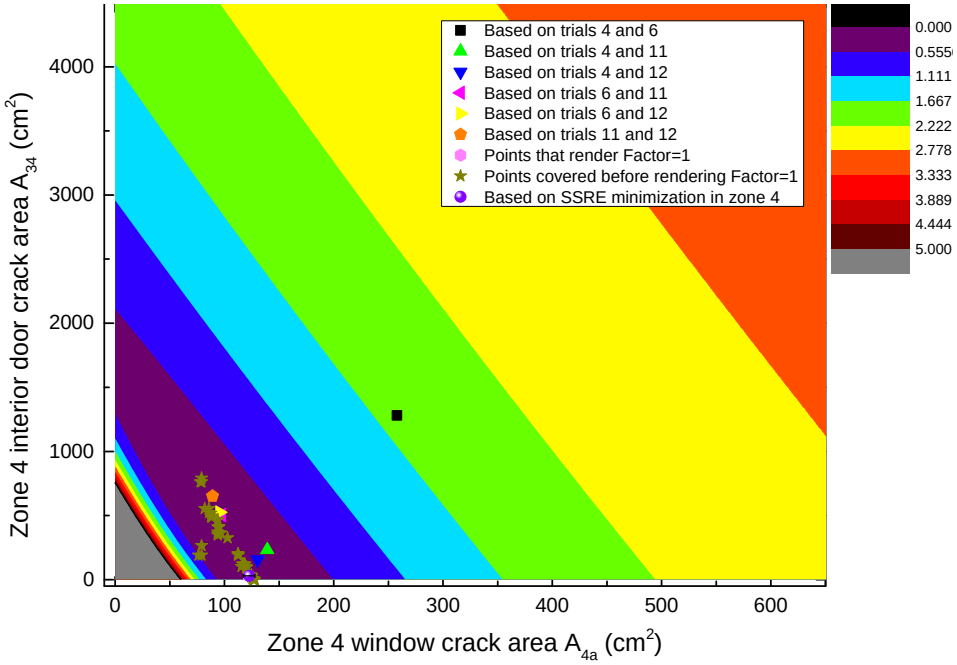

(e) $SSRE_4^*$ contours in zone 4 (Figure 2.4 (cont.))

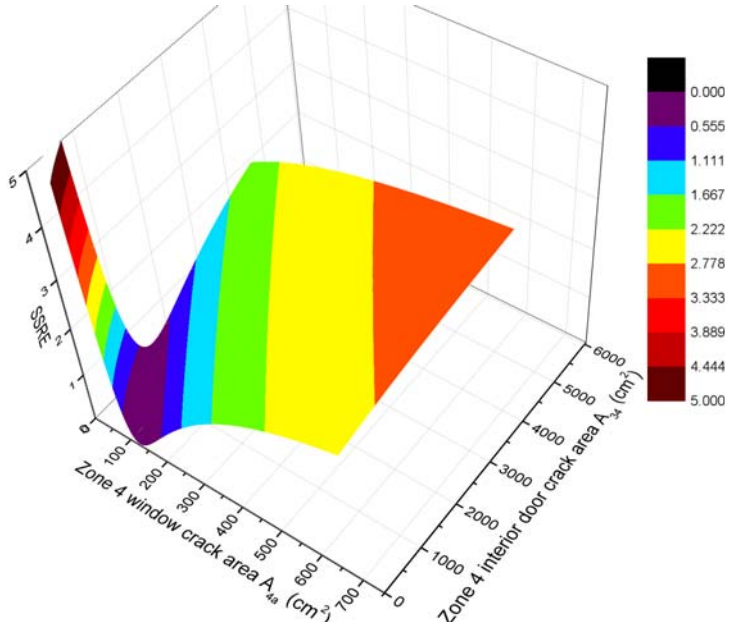

(f) 3D $SSRE_4^*$ plot in zone 4

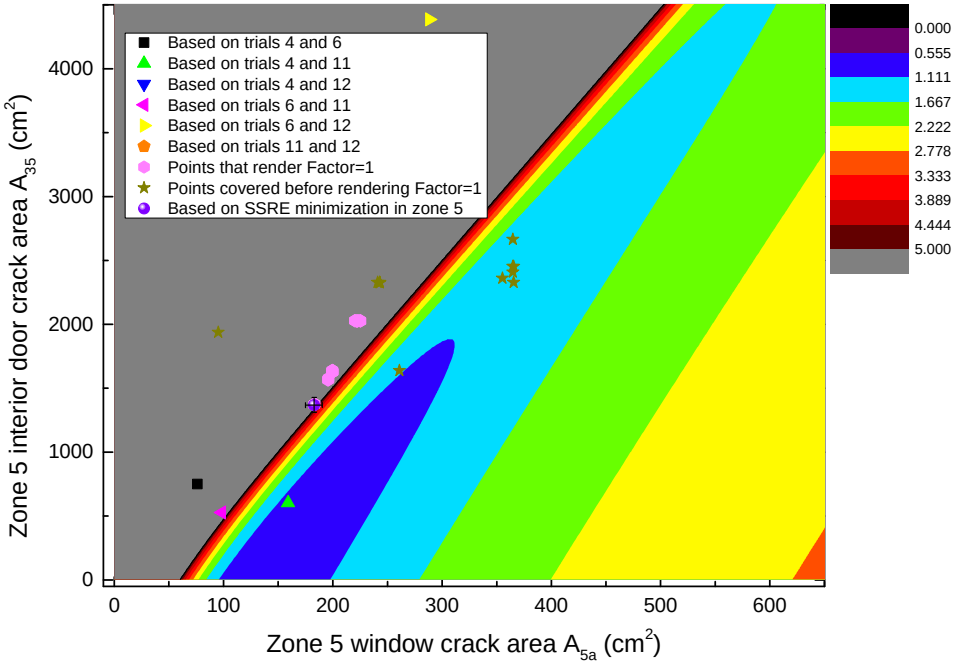

(g) $SSRE_5^*$ contours in zone 5 (Figure 2.4 (cont.))

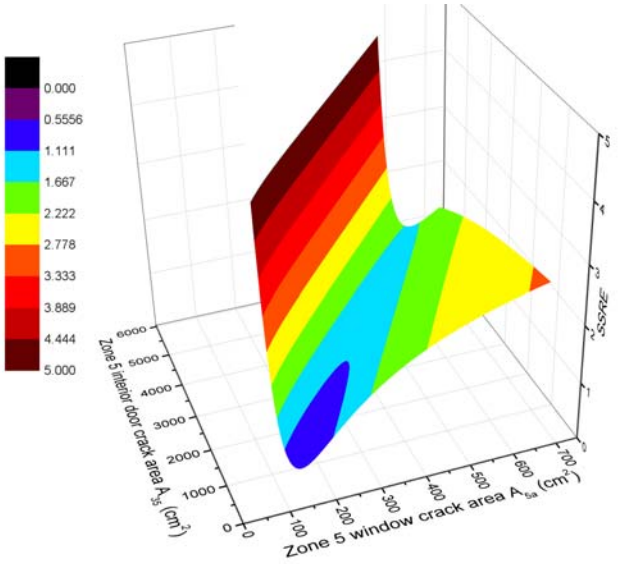

(h) 3D $SSRE_5^*$ plot in zone 5

Figure 2.4 Crack area optimization in zones 1, 2, 4 and 5

Following a similar procedure, zone-3 and -6 crack areas can be determined. A summary of the crack areas is listed in Table 2.7. A CONTAM 3.0 model was constructed using the obtained crack areas and simulated pressure differences are obtained and shown in Figure 2.5 following a procedure similar to that in the whole-facility approach.

Table 2.7 Calculated leakage area in each opening

Parameter	Crack area (cm^2)	Estimated crack width (uniform around each opening) (cm)
A_{1a}	314.21	0.79
A_{31}	2100.01	3.50
A_{2a}	139.68	0.35
A_{32}	0.04	0.0001
A_{4a}	122.74	0.31
A_{34}	29.16	0.05
A_{5a}	182.86	0.46
A_{35}	1367.69	2.28
A_{3nda}	42.91	0.07
A_{3nwa}	0.46	0.0011
A_{3swa}	105.16	0.26
$A_{3sdampera}$	21.37	NA
A_{36}	17.14	0.03
A_{6a}	7.76	0.02

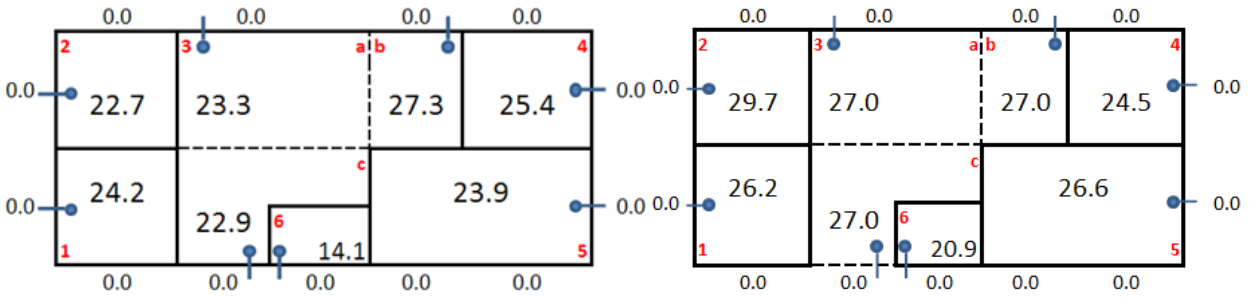

(a) Experimental overpressures (Pa) in trial 4 (b) Simulated overpressures (Pa) in trial 4

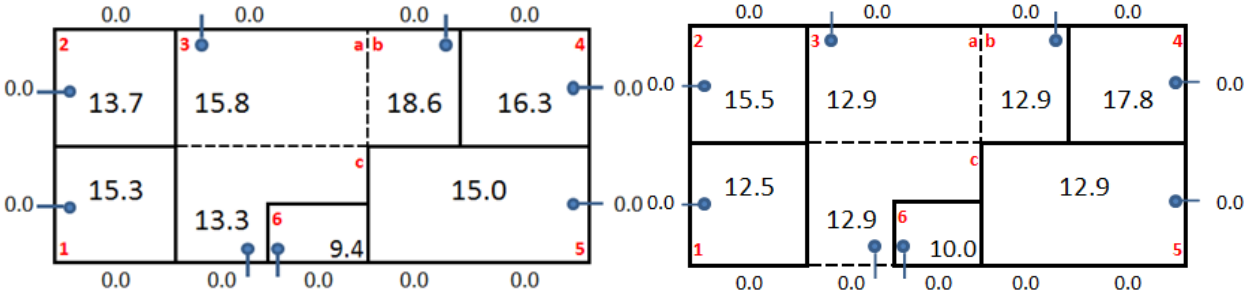

(c) Experimental overpressures (Pa) in trial 6 (d) Simulated overpressures (Pa) in trial 6

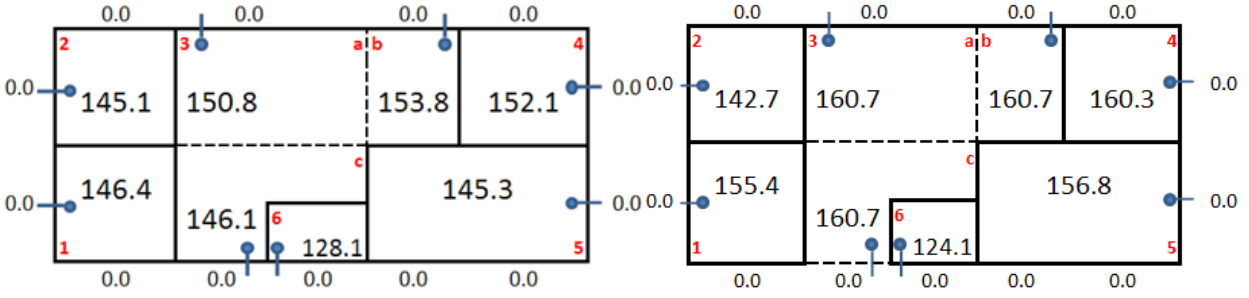

(e) Experimental overpressures (Pa) in trial 11 (f) Simulated overpressures (Pa) in trial 11

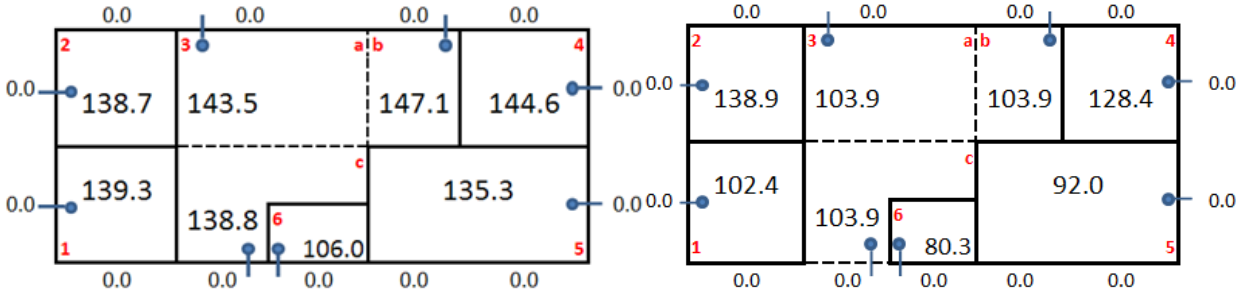

(g) Experimental overpressures (Pa) in trial 12 (h) Simulated overpressures (Pa) in trial 12

Figure 2.5 Empirical validation using calculated leakage areas in Table 2.5

Following the ASTM D5157-97 standard (ASTM, 2008), Table 2.8 can be obtained based on Figure 2.5. It can be seen that all of the results (48 out of 48) are within specified

ranges of the standard, which shows an excellent model performance following the zone-by-zone approach.

Table 2.8 Model performance evaluation for the zone-by-zone crack estimation approach

Parameter	Range	Zone							
		1	2	3a	3b	3c	4	5	6
Correlation coefficient, r	(r≥0.9)	0.96	1.00	0.95	0.95	0.95	0.99	0.94	0.98
Regression slope, m	(0.75≤m≤1.25)	0.90	0.96	0.89	0.88	0.91	0.97	0.89	0.85
Regression intercept, b	($\lvert b/\bar{C}\ o\rvert$≤0.25)	0.01	0.06	0.02	0.01	0.03	0.01	0.02	0.06
NMSE	($\lvert NMSE\rvert$≤0.25)	0.060	0.002	0.067	0.075	0.059	0.012	0.088	0.048
FB	($\lvert FB\rvert$≤0.25)	0.092	0.020	0.091	0.118	0.054	0.022	0.103	0.090
FS	($\lvert FS\rvert$≤0.50)	0.120	0.087	0.131	0.159	0.077	0.038	0.111	0.282

2.4.4 Discussion

Comparing Table 2.6 to Table 2.8, it can be seen that the zone-by-zone approach generally renders better model performance than the whole-facility approach, due to the fact that all the crack areas are not necessarily the same in reality. However, the current simplification of the leakage function form (especially the flow exponent 0.65 or 0.5) may not be the exact representation of reality.

A possible direction for improvement is to quantify all the involved parameters. Take zone 1 in Figure 2.2 for instance, the mass conservation can be expressed as

$$Q_1 = C_{1a}^{*}\Delta p_{1a}^{n_{1a}} A_{1a} + C_{13}^{*}\Delta p_{13}^{n_{13}} A_{13} \tag{2.15}$$

where the supply airflow rate is divided into two streams: exfiltration flow $Q_{1a} = C_{1a}^{*}\Delta p_{1a}^{n_{1a}} A_{1a}$ through the window and inter-zone flow $Q_{13} = C_{13}^{*}\Delta p_{13}^{n_{13}} A_{13}$ through the door. For each crack flow, there are four elements: 1) modified flow coefficient D to represent the flow resistance due to crack shape and dimension; 2) pressure difference Δp across the crack; 3) flow exponent n; and 4) crack area A. Following the reasoning in Equations (2.6)-(2.8), the flow coefficients may not be necessary. This will reduce Equation (2.15) into Equation (2.16).

$$Q_1 = \Delta p_{1a}^{n_{1a}} A_{1a} + \Delta p_{13}^{n_{13}} A_{13} \tag{2.16}$$

Even after the parameter reduction, there are still four parameters that need to be determined through LSM following a zone-by-zone approach in zone 1. Similarly four parameters in zones 2 and 4, six in zone 5, ten in zone 3 and two in zone 6. It is worth noting that both the flow exponent n and the crack area A now vary within a wide range (for instance, $0<A<0.01$ m^2, $0.5<n<1$ for small cracks and $0.1<n<0.5$ for big cracks). In addition, the number of unknown parameters increases from 13 to 26. Thus, the above treatment significantly elevates the difficulty level of obtaining reasonable results and increases the optimization time.

Even though there are some simplified assumptions in the whole-facility approach, it is still desirable because it provides good estimation results and costs less time than the zone-by-zone approach. The zone-by-zone approach costs more time, but it can generally render better model performance. In the present study, 91.7% of the indicator values lie within ranges of the standard using the whole-facility approach while 100% of the indicator values are within ranges of the standard using the zone-by-zone approach. The consumed time increases roughly by a factor of n (n is the number of zones in the facility) by switching from whole-facility approach to the zone-by-zone approach.

The two approaches are promising, because 1) they can be realized using existing building air-delivery duct system instead of setting up fans to perform a "blower-door" test; 2) they allow estimation of inter-zone leakage information in buildings. The general validity of airflow conservation law and the power-law crack flow suggests that as long as volume flow rate and overpressure measurements can be provided, and ambient wind pressures measured or determined through CFD simulations, the present model can be applied to any multizone buildings.

2.5 Summary

A crack area estimation model was demonstrated in which two approaches (zone-by-zone approach and whole-facility approach) were introduced. A CONTAM 3.0 model was constructed using the above estimated crack areas for simulation. An evaluation method following ASTM D5157-97 standard (ASTM, 2008) was taken to evaluate the CONTAM model simulation performance in terms of pressure difference prediction, and it was shown that the model performance was very good: 91.7% of indicator values were within ranges of the standard for the whole-facility approach and 100% for the zone-by-zone approach.

CHAPTER 3-VENTILATION SYSTEM AND CONTAMINANT MITIGATION STRATEGY

After characterization of the testbed, comparisons were performed between different ventilation systems using CONTAM to select a suitable ventilation system. The three candidate systems under investigation were: 1) central unbalanced ventilation system (CUBVS), using which a building was pressurized due to the net outdoor air intake; 2) distributed unbalanced ventilation system (DUBVS), using which a building was pressurized due to the net outdoor air intake; and 3) distributed balanced ventilation system (DBVS), using which neutral indoor pressure was maintained due to the net zero outdoor air intake. The three configuration plans for air filters were: 1) OA filter only; 2) recirculated air (RA) filter only; and 3) both the OA and the RA filters. Ventilation and mitigation strategies were explored using CONTAM. As a result, a DUBVS was selected as a suitable ventilation system, because 1) it can provide positive pressure difference across the building envelope to prevent exterior contaminant infiltration from the ambient environment and the vestibule; and 2) some contaminated indoor zones can be "isolated" from adjacent ones by adjusting the relative pressure differences. More detail is provided in Appendix D regarding the two case studies. The current focus is to demonstrate a framework of IAQ evaluation through investigating the system performance in terms of "Protection factor *vs*. Filtration power." Compared to the DUBVS, a CUBVS is more commonly utilized in buildings as it is more easily manageable. Thus, even though the DUBVS was a superior ventilation system, the CUBVS was selected as the ventilation system for simulation purposes.

3.1 Simulation Scenario

The simulation scenario was as follows, starting at t=0, a particle plume passed by a facility at a constant particle number density for 5 hours, and the ambient concentration immediately dropped to zero after that (t=5 hrs+). During the plume, some people tried to seek shelter in the facility vestibule 1 minute after the ambient plume started. It was assumed that at t_1=62 seconds that the particles brought by incoming people were deposited into the vestibule as a burst source. The burst source was assumed to be able to elevate the contaminant concentration in the vestibule to the same level as the ambient after mixing. It was crucial to efficiently mitigate the hazard introduced by people in the vestibule before access permission was granted. The facility was subjected to "southeast" wind at a wind speed in the range of 0-11.18 m/s. The

facility was installed with a CUBVS in zones 1-5 and a DBVS in zone 6. Three spore distributions were investigated (Carrera, *et al*., 2007; Carrera *et al*., 2008; Reponen *et al*., 1998), with the first two treated as sensitivity analysis for *the* third one, as shown in Table 3.1. The differences between these three distributions were the geometrical mean diameter and standard deviation.

The wind pressure profile corresponding to each wind speed was estimated based on ASHRAE Handbook (ASHRAE, 2009). A small leakiness (0.0005 $m^3/s/m^2$ of building envelope area @ 75 Pa) was selected for the facility for the purpose of simulation.

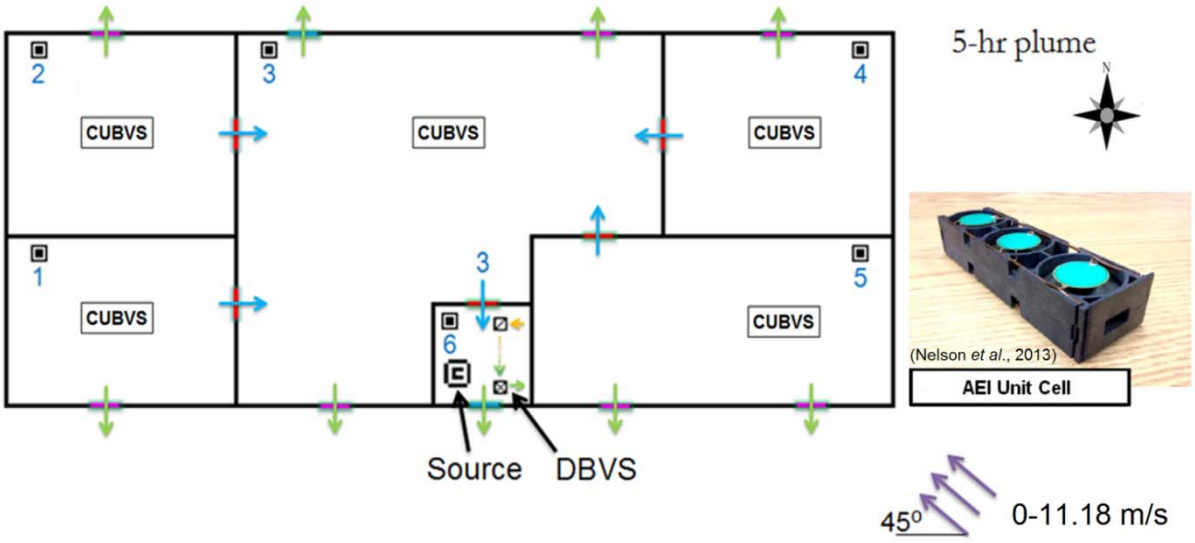

Figure 3.1 A sketch of the facility in the simulation scenario

Table 3.1 Contaminant properties

Particles / Species Property	Distribution 1	Distribution 2	Distribution 3
Diffusion coefficient (m^2/s)	2×10^{-5}	2×10^{-5}	2×10^{-5}
Geometrical mean diameter (μm)	10	0.8774	0.8
Geometrical standard deviation	5	1.07	1.54
Diameter range (μm)	0.5-150	0.5-2.5	0.5-2.5
Bins	28	20	20
Number density (#/cm^3)	328	106,000	106,000
Effective density (kg/m^3)	1,165	1,165	1,165

3.2 Determining the Baseline OA Fraction

In order to design a new central ventilation system for the facility, it was important to determine a baseline condition. To be specific, it was of interest to explore OA fractions at different ambient "southeast" wind speeds and determine a baseline among all the possible ratios. It was demonstrated that as long as a sufficient positive pressure prevailed, ambient contaminant infiltration would not occur. In this section, the sufficient positive pressure level was set to be 5 Pa, that is, the smallest pressure difference across vestibule exterior door should be at least and as close as possible to 5 Pa.

There were some design requirements:

- Design flow (supply air into the facility) range: 0.283 m^3/s - 0.472 m^3/s
- Small leakiness assumed (0.0005 $m^3/s/m^2$ of building envelope area @ 75 Pa), i.e., 9.94 cm^2/m^2 unit crack area for each opening; window area: 1 m^2; door area: 2.5 m^2
- All supply air went through a coarse filter (MERV 8)
- Design OA flow rate based on ASHRAE Standard 62.1-2010 (ASHRAE, 2010a)
- Ventilation rate per unit floor area in zones 1-5 was set to be the same
- The vestibule was not ventilated

With the above details set, a range of OA fractions at two wind speeds (0 m/s and 11.18 m/s) and three leakiness values (0.0005, 0.0015 and 0.0040 $m^3/s/m^2$ @ 75 Pa) were obtained, as listed in Tables 3.2a and 3.2b. A recommended range of OA fractions are highlighted in green color, where the lower bound of the OA fraction corresponds to a higher supply air flow rate (near the upper bound 0.472 m^3/s) and the upper bound of the OA fraction corresponds to a lower supply air flow rate (near the lower bound 0.283 m^3/s). The OA fraction below the tabulated lower bound (each cell in white color) means that sufficient positive pressure cannot be achieved even with the 0.472 m^3/s SA flow rate. The OA fraction beyond the upper bound means that the SA flow rate together with that OA fraction can provide more than sufficient positive pressure (each cell in yellow color), making it a less economical option. Based on Tables 3.2b, an OA fraction range of 25%-40% needs to be further explored for small-leakiness buildings.

Table 3.2a OA fractions to provide sufficient positive pressures at 0 m/s ambient wind

Leakiness ($m^3/s/m^2$ @ 75 Pa)	OA Fraction											
	10%	15%	20%	25%	30%	40%	50%	60%	70%	80%	90%	100%
0.0005												
0.0015												
0.0040												
	Both Δp_{5rw} and Δp_6 cannot reach 5 Pa, because OA is not sufficient											
	Both Δp_{5rw} and Δp_6 can reach ⩾ 5 Pa, provided by a SA flow rate within the bounds											
	Both Δp_{5rw} and Δp_6 can reach ⩾ 5 Pa, provided by a SA flow rate lower than the lower bound											

Table 3.2b OA fractions to provide sufficient positive pressures at 11.18 m/s ambient wind

Leakiness ($m^3/s/m^2$ @ 75 Pa)	OA Fraction											
	10%	15%	20%	25%	30%	40%	50%	60%	70%	80%	90%	100%
0.0005												
0.0015												
0.0040												
	Both Δp_{5rw} and Δp_6 cannot reach 5 Pa, because OA is not sufficient											
	Both Δp_{5rw} and Δp_6 can reach ⩾ 5 Pa, provided by a SA flow rate within the bounds											
	Both Δp_{5rw} and Δp_6 can reach ⩾ 5 Pa, provided by a SA flow rate lower than the lower bound											

Similar tables can be made to cover various wind speeds and generate Table 3.3, where suitable ranges of OA fraction can be found that will provide just sufficient positive pressures at various wind speeds with a SA flow rate of 0.283~0.472 m^3/s. Based on Table 3.3, an OA fraction of 25% and 40% was selected as the lower and upper bound of OA fraction of the central unbalanced ventilation system for small-leakiness buildings.

Table 3.3 Suitable OA fraction range at each wind speed and leakiness

Wind speed (m/s)	Leakiness ($m^3/s/m^2$ @ 75 Pa)	
	Small (0.0005)	Average (0.0015)
0	15%-20%	35%-65%
2.24	15%-20%	40%-60%
4.47	15%-25%	45%-75%
6.71	20%-30%	60%-90%
8.94	25%-35%	70%-100%
11.18	25%-40%	80%-100%
OA fraction to be explored:	25%, 40%	NA

3.3 Determining Different Filter Efficiencies

When the AEI device was powered off, it can be treated as a MERV filter with a reported purification efficiency of 71.2% ± 8.3% (Nelson, 2011). According to the model predictions in Figure 3.2 (Kowalski and Bahnfleth, 2002), both MERV 12 and 13 filters fit relatively well. In order to make conservative predictions, the MERV 12 filter was chosen to be the approximated one for the AEI device when it was powered off (noted as "AEI off" hereafter).

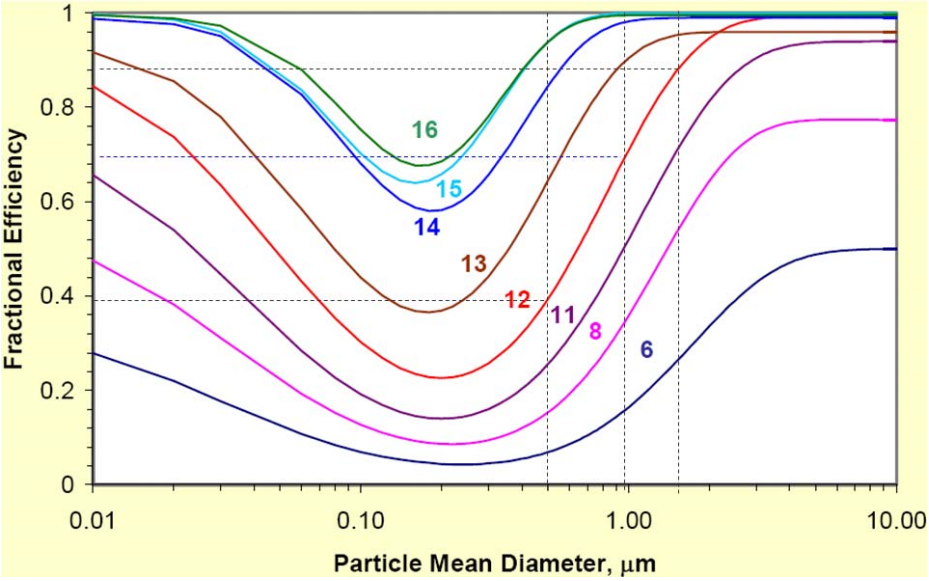

Figure 3.2 MERV 12 approximated for AEI device (AEI off) (Kowalski and Bahnfleth, 2002)

When the AEI device (shown in Figure 3.3) was powered on (noted as "AEI on" hereafter), its efficiency can be extrapolated based on experimental data provided by Applied Research Associates (ARA), as shown in Figure 3.4 (a). In his experiments, Nelson (2011) bundled 60 cells of the AEI device to make a unit. The maximum design flow rate for one unit was 0.024 m^3/s with a channel flow velocity of 2.16 m/s. In the present study, this flow velocity was kept the same. Thus, some extrapolation was necessary based on the ARA data. With necessary rearrangement, the "AEI on" efficiency was obtained that varied with particle size, as shown in Figure 3.4 (b).

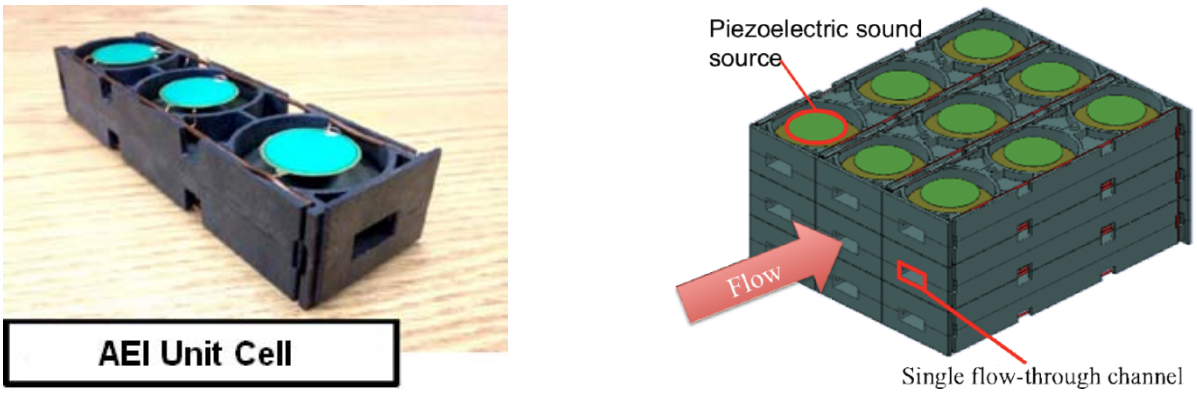

(a) (b)

Figure 3.3 AEI device: a) unit cell (Nelson *et al.*, 2013), b) a bundle (Gallia *et al.*, 2010)

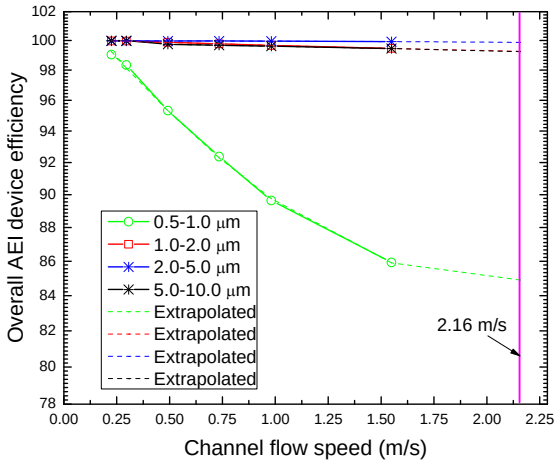

(a)

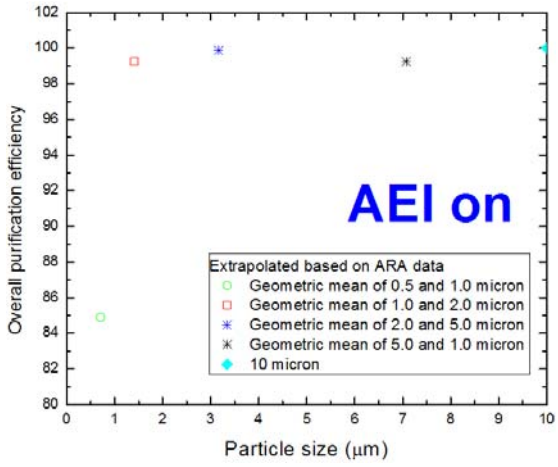

(b)

Figure 3.4 a) AEI efficiencies based on ARA data, b) AEI efficiency *vs*. particle size

The variation of filter efficiency with particle size was taken into consideration in this section. The HEPA filter and MERV 8 filter efficiencies were predicted according to the models by Kowalski *et al*. (1999) and Kowalski and Bahnfleth (2002), as shown in Figures 3.5 and 3.6. A size range of 0.3 to 0.67 μm was the "danger zone" for the HEPA filters. In this section, the model prediction of the HEPA filter efficiency shown in Figure 3.5 was used in CONTAM simulations. There is only one data point (the nominal rating point: 99.97% efficiency at 0.3 μm) in Figure 3.5 for the HEPA filters because other points were typically unavailable in the manufacturer catalog data. In the adopted model, this data point was taken into consideration.

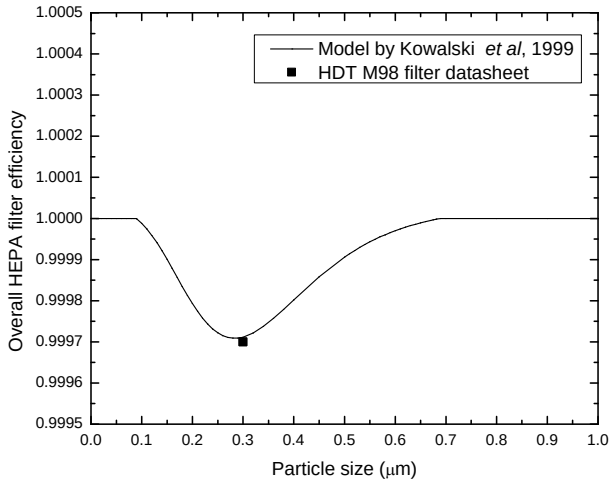

Figure 3.5 HEPA filter model prediction (Kowalski *et al*., 1999)

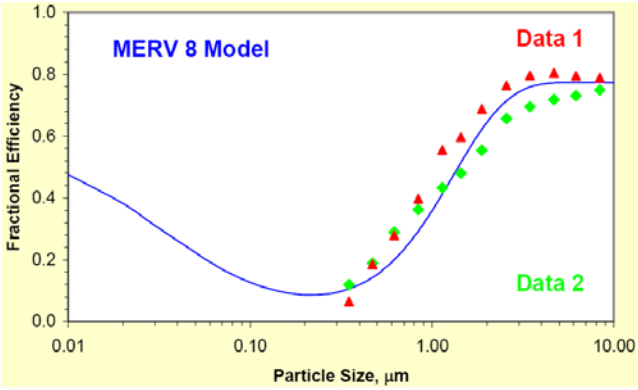

Figure 3.6 MERV 8 filter model prediction (Kowalski and Bahnfleth, 2002)

3.4 Determining Filtration Power Consumption

The selected HEPA filter was M98 from HDT Engineered Technologies. The MERV 8 filter was Camfil Farr pleated panel filter 30/30. Pressure drop information of the two filters is listed in Table 3.4.

Table 3.4 Pressure drop of the HEPA filter and the MERV 8 filter

	Initial resistance (Pa)	Final resistance (Pa)	Air flow capacity (m^3/s)	Rated Air flow for one unit (m^3/s)	Multiple units combinable
HEPA filter	250	1000		0.094	2-7
MERV 8 filter	57.5	250	0.557	-	-

The relevant filter efficiencies and corresponding power consumptions are summarized in Table 3.5. When calculating total filtration power consumption, the old filter was chosen instead of the new one for the HEPA filter. Generally, the pressure drop varied linearly with flow rate for the HEPA filter (Novick *et al*., 1992). The filtration power due to the M98 HEPA filter resistance was a quadratic function of the flow rate, because it was taken as the product of the pressure drop across the filter and the air flow rate. The unit activation power was estimated to be 0.1 J/L for the AEI device. Thus, its total AEI filtration power was the sum of activation power and friction power. Here the *friction power* was the power consumed to overcome the friction in the flow channel and *filtration power* was the summed power consumed to accomplish the filtration.

Table 3.5 Summary of the filter efficiency and the power consumption

Parameter / Filter	Filter efficiency (MERV rating)	Benchmark (m^3/s)	Unit energy or pressure drop at benchmark (max)	Friction power at a flow rate of Q m^3/s (W)	Filtration power at a specific flow rate of Q m^3/s (W)
New HEPA filter	Figure 3.26	0.661	250 (Pa)	$250*Q^2/0.661$	$250*Q^2/0.661$
Old HEPA filter	Figure 3.26	0.661	1000 (Pa)	$1000* Q^2/0.661$	$1000* Q^2/0.661$
AEI device (off)	Figure 3.29	0.024	120 (Pa)	2.8 W per 0.024 m^3/s per AEI unit	2.8*Q/0.024
AEI device (on)	Figure 3.31(c)	0.024	0.1 (J/L) (unit activation power)	2.8 W per 0.024 m^3/s per AEI unit	2.8*Q/0.024+0.1*Q*1000
MERV 8 filter	Figure 3.27	0.557	57.5 (Pa)	$57.5* Q^2/0.557$	$57.5* Q^2/0.557$

3.5 Filtration Schemes and a Performance Metric

There were sixteen filtration plans (Table 3.6) examined for a ventilation system shown in Figure 3.7. It was of interest to examine all of these sixteen filtration plans at the above mentioned OA fractions (25% and/or 40%) for the small-leakiness facility and determine the corresponding protection factor (PF) and filtration power consumption. Through comparing the sixteen filtration plans, some ventilation and mitigation strategy can be obtained for zones 1-5.

In the present study, the protection factor (PF) is defined as follows,

$$PF = \int_0^{t_2} c_{out}\, d\tau \Big/ \int_0^{t_2} c_{in}\, d\tau \qquad \left(t_2 \text{ is the concerned time frame}\right) \tag{3.1}$$

where c_{out} is specified in Table 3.1 and c_{in} is obtained through a CONTAM simulation, the concerned time frame t_2 is normally a period within which a significant change of either c_{out} or c_{in} occurs. The classification of "significant change" is out of the scope of the present study as the "change" is dependent on ambient/indoor particle number densities, particle toxicity, human respiratory rate, and possibility of survival upon accumulation of a threshold amount of the particle(s). If the particles are of indoor origin, the PF is dominantly determined by the particle number densities. Any attempt to get meaningful uniform conclusion regarding the PF in the presence of various indoor particle source strengths will fail, as concluded by Chen and Zhao (2011). This is because the changes of indoor and outdoor concentration are independent events. A case-by-case analysis of the PF value and the time frame is suggested in this case. As a comparison, if the particles are of outdoor origin only, the changes of indoor and outdoor concentration are dependent events because c_{in} is dependent on c_{out}. In addition, the time frame of significant change of the indoor concentration is typically close to that of the outdoor concentration. The PF is generally applicable in this case because the I/O ratio is typically not dependent on the ambient source strength or the time frame. In the present study, the PF was explored for scenarios where only outdoor sources were present. The typical time frame t_2 can be long or short, depending on the ambient source strength and ambient wind speed. t_2 was chosen to be five hours for the purpose of simulation.

The protection factor PF is an indicator intended to quantify the safety level of a protected facility against particulate matter such as biological agents that pose life threats based on accumulative dosage through inhalation. For instance, if a person stays in a protected facility

with a PF of 150 and maintains the same respiratory rate as in the ambient, it will take 150 times of the time he would have had in the polluted ambient environment before he accumulates a dosage that renders him 50% possibility of ending up in death. This dosage is often called LD_{50}. A building with very high PF value (for instance, 1000) does not necessarily mean that a person staying inside is definitely safe, because the ambient spore number density also plays an important role in determining the time frame within which a person accumulates a lethal dosage through inhalation. The determination of ambient spore number density is out of the scope of this study due to its unpredictable nature. Considering the above aspects, the PF was adopted as an IAQ performance metric.

Table 3.6 Sixteen filtration plans

Filtration scheme	SA filter	OA filter	RA filter
1	MERV8	HEPA	-
2	MERV8	HEPA	AEI off
3	MERV8	HEPA	AEI on
4	MERV8	HEPA	HEPA
5	MERV8	AEI on	-
6	MERV8	AEI on	AEI off
7	MERV8	AEI on	AEI on
8	MERV8	AEI on	HEPA
9	MERV8	AEI off	-
10	MERV8	AEI off	AEI off
11	MERV8	AEI off	AEI on
12	MERV8	AEI off	HEPA
13	MERV8	-	-
14	MERV8	-	AEI off
15	MERV8	-	AEI on
16	MERV8	-	HEPA

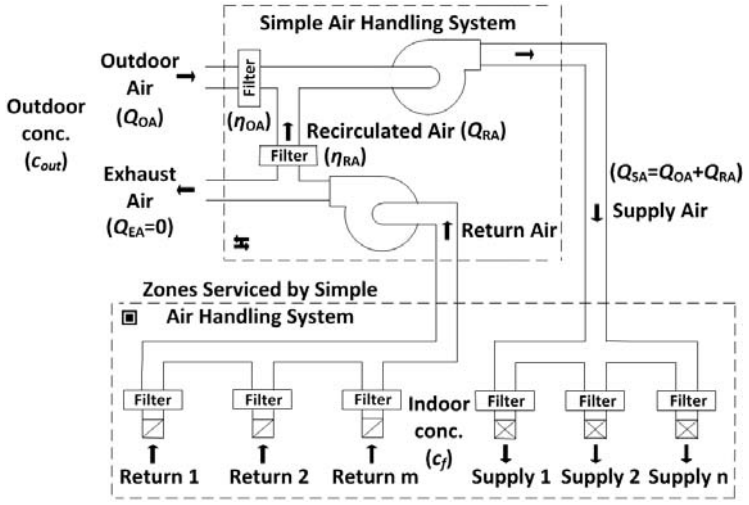

Figure 3.7 A representative ventilation system

3.6 Particle Distribution 1

In this section, the ambient particles followed the log-normal distribution-1 listed in Table 3.1, as shown in Figure 3.8.

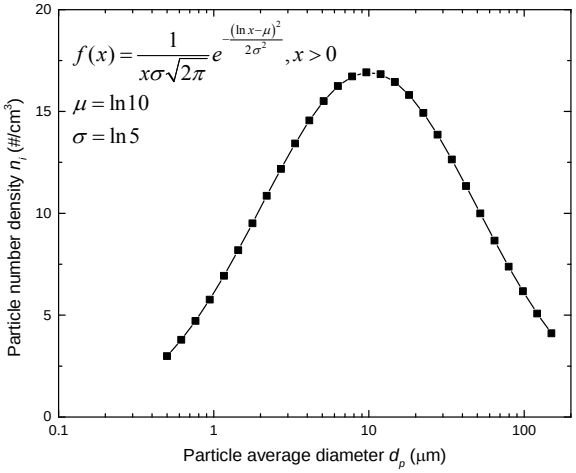

Figure 3.8 Log-normal distribution 1 of particles in Table 3.1

For the small-leakiness facility, an OA fraction of 25% was explored at different ambient "southeast" wind speeds, as shown in Figure 3.9. The ventilation rates were selected to provide the satisfying and smallest possible positive pressures in the vestibule within the supply air flow rate range of 0.283 m^3/s to 0.472 m^3/s. The ambient pressure values were gauge readings, and the pressure values in each zone was the positive pressure difference across the red-highlighted

crack(s) in each zone. It was worth noticing that at wind speeds below 3.13 m/s the ventilation rate was kept the same as that at 3.13 m/s, because 0.283 m^3/s was the SA flow rate lower bound.

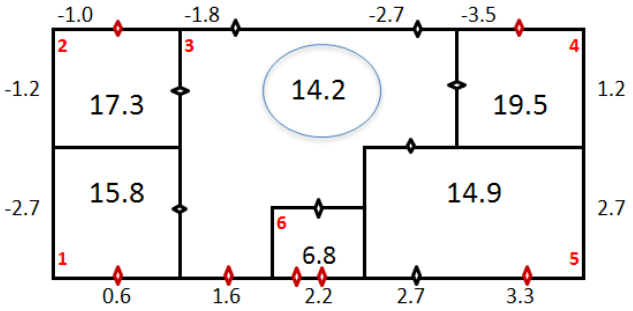

(a) Pressure distribution at 3.13 m/s

Zone	OA (m^3/s)	RA (m^3/s)	SA (m^3/s)
1	0.008	0.024	0.033
2	0.008	0.024	0.033
3	0.030	0.089	0.119
4	0.008	0.024	0.033
5	0.017	0.050	0.067
Sum	0.071	0.212	0.283

(b) OA, RA and SA flow rate

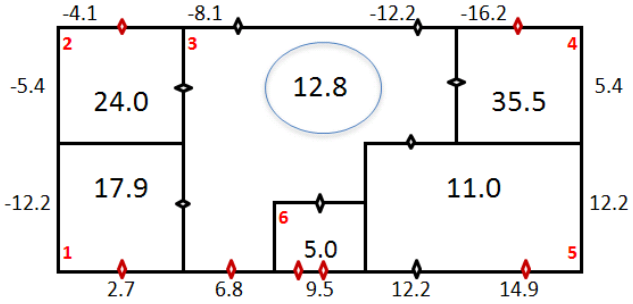

(c) Pressure distribution at 6.71 m/s

Zone	OA (m^3/s)	RA (m^3/s)	SA (m^3/s)
1	0.009	0.028	0.037
2	0.009	0.028	0.037
3	0.034	0.102	0.136
4	0.009	0.028	0.037
5	0.019	0.058	0.077
Sum	0.081	0.244	0.326

(d) OA, RA and SA flow rate

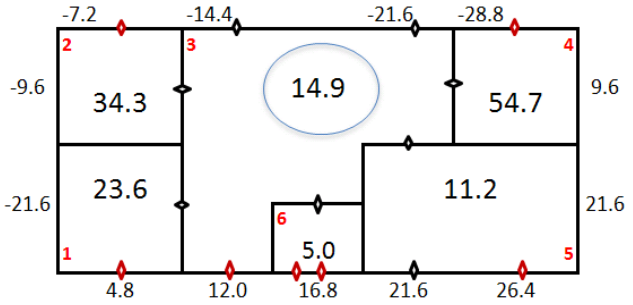

(e) Pressure distribution at 8.94 m/s

Zone	OA (m^3/s)	RA (m^3/s)	SA (m^3/s)
1	0.011	0.034	0.046
2	0.011	0.034	0.046
3	0.042	0.125	0.166
4	0.011	0.034	0.046
5	0.023	0.070	0.094
Sum	0.099	0.298	0.398

(f) OA, RA and SA flow rate

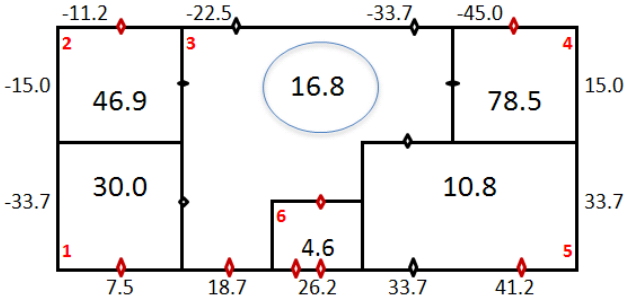

(g) Pressure distribution at 11.18 m/s

Zone	OA (m^3/s)	RA (m^3/s)	SA (m^3/s)
1	0.014	0.041	0.054
2	0.014	0.041	0.054
3	0.049	0.148	0.197
4	0.014	0.041	0.054
5	0.028	0.084	0.112
Sum	0.118	0.354	0.472

(h) OA, RA and SA flow rate

Figure 3.9 Pressure distribution and ventilation rates at various wind speeds (25% OA)

"PF *vs*. filtration power" figures in Figure 3.10 were obtained based on ventilation flow rates in Figure 3.9 to show the effect of wind speed and filter on PF and filtration power consumption. The PF values were calculated based on CONTAM simulations and Equation (3.1). The filtration power was calculated based on Table 3.5. The ventilation flow rates stayed the same at 0.283 m^3/s for cases where wind speeds were below 3.13 m/s, making the protection factor in zones 1-5 the same for all these cases. As wind speed increased from 3.13 m/s to 11.18 m/s, it was seen from Figure 3.10 that the filtration power consumption increased with the wind speed, but the PF was influenced very little by the wind speed. This suggests that for a given OA fraction and filtration scheme, as long as the positive pressure is sufficient, the ventilation rate has little impact on the PF.

Apparently there are four levels of PF values that are impacted dominantly by the OA filter efficiency ($\eta_{HEPA} > \eta_{AEI(on)} > \eta_{AEI(off)}$), and leaving the OA unfiltered is certainly not suggested (compare Plans 1-12 to Plans 13-16). The effect of the RA filter on the PF is insignificant compared to that of the OA filter. With an OA filter fixed, having the HEPA filter for the RA consumes the most amount of power among the three filters: HEPA filter, AEI device (on) and AEI device (off). The above trends stay the same for all the simulations in the present study. The above findings generally hold true for any multizone buidings with outdoor particles.

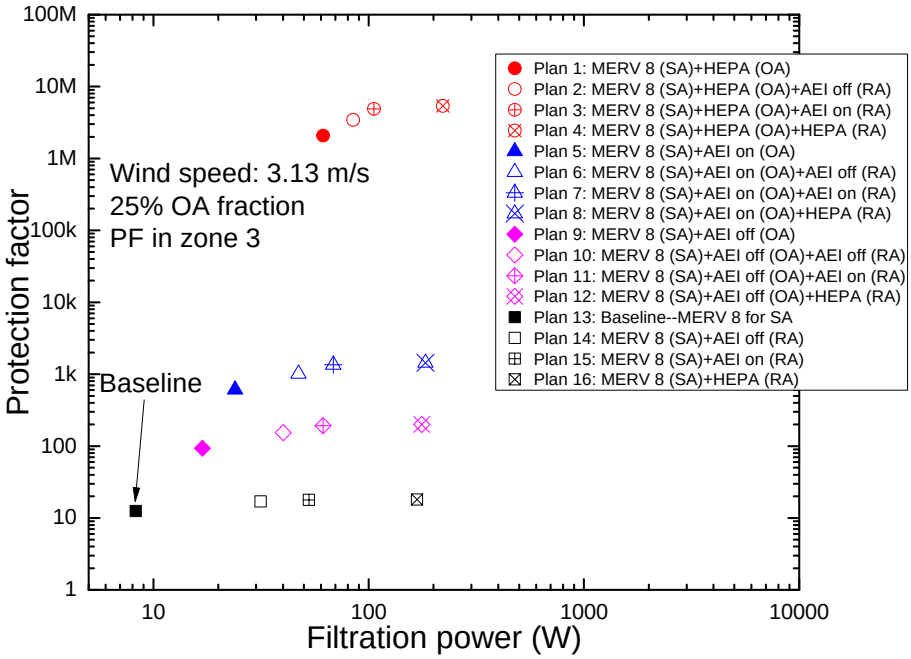

(a) Figure 3.10 (cont.)

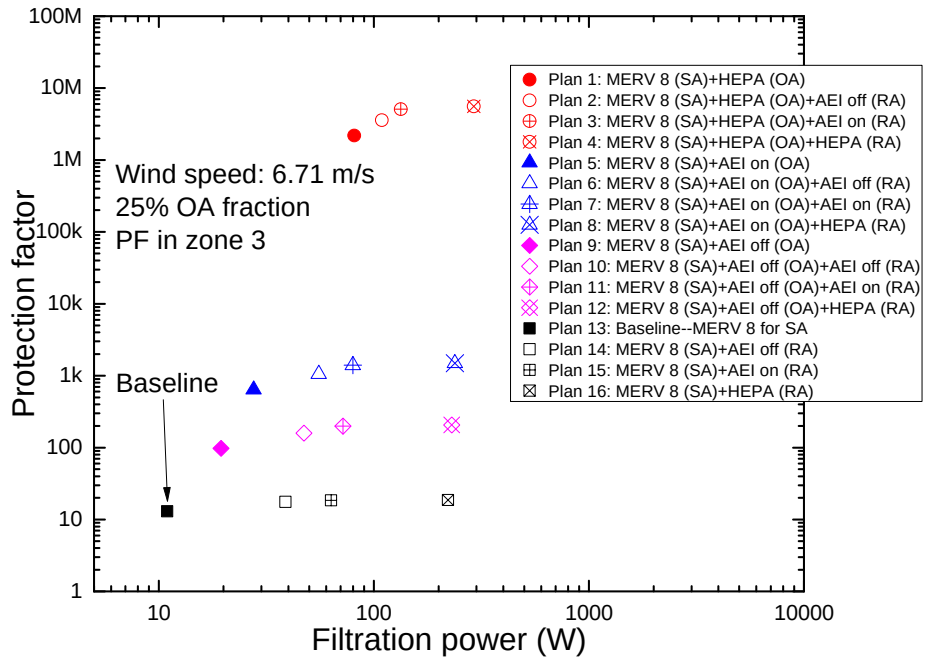

(b)

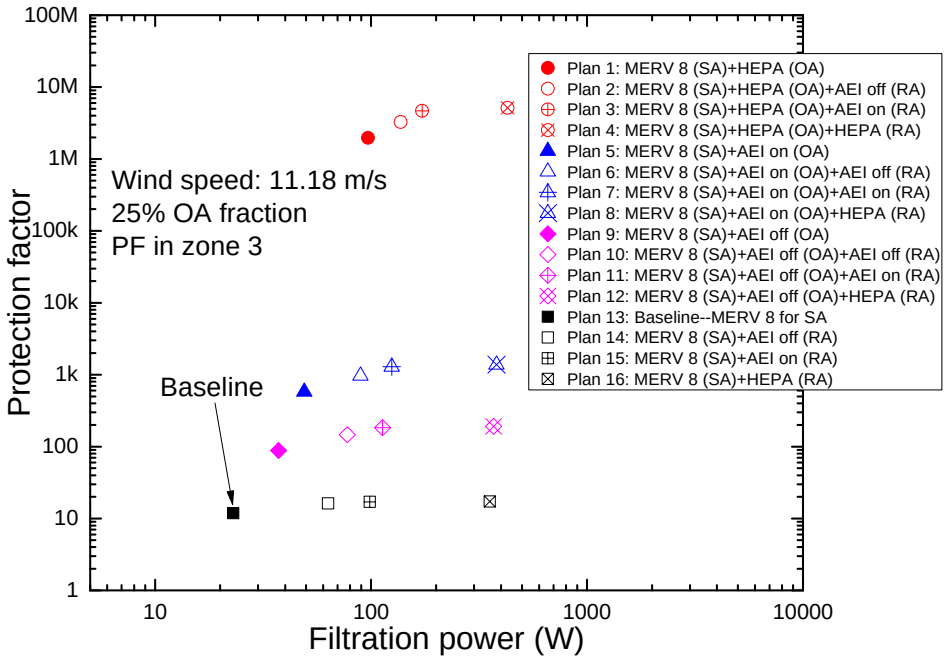

(c)

Figure 3.10 Protection factor *vs*. filtration power at different wind speeds for 25% OA

For the small-leakiness facility, another OA fraction of 40% was explored at different ambient "southeast" wind speeds, as shown in Figure 3.11. The ventilation rates were selected to provide the satisfying and smallest possible positive pressures in the vestibule within the central

ventilation system SA flow rate range of 0.283 m^3/s to 0.472 m^3/s. The ambient pressure values were gauge values, and the pressure values in each zone was the positive pressure difference across the red-highlighted crack(s) in each zone. At wind speeds below 8.94 m/s, the ventilation rate was kept the same as that at 8.94 m/s, due to the fact that 0.283 m^3/s was the lower bound of the SA flow rate. Only at 11.18 m/s did the ventilation flow rate increase a little. What this meant was that the corresponding filtration power consumption at 11.18 m/s was just a little larger than that at and below 8.94 m/s.

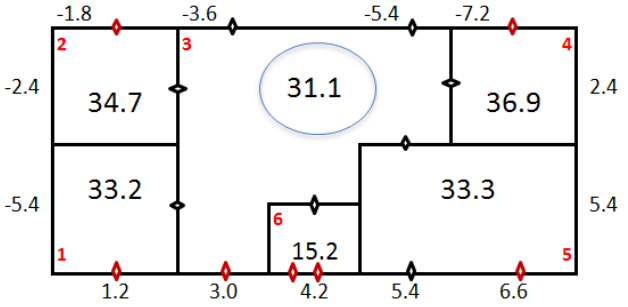

(a) Pressure distribution at 3.13 m/s

Zone	OA (m^3/s)	RA (m^3/s)	SA (m^3/s)
1	0.013	0.020	0.033
2	0.013	0.020	0.033
3	0.047	0.071	0.119
4	0.013	0.020	0.033
5	0.027	0.040	0.067
Sum	0.113	0.170	0.283

(b) OA, RA and SA flow rate

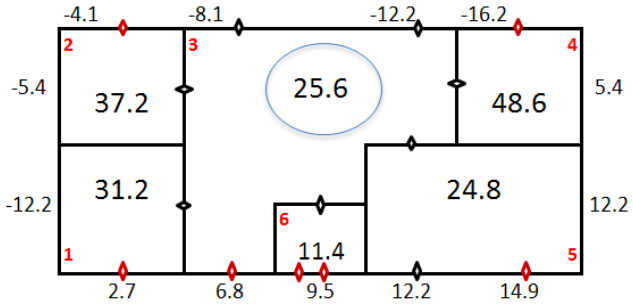

(c) Pressure distribution at 6.74 m/s

Zone	OA (m^3/s)	RA (m^3/s)	SA (m^3/s)
1	0.013	0.020	0.033
2	0.013	0.020	0.033
3	0.047	0.071	0.119
4	0.013	0.020	0.033
5	0.027	0.040	0.067
Sum	0.113	0.170	0.283

(d) OA, RA and SA flow rate

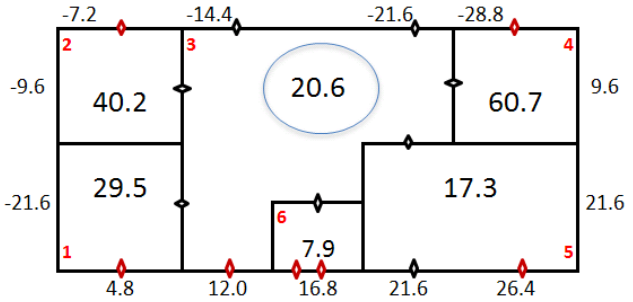

(e) Pressure distribution at 8.94 m/s

Zone	OA (m^3/s)	RA (m^3/s)	SA (m^3/s)
1	0.013	0.020	0.033
2	0.013	0.020	0.033
3	0.047	0.071	0.119
4	0.013	0.020	0.033
5	0.027	0.040	0.067
Sum	0.113	0.170	0.283

(f) OA, RA and SA flow rate

(Figure 3.11 (cont.))

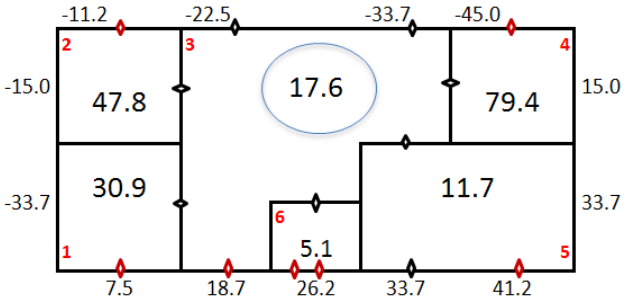

(g) Pressure distribution at 11.18 m/s

Zone	OA (m^3/s)	RA (m^3/s)	SA (m^3/s)
1	0.014	0.021	0.035
2	0.014	0.021	0.035
3	0.050	0.075	0.126
4	0.014	0.021	0.035
5	0.028	0.043	0.071
Sum	0.120	0.180	0.300

(h) OA, RA and SA flow rate

Figure 3.11 Pressure distribution and ventilation rates at various wind speeds (40% OA)

Similar to the previous case with a 25% OA fraction, the ventilation rates stayed the same for the cases where wind speeds were no larger than 8.94 m/s at the current OA fraction of 40%. Thus, the PF for all these cases were the same. At 11.18 m/s, the corresponding filtration power consumption was a little larger than that at 8.94 m/s, but the PF was very close to that at 8.94 m/s, as shown in Figure 3.12.

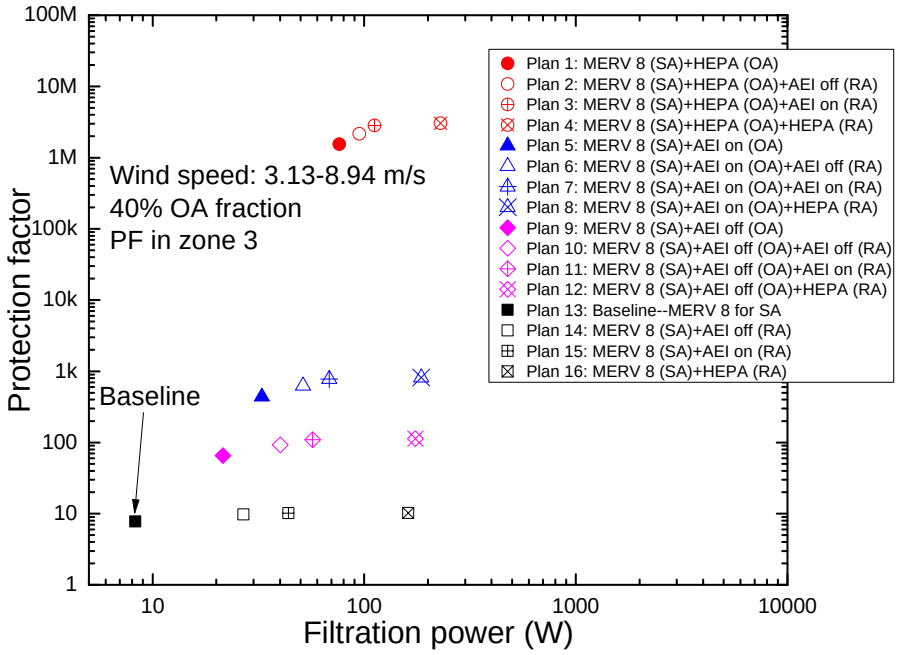

(a) Figure 3.12 (cont.)

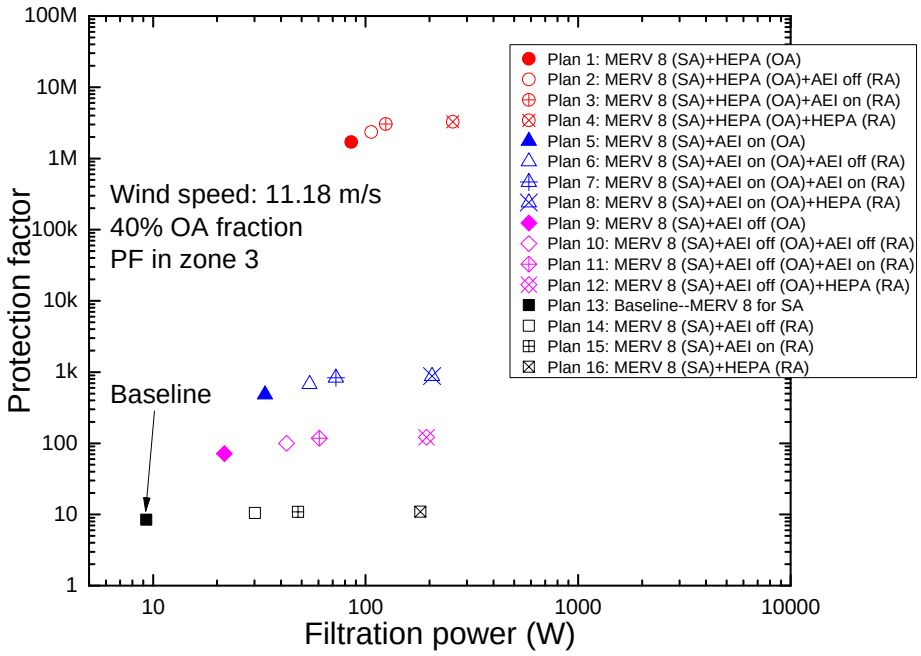

(b)

Figure 3.12 Protection factor *vs*. filtration power at different wind speeds for 40% OA

Comparing Figure 3.10 (a) to 3.12 (a), it was seen that the PF value at the 40% OA fraction was lower than at the 20% OA fraction. The two cases were at the same ventilation rate (0.283 m^3/s) and wind speed (3.13 m/s); therefore, the difference in the PF was solely caused by the difference in OA fraction. To be specific, as the OA fraction increased from 25% to 40% a larger proportion of the contaminated OA was introduced indoors but a relatively smaller proportion went through the RA filtration, leading to the reduction of the PF. What this suggests is that with other conditions kept the same, a higher OA fraction ratio will lower the PF, not to mention it would certainly lead to an increase of energy consumption due to necessary processing and conditioning of the OA.

In this section, a series of wind speeds and two OA fractions were covered in making "PF *vs*. filtration power" plots. The ranges of wind speeds and OA fractions are common condition ranges for any ventilation systems and any multizone buildings. Provided that sufficient positive pressure differences prevail, the four findings generally hold true for any multizone buidings: 1) ventilation flow rate have insignificant effect on the PF; 2) OA filter efficiency dominates the PF; 3) the effect of the RA filter on the PF is insignificant compared to that of the OA; and 4) a higher OA fraction lowers the PF with other conditions being the same.

3.7 Particle Distributions 2 and 3

The ambient particles in this section followed the last two log-normal distributions listed in Table 3.1, as shown in Figure 3.13. Simulated distributions in Figures 3.13 (b) and 3.13 (d) were obtained based on the original data in Figures 3.13 (a) and 3.13 (c).

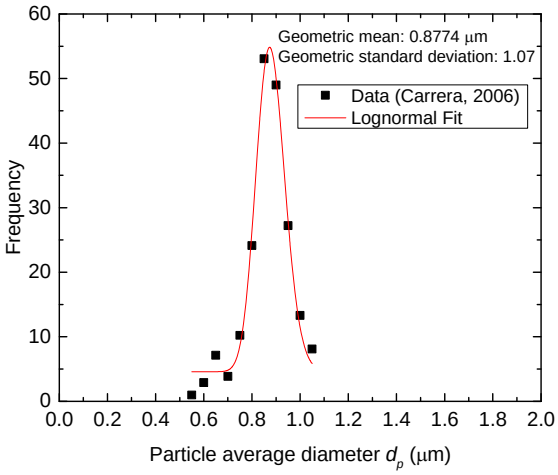

(a) Distribution 2, original data

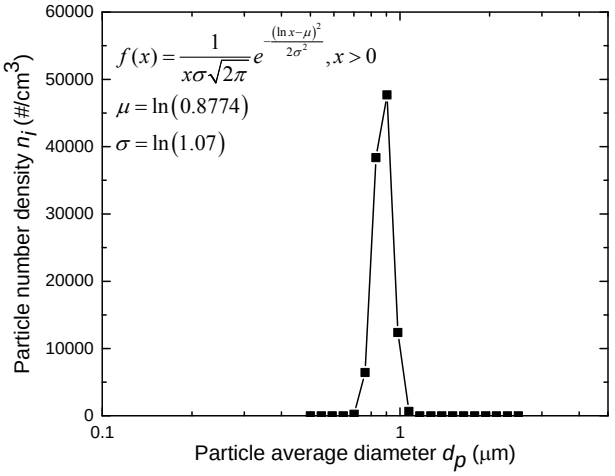

(b) Distribution 2, used in the simulation

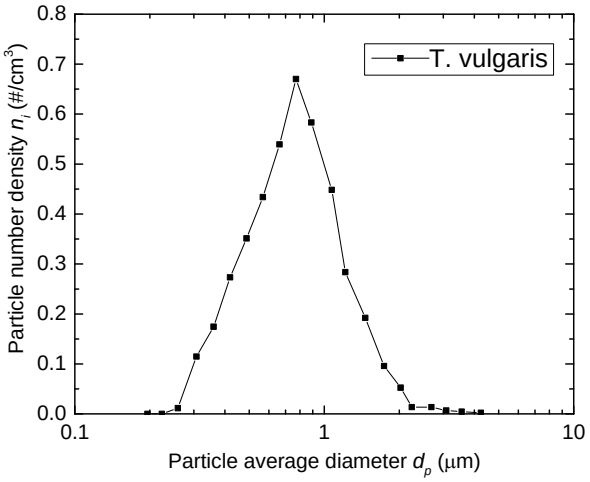

(c) Distribution 3, original data

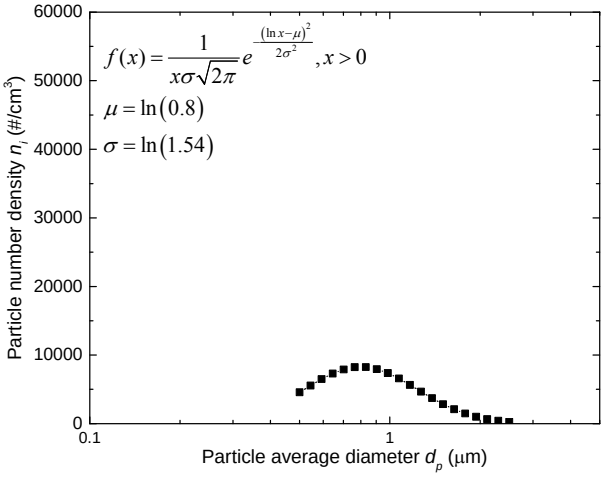

(d) Distribution 3, used in the simulation

Figure 3.13 The log-normal distributions 2 and 3 of particles in Table 3.1

In this section, the HEPA filter efficiency curve was updated, as shown in Figure 3.14. This update was inspired by a study (Kowalski *et al*., 1999) where the authors tested their filter efficiency model with 89 airborne pathogens and identified 27 of them as the most penetrating microorganisms among others in the same size ranges. They also obtained a transmittance value

(transmittance=1-filtration efficiency) of each of the 27 microorganisms, as shown in Figure 3.14. In order to make conservative predictions, the above finding was adopted in the present study to set the extreme situation for the HEPA filter. It was noteworthy that the HEPA filter efficiency was below its nominal value (99.97%) at 0.3 μm.

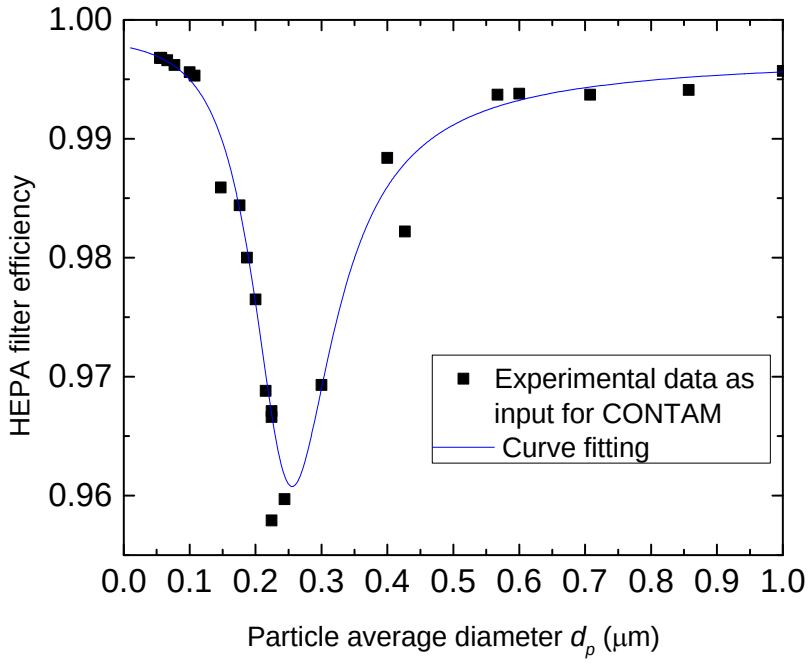

Figure 3.14 Updated HEPA filter efficiency for extreme situations (Kowalski *et al*., 1999)

A "*PF vs*. filtration power" plot was generated for each particle distribution in the zone 3, as shown in Figure 3.15. In the simulations, zone 1-3, 2-3, 4-3, 5-3 interior doors were fully open. There was only one central return in zone 3 for the CUBVS in the facility. The PF was based on spore count. The findings in Figure 3.15 were consistent with those in Figures 3.10 and 3.12. Furthermore, a "*PF vs*. filtration power" plot was generated for each distribution in the vestibule (zone 6), as shown in Figure 3.16. It was seen that protecting the indoor zones 1-5 with HEPA filters for the OA can enhance the protection of the vestibule, because the inter-zone flow from zone 3 to zone 6 can affect the cleaning of the vestibule. According to Figure 3.16, when there is no ambient hazard, the AEI device is not required to be turned on, and the corresponding PF is fine. When there is moderate to severe ambient hazard, turning the AEI on to filter the OA may be sufficient because the corresponding PF value is just slightly lower than that obtained by using the HEPA filter. When the ambient hazard is severe and lethal, it is necessary to switch to

the HEPA filter for the OA to increase in PF. What Figure 3.16 implies is that a control scheme is necessary for the DBVS in the vestibule such that some energy can be saved without compromising the PF of the facility when the ambient hazard is not severe.

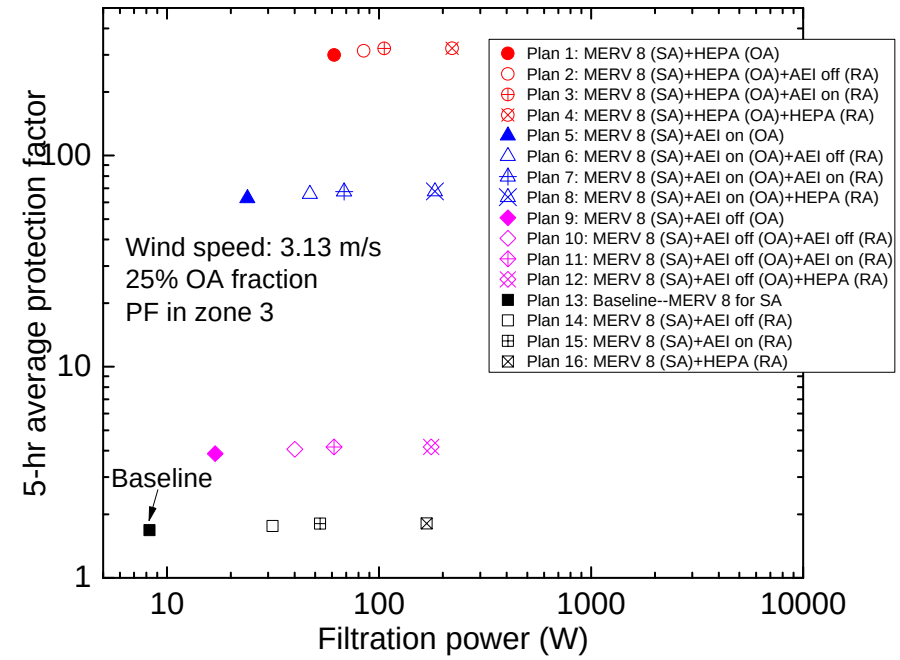

(a)

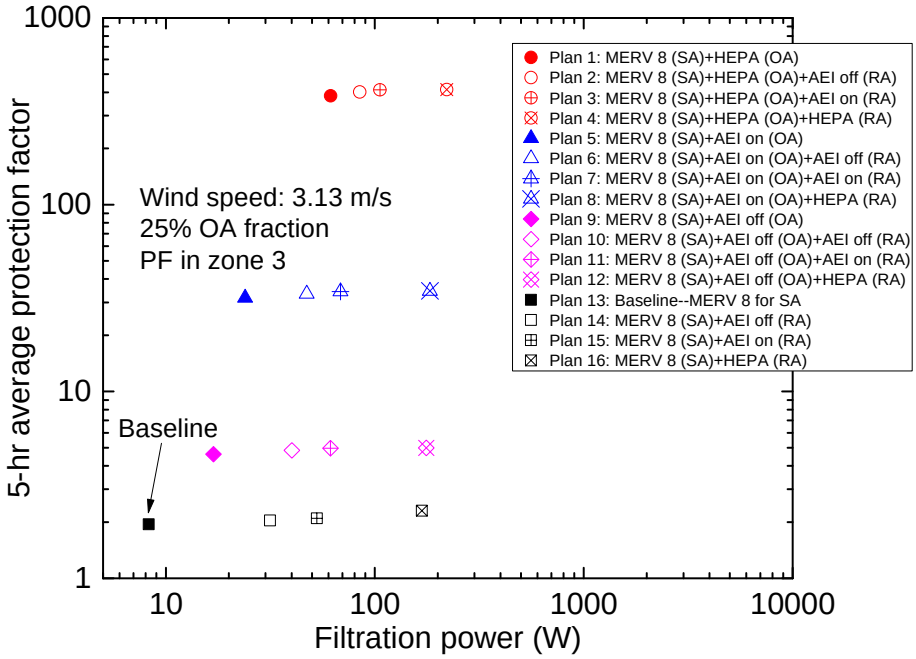

(b)

Figure 3.15 PF *vs*. filtration power in zone 3: a) distribution 2, b) distribution 3

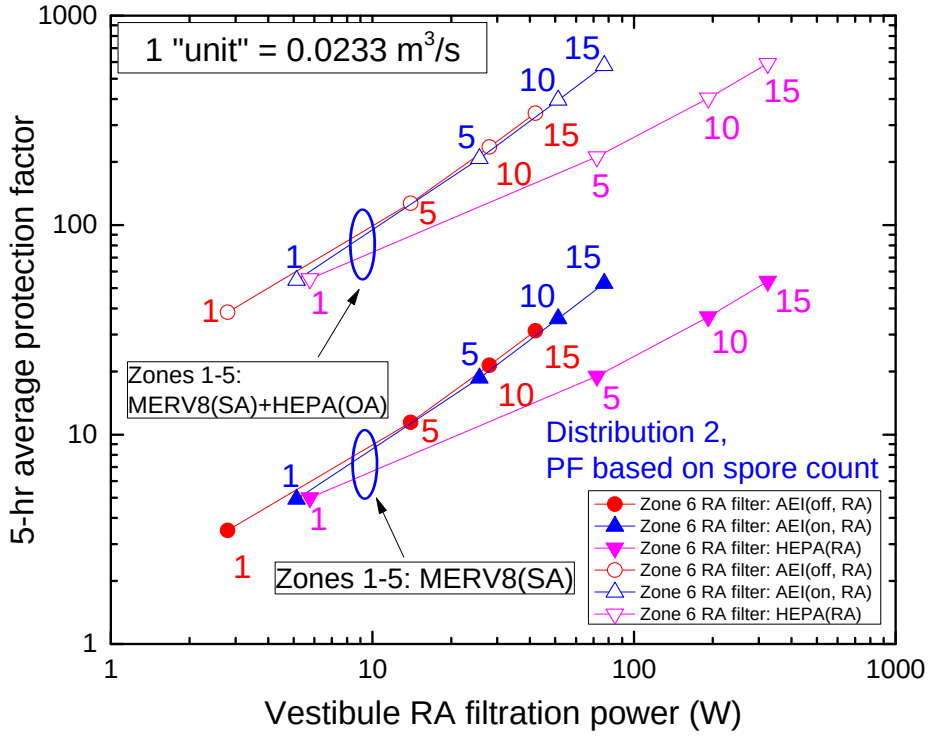

(a)

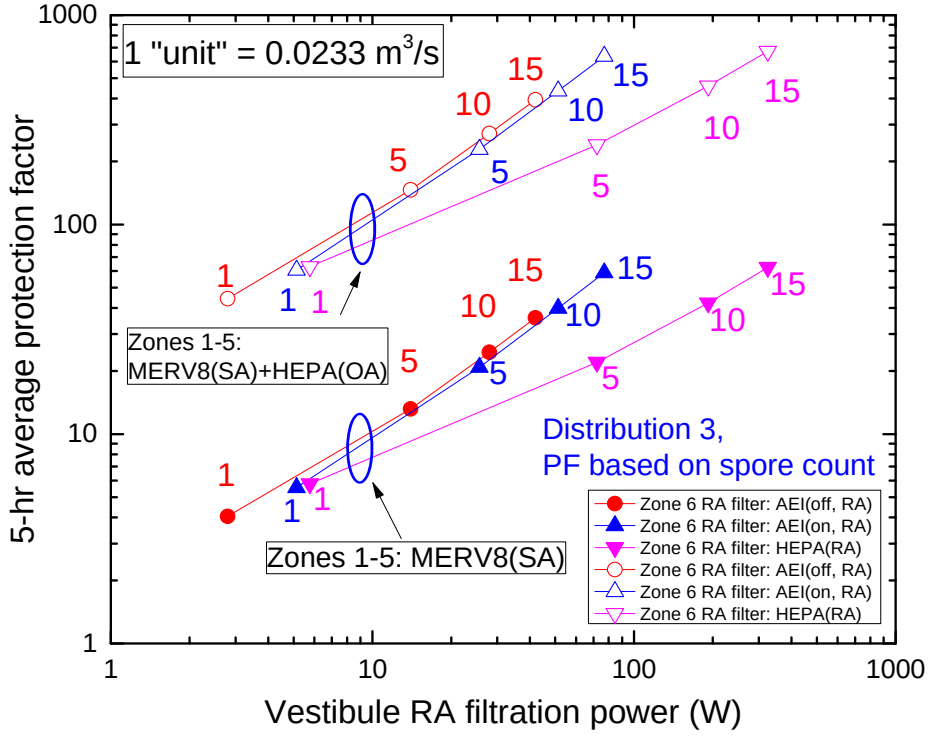

(b)

Figure 3.16 PF *vs.* filtration power in the vestibule: a) distribution 2, b) distribution 3

3.8 Summary

The performance of the AEI device/MERV filters/HEPA filters in terms of "Protection factor *vs*. Filtration power" was investigated using CONTAM for a representative facility. The framework outlined in this chapter contained four elements: 1) performance metric PF; 2) filtration power calculation; 3) any type of filter (as long as the filter efficiency curve is known); and 4) particle distribution.

Intuitive findings can be obtained following the framework. For instance, the simulation results indicated that 1) a higher OA fraction lowered the indoor PF with other conditions being the same; 2) the PF was mainly dependent on the OA filter efficiency, so utilizing a more efficient filter for the OA was preferred to achieve a higher PF value.

Some non-intuitive findings can also be obtained using the framework. For instance, it was found out that the effect of the RA filter on the indoor PF was much less than that of the OA in a CUBVS system. This finding could lead to significant savings in investment cost of the RA filter and/or operating cost associated with the flow resistance of the filter. In other words, the residents can choose not to have any RA filter in their CUBVSs or substitute the HEPA filter with a MERV 11 filter for filtering the RA to save some operating cost.

The framework can be used for system or component comparison. Following this framework in the present study, it was found out that the AEI device can be a good substitute for the HEPA filter in the DBVS for protecting the vestibule. In terms of indoor environment protection, the AEI device cannot compete with the HEPA filter in OA filtration.

As demonstrated, this framework is suitable and generalizable for other multizone IAQ evaluations using other ventilation/filtration systems, to identify the best filtration scheme for pressurization-protection of multizone buildings and/or protection of the vestibules.

CHAPTER 4 – MODELING OF A PROTECTED FACILITY

CONTAM has been demonstrated in Chapter 3 as a suitable tool for transient and steady-state simulation in complex multizone buildings, but the results are not in an analytical form. An analytical relationship between the PF, the ventilation flow rates, the filtration scheme and the room characteristics can be helpful because it facilitates understanding and implementation. This analytical relationship is typically not obtainable in complex buildings except in some special cases. However, for situations where only a big lobby and a vestibule are involved, deriving an analytical or approximated solution for contaminant concentration is feasible. As a subset of complex multizone buildings, a simplified "lobby+vestibule" facility still contains the main elements affecting indoor contaminant concentration. A modeling of the simplified facility can identify the contribution of each parameter, predict the PF and provide guidance for ventilation system operation (ventilation flow rate and filtration scheme). All of the findings can be transferable to understand the more complicated parameter interaction in complex multizone buildings.

In this chapter the following were provided: 1) An approximated solution of contaminant concentration was obtained for a multizone facility in a special case; 2) Extension of an existing model (Ginsberg and Bui, 2013) was made to predict the steady-state PF in the simplified "lobby+vestibule" facility; 3) For periodic contaminant source deposition scenarios in the vestibule, analytical solutions were obtained to identify the smallest period necessary to prevent the deposited contaminant from accumulating in the vestibule; and 4) Based on the PF contour plots, the effects of ventilation flow rates in the room and the vestibule were identified to guide ventilation flow rate determination.

4.1 Approximated Contaminant Concentration

For demonstration purposes, the facility was protected by the DUBVSs for zones 1-5, each equipped with a MERV 8 filter for the SA, a HEPA filter for the OA and/or a filter for the RA, as shown in Figure 4.1. A DBVS was installed in the vestibule (zone 6) but it was not turned on. Four interior doors (zone 3-1, zone 3-2, zone 3-4, zone 3-5 doors) were kept fully open. In this section, it was of interest to analytically predict the contaminant concentration in zone 3. The contaminant particles followed Distribution 3 in Table 3.1.

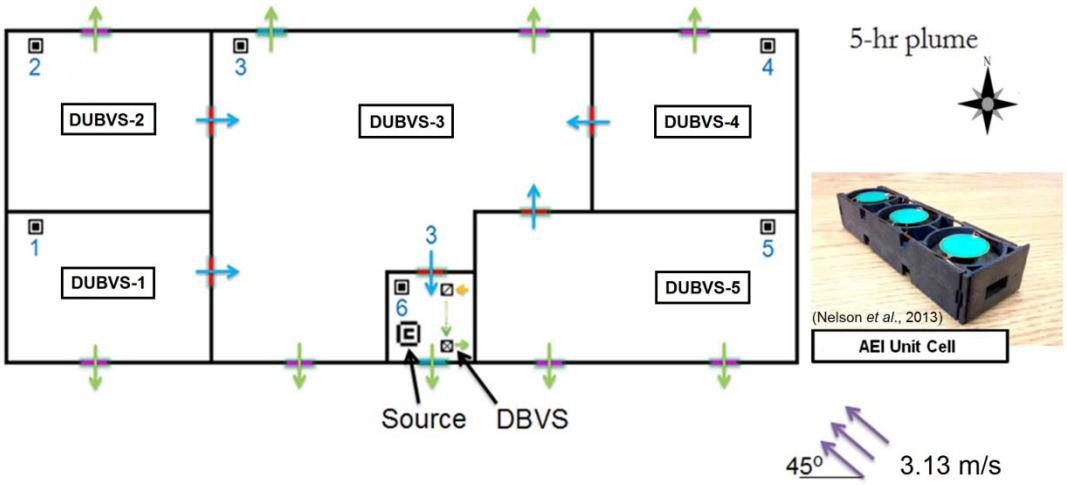

Figure 4.1 Sketch of the facility with DUBVSs and a DBVS

4.1.1 A State Space Equation

Based on contaminant conservation, the contaminant concentrations in zones 1, 2, 4, 5 and zone 3 are shown in Equations 4.1 and 4.2 for Bin *i* of particle distribution in zone *n*.

$$\frac{dc_{i,n}}{dt} = \underbrace{\left(-\frac{Q_{RA,n}}{V_n} + \frac{Q_{RA,n}}{V_n}(1-\eta_{i,RA})(1-\eta_{i,SA}) - \frac{Q_{OA,n}}{V_n} \right)}_{\lambda_n} c_{i,n} + \underbrace{\frac{Q_{OA,n}}{V_n}(1-\eta_{i,OA})(1-\eta_{i,SA})}_{\gamma_n} c_{i,out} \qquad (n = 1,2,4,5) \tag{4.1}$$

where the c means concentration, Q means air flow rate, V is zone volume and η is the filter efficiency.

$$\frac{dc_{i,3}}{dt}=\left(\underbrace{-\frac{Q_{RA,3}}{V_3}+\frac{Q_{RA,3}}{V_3}(1-\eta_{i,RA})(1-\eta_{i,SA})-\frac{Q_{OA,3}}{V_3}}_{\lambda_3}-\underbrace{\left[\frac{Q_{13}}{V_3}+\frac{Q_{23}}{V_3}+\frac{Q_{43}}{V_3}+\frac{Q_{53}}{V_3}\right]}_{\lambda_3^*}\right)c_{i,3}$$
$$+\underbrace{\frac{Q_{OA,3}}{V_3}(1-\eta_{i,OA})(1-\eta_{i,SA})}_{\gamma_3}c_{i,out}+\underbrace{\frac{Q_{13}}{V_3}}_{\beta_1}c_{i,1}+\underbrace{\frac{Q_{23}}{V_3}}_{\beta_2}c_{i,2}+\underbrace{\frac{Q_{43}}{V_3}}_{\beta_4}c_{i,4}+\underbrace{\frac{Q_{53}}{V_3}}_{\beta_5}c_{i,5} \tag{4.2}$$

With a general form of the state space equation (Equation 4.3) and Equations (4.1)-(4.2), the system matrix *A* and input matrix *B* are shown in Equation 4.4.

$$\frac{d\vec{c}}{dt}=A\vec{c}+B\vec{u} \tag{4.3}$$

$$\frac{d\vec{c}}{dt}=\underbrace{\begin{bmatrix}\lambda_1 & 0 & 0 & 0 & 0\\ 0 & \lambda_2 & 0 & 0 & 0\\ \beta_1 & \beta_2 & \lambda_3-\lambda_3^* & \beta_4 & \beta_5\\ 0 & 0 & 0 & \lambda_4 & 0\\ 0 & 0 & 0 & 0 & \lambda_5\end{bmatrix}}_{A}\begin{bmatrix}c_{i,1}\\ c_{i,2}\\ c_{i,3}\\ c_{i,4}\\ c_{i,5}\end{bmatrix}+\underbrace{\begin{bmatrix}\gamma_1 & 0 & 0 & 0 & 0\\ 0 & \gamma_2 & 0 & 0 & 0\\ 0 & 0 & \gamma_3 & 0 & 0\\ 0 & 0 & 0 & \gamma_4 & 0\\ 0 & 0 & 0 & 0 & \gamma_5\end{bmatrix}}_{B}\begin{bmatrix}c_{i,out}\\ c_{i,out}\\ c_{i,out}\\ c_{i,out}\\ c_{i,out}\end{bmatrix} \tag{4.4}$$

The parameters that influenced indoor contaminant concentration were connected in the state space equation: ventilation flow rate, inter-zone crack flow rate, zone volume and filter efficiency. With the above state space equation established, it was then possible to derive an analytical solution of concentration for a specific zone in the facility using some simplification.

4.1.2 Approximated Solution of Contaminant Concentration

For simplification, DUBVSs in zones 1-5 were considered with only the OA in zones 1, 2, 4 and 5 and with only one central return in zone 3. From the simulation results in Figure 4.2, it was seen that the magnitude of each exfiltration flow rate (green bar) was very small in zones 1, 2, 4 and 5 compared to the OA flow rate in each of the four zones. Thus, it was approximated that all of the OA in zones 1, 2, 4 and 5 flew into zone 3 and exfiltrated zone-3 exterior openings.

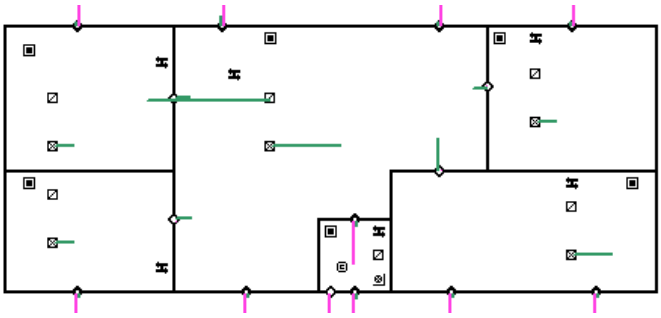

Figure 4.2 Air flow rate magnitude (green bar) in the facility

In this scenario, the governing equation for contaminant concentration in zones 1, 2, 4, 5 and zone 3 was reduced to Equations 4.5 and 4.7, respectively. In result, solutions for concentration are shown in Equations 4.6 and 4.8.

$$\frac{dc_{i,n}}{dt} = \underbrace{\left(-\frac{Q_{OA,n}}{V_n}\right)}_{\lambda_n} c_{i,n} + \underbrace{\frac{Q_{OA,n}}{V_n}(1-\eta_{i,OA})(1-\eta_{i,SA})}_{\gamma_{i,n}} c_{i,out} \quad (n=1,2,4,5) \tag{4.5}$$

$$c_{i,n} = \frac{\gamma_{i,n}}{\lambda_n} c_{i,out}\left(e^{\lambda_n t}-1\right) = (1-\eta_{i,OA})(1-\eta_{i,SA}) c_{i,out}\left(1-e^{-\frac{Q_{OA,n}}{V_n}t}\right) \quad (n=1,2,4,5) \tag{4.6}$$

$$\frac{dc_{i,3}}{dt} = \left(\underbrace{-\frac{Q_{RA,3}}{V_3} + \frac{Q_{RA,3}}{V_3}(1-\eta_{i,RA})(1-\eta_{i,SA}) - \frac{Q_{OA,3}}{V_3}}_{\lambda_3} \underbrace{- \left[\frac{Q_{OA,1}+Q_{OA,2}+Q_{OA,4}+Q_{OA,5}}{V_3}\right]}_{\lambda_3^*} \right) c_{i,3} \tag{4.7}$$

$$+ \underbrace{\frac{Q_{OA,3}}{V_3}(1-\eta_{i,OA})(1-\eta_{i,SA})}_{\gamma_{i,3}} c_{i,out} + \underbrace{\frac{Q_{OA,1}}{V_3}}_{\beta_1} c_{i,1} + \underbrace{\frac{Q_{OA,2}}{V_3}}_{\beta_2} c_{i,2} + \underbrace{\frac{Q_{OA,4}}{V_3}}_{\beta_4} c_{i,4} + \underbrace{\frac{Q_{OA,5}}{V_3}}_{\beta_5} c_{i,5}$$

$$c_{i,3} = \left[\frac{-D}{\lambda_1 - \left(\lambda_3 - \lambda_3^*\right)} \exp\left(\lambda_1 t\right) + E \exp\left[\left(\lambda_3 - \lambda_3^*\right)t\right]\right] - \frac{\gamma_{i,3} c_{i,out} + D}{\lambda_3 - \lambda_3^*} \tag{4.8}$$

where

$$D = \left(\beta_1 + \beta_2 + \beta_4 + \beta_5\right)(1-\eta_{i,OA})(1-\eta_{i,SA}) c_{i,out} \tag{4.9}$$

$$E = \frac{D}{\lambda_1 - \left(\lambda_3 - \lambda_3^*\right)} + \frac{\gamma_{i,3} c_{i,out} + D}{\lambda_3 - \lambda_3^*} \tag{4.10}$$

In order to get a clearer understanding of the physical meaning of the above solution for contaminant concentration in zone 3, Equation 4.8 was rearranged:

$$c_{i,3} = E\exp\left[\left(\lambda_3 - \lambda_3^*\right)t\right] - F\exp(\lambda_1 t) + G \tag{4.11}$$

where

$$\lambda_1 = -\frac{Q_{OA,1}}{V_1} = -\frac{Q_{OA,n}}{V_n} \qquad (n = 1,2,3,4,5) \tag{4.12}$$

$$\lambda_3 - \lambda_3^* = -\frac{Q_{SA,tot}}{V_3} + \frac{Q_{RA,tot}}{V_3}(1-\eta_{i,RA})(1-\eta_{i,SA}) \tag{4.13}$$

$$E = F - G \tag{4.14}$$

$$F = \frac{\left(Q_{OA,tot} - Q_{OA,3}\right)(1-\eta_{i,OA})(1-\eta_{i,SA})c_{i,out}}{Q_{SA,tot} - Q_{OA,1}V_3/V_1 - Q_{RA,tot}(1-\eta_{i,RA})(1-\eta_{i,SA})} \tag{4.15}$$

$$G = \frac{Q_{OA,tot}(1-\eta_{i,OA})(1-\eta_{i,SA})c_{i,out}}{Q_{SA,tot} - Q_{RA,tot}(1-\eta_{i,RA})(1-\eta_{i,SA})} \tag{4.16}$$

The transient concentration in zone 3 showed that its characteristics were determined by two time constants, one representing the contaminant intake rate (Equation 4.12) and the other representing the diluting and filtration rate (Equation 4.13). It was seen in Figure 4.3 that the approximated solutions of contaminant concentration in zones 1 and 3 agreed reasonably well with the CONTAM simulation results at steady state. This meant that it was feasible to utilize the approximated solution to predict the transient concentration in the facility protected by the DUBVSs. If another CUBVS was used instead of the DUBVSs, the contaminant concentration in each zone would be coupled due to the central return. Thus, it was very difficult to find an analytical solution for that case.

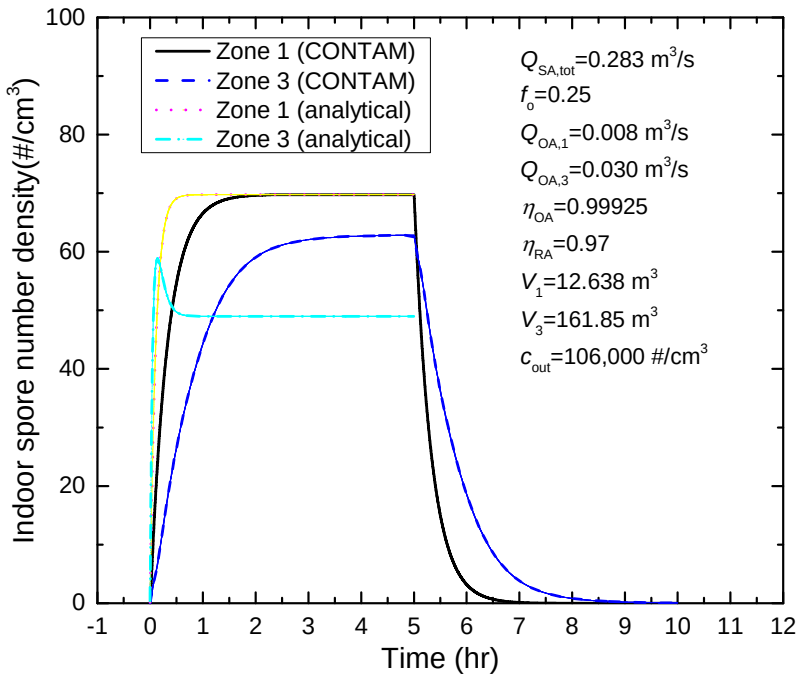

Figure 4.3 Comparison of contaminant concentrations in zones 1 and 3

An example demonstration of utilizing the state space equation to obtain the analytical solution of contaminant concentration is provided in this section. Modeling of a simplified "lobby+vestibule" facility is presented in Section 4.2, where the PFs are linked to the characteristics of ventilated rooms and vestibules.

4.2 Characteristics of Ventilated Rooms

Aiming at building protection, a model developed by Ginsberg and Bui (2013) was extended to explore common building-pressurization scenarios. Three pressurization-protection scenarios were investigated in the present study as comparisons to the three non-pressurized scenarios explored by Ginsberg and Bui (2013). The schematics of the facility in Sections 4.2-4.3 were based on Gingsberg and Bui's work, with adjustments permitted by the authors.

4.2.1 A Pressurized Room with Leakage and a Vestibule

As shown in Figure 4.4, there is a room (marked as "indoors") connected to a vestibule. There is some leakage area in this room and it is equipped with an unbalanced ventilation system. The supply flow rate is R; return flow rate is $f_{RA}R$ (f_{RA} means the RA fraction); exhaust flow rate is 0; outdoor air (or make-up air) is $(1\text{-}f_{RA})R$ in the unbalanced ventilation system for the room;

and the exfiltration flow rate through the room is $(1\text{-}f_{RA})R$. The RA flow rate in the balanced ventilation system for the vestibule is R_V. The opening of the exterior and interior door of the vestibule incurs an air exchange volume of α and β, respectively. The filter transmittance (or "1-filter efficiency") of the OA filter and the RA filter in the unbalanced ventilation system is T_{OA} and T_{IA}, respectively. The filter transmittance of the RA filter in the balanced ventilation system is T_V.

It is assumed in the modeling that a person tries to go through a vestibule quickly such that there is negligible time lag in his opening both the exterior and the interior doors of the vestibule. Once this person steps in the vestibule but before he pushes open the interior door of the vestibule, the contaminant introduced in the vestibule in the α air exchange volume gets well mixed instantaneously in the vestibule. When the person pushes open the interior door of the vestibule, another air exchange volume β is incurred. The air exchanges are modeled as Dirac delta functions, and assumed to have no effect on all other existing flows such as inter-zone leakage flow, exfiltration flow in the room, OA and RA flows, *etc*.

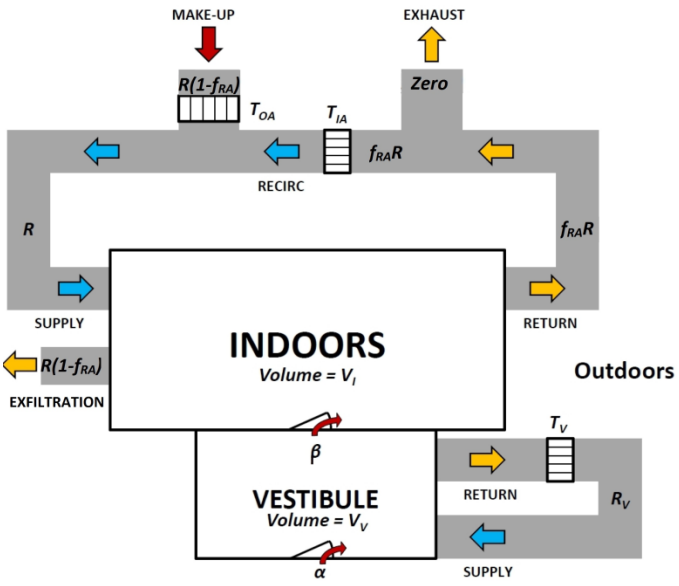

Figure 4.4 A pressurized room with leakage and a vestibule

A state space equation for such a pressurized room with leakage and a vestibule is as follows,

$$\begin{pmatrix} \dot{c}_i \\ \dot{L}_i \\ \dot{c}_V \end{pmatrix} = \begin{pmatrix} a - g\delta(t-t_0) & 0 & g\delta(t-t_0) \\ \theta & 0 & 0 \\ f\delta(t-t_0)+j & 0 & c - f\delta(t-t_0) - h\delta(t-t_0) - j \end{pmatrix} \begin{pmatrix} c_i \\ L_i \\ c_V \end{pmatrix} + \begin{pmatrix} \gamma H(t) \\ 0 \\ hH(t)\delta(t-t_0) \end{pmatrix} \tag{4.17a}$$

$$a = -R\left(1 - f_{RA}T_{IA}\right)/V_I \tag{4.17b}$$

$$b = \theta / V_I \tag{4.17c}$$

$$c = -R_V\left(1 - T_V\right)/V_V \tag{4.17d}$$

$$f = \beta / V_V \tag{4.17e}$$

$$g = \beta / V_I \tag{4.17f}$$

$$h = \alpha / V_V \tag{4.17g}$$

$$j = R_{IV} / V_V \tag{4.17h}$$

$$\gamma = R\left(1 - f_{RA}\right)T_{OA} / V_I \tag{4.17i}$$

where c_i and c_V are contaminant concentration indoors and in the vestibule; L_i is the contaminant intake into a person's lung; c_{out} is ambient contaminant concentration; $H(t)$ and $\delta(t-t_0)$ are Heaviside and Dirac delta function, respectively; t_0 is the instant both the vestibule exterior and interior doors are opened; R_{IV} is inter-zone leakage rate from the room to the vestibule; V_I and V_V are room volume and the vestibule volume, respectively; Θ is the respiratory rate of an adult.

Take a Laplace transform of the c_i equation in Equation 4.17a, and assume the source deposition (opening of both vestibule doors) is periodic:

$$c_i(s) = \frac{1}{s-a}\frac{ge^{-t_0 s}}{1-e^{-T_0 s}}\left[c_V(t_0) - c_i(t_0)\right] + \frac{\gamma c_{out}}{s(s-a)} + \frac{c_i(0)}{(s-a)} \tag{4.18}$$

where $c_i(t_0)$ and $c_V(t_0)$ are assumed to be the steady-state indoor and vestibule contaminant concentration; T_0 is the door opening period.

$$c_i(t_0) = \frac{T_{OA}}{1 + \left(1/\left(1 - f_{RA}\right) - 1\right)\left(1 - T_{IA}\right)} c_{out} = -\frac{\gamma}{a} c_{out} \tag{4.19a}$$

$$c_V(t_0) = \frac{R_{IV}}{R_{IV} + R_V\left(1 - T_V\right)} c_i(t_0) = -\frac{\gamma}{a}\frac{R_{IV}}{R_{IV} + R_V\left(1 - T_V\right)} c_{out} = m c_{out} \tag{4.19b}$$

Apply the Final Value Theorem to Equation 4.18 and get

$$\frac{1}{PF_i} = \lim_{t\to\infty}\frac{c_i(t)}{c_{out}} = \lim_{s\to 0}\frac{sc_i(s)}{c_{out}} = -\frac{g\left(m+\gamma/a\right)}{aT_0} - \frac{\gamma}{a} \tag{4.20}$$

Similarly, the following can be obtained based on the c_V equation in Equation 4.17a:

$$\frac{1}{PF_V} = \frac{\left[h\left(1-m\right)-f\left(\gamma/a+m\right)\right]}{\left(j-c\right)T_0} + \frac{j}{j-c}\left[-\frac{g\left(m+\gamma/a\right)}{aT_0} - \frac{\gamma}{a}\right] \tag{4.21}$$

It is shown from Equations 4.20 and 4.21 that the PF is connected to the ventilation flow rate, inter-zone leakage flow rate, exchange flow volume due to the door opening, filter transmittance, door opening period and room volume.

4.2.2 A Pressurized Room with Leakage and a Door

The only difference between this scenario and the previous one is that there is no vestibule to protect the room.

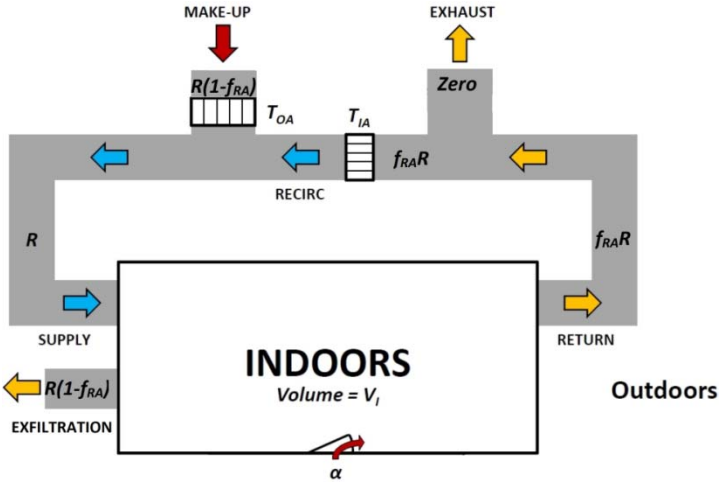

Figure 4.5 A pressurized room with leakage and a door

A state space equation for such a pressurized room with leakage and a door is as follows,

$$\begin{pmatrix}\dot{c}_i\\ \dot{L}_i\end{pmatrix} = \begin{pmatrix}a-d\delta\left(t-t_0\right) & 0\\ \theta & 0\end{pmatrix}\begin{pmatrix}c_i\\ L_i\end{pmatrix} + \begin{pmatrix}\gamma H\left(t\right)+dH\left(t\right)\delta\left(t-t_0\right)\\ 0\end{pmatrix}c_{out} \tag{4.22a}$$

$$d = \alpha / V_I \tag{4.22b}$$

Follow a similar approach as the above to get

$$\frac{1}{PF_i} = \lim_{t\to\infty}\frac{c_i(t)}{c_{out}} = \lim_{s\to 0}\frac{sc_i(s)}{c_{out}} = -\frac{d\left(1+\gamma/a\right)}{aT_0} - \frac{\gamma}{a} \tag{4.23}$$

4.2.3 A Pressurized Room with Leakage but No Door

The difference between this scenario and the one in Section 4.2.2 is that there is no door.

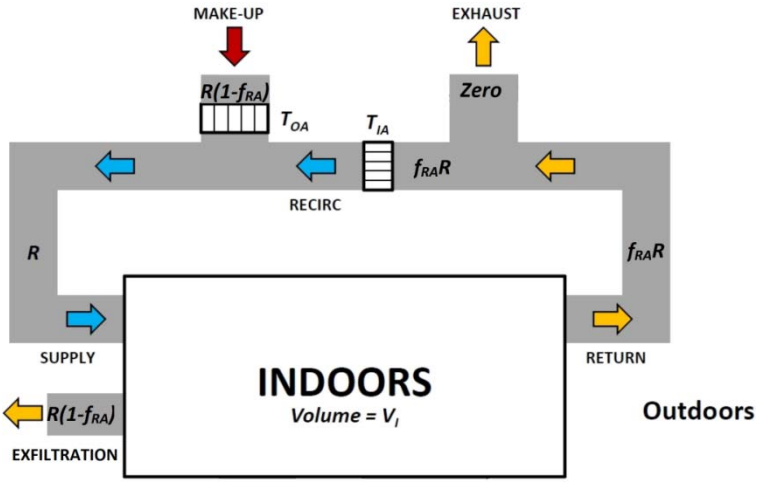

Figure 4.6 A pressurized room with leakage but no door

A state space equation for such a pressurized room with leakage but no door is as follows,

$$\begin{pmatrix}\dot{c}_i\\ \dot{L}_i\end{pmatrix} = \begin{pmatrix}a & 0\\ \theta & 0\end{pmatrix}\begin{pmatrix}c_i\\ L_i\end{pmatrix} + \begin{pmatrix}\gamma H(t)\\ 0\end{pmatrix} c_{out} \tag{4.24}$$

Follow a similar approach to get

$$\frac{1}{PF_i} = \lim_{t\to\infty}\frac{c_i(t)}{c_{out}} = \lim_{s\to 0}\frac{sc_i(s)}{c_{out}} = -\frac{\gamma}{a} \tag{4.25}$$

4.2.4 An Idealized Non-pressurized Room with No Leakage

As a comparison, the scenarios explored by Ginsberg and Bui (2013) are presented in Sections 4.2.4-4.2.6. In these three sections, α and β are the air exchange flow rates because the air and contaminant exchange are assumed to occur constantly.

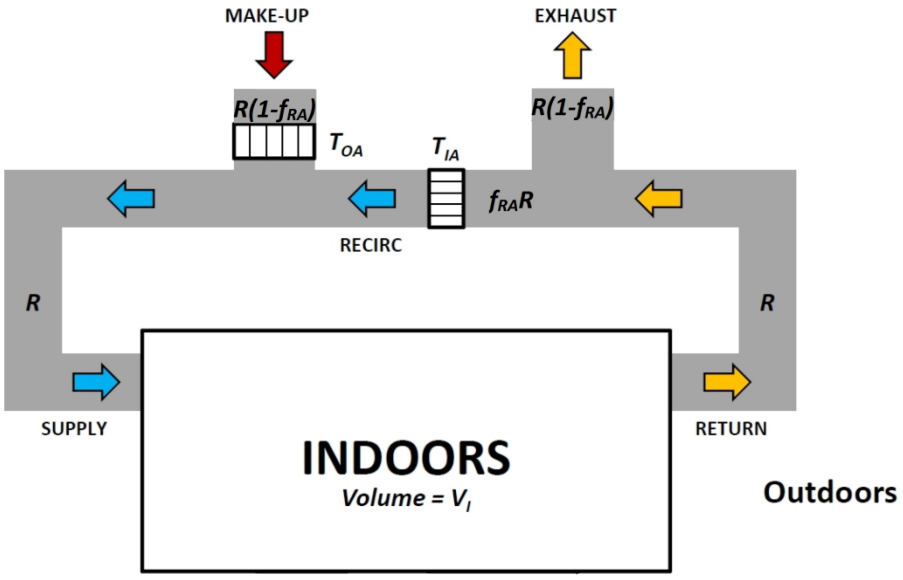

Figure 4.7 A non-pressurized room with no leakage

A state space equation for such a non-pressurized room with no leakage is as follows,

$$\begin{pmatrix} \dot{c}_i \\ \dot{L}_i \end{pmatrix} = \begin{pmatrix} a & 0 \\ \theta & 0 \end{pmatrix} \begin{pmatrix} c_i \\ L_i \end{pmatrix} + \begin{pmatrix} \gamma H(t) \\ 0 \end{pmatrix} c_{out} \tag{4.26}$$

Follow a similar approach to get

$$\frac{1}{PF_i} = \lim_{t\to\infty} \frac{c_i(t)}{c_{out}} = \lim_{s\to 0} \frac{sc_i(s)}{c_{out}} = -\frac{\gamma}{a} \tag{4.27}$$

This result is exactly the same as that in Section 4.2.3. What this means is that as long as the exhaust air flow rate for the idealized non-pressurized room is equal to the exfiltration flow rate of the pressurized room with no door and the two ventilation schemes are the same, the protection factor will remain the same for the two cases.

4.2.5 A Non-pressurized Room with Leakage due to a Door

The differences between this section and Section 4.2.2 are: 1) the walls are well sealed and the only leakage of the room is due to the door; 2) the room is at neutral pressure because the exhaust air flow rate is equal to the outdoor air (or make-up air) flow rate.

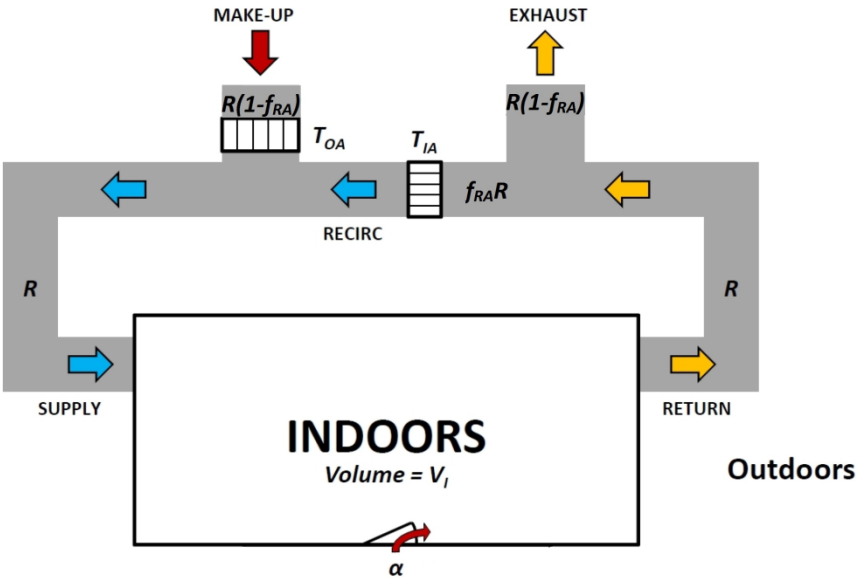

Figure 4.8 A non-pressurized room with leakage due to a door

A state space equation for such a non-pressurized room with leakage due to a door is,

$$\begin{pmatrix} \dot{c}_i \\ \dot{L}_i \end{pmatrix} = \begin{pmatrix} a-d & 0 \\ \theta & 0 \end{pmatrix} \begin{pmatrix} c_i \\ L_i \end{pmatrix} + \begin{pmatrix} \gamma H(t) + dH(t) \\ 0 \end{pmatrix} c_{out} \tag{4.28a}$$

$$d = \alpha / V_I \tag{4.28b}$$

Follow a similar approach to get

$$\frac{1}{PF_i} = \frac{\gamma + \alpha}{-a + d} = \frac{T_{OA}(1 - f_{RA}) + \alpha / R}{1 - f_{RA} T_{IA} + \alpha / R} \tag{4.29}$$

4.2.6 A Non-pressurized Room with Leakage due to a Vestibule

The differences between this scenario and that in Section 4.2.1 are: 1) the walls are well sealed and the only leakage of the room is due to the vestibule door; 2) the room is at neutral pressure because the exhaust air flow rate is equal to the outdoor air (or make-up air) flow rate; and 3) the contaminant and air exchange between the room and the vestibule is assumed at a constant rate, whereas in Section 4.2.1 the exchange only occurs when a vestibule door is opened.

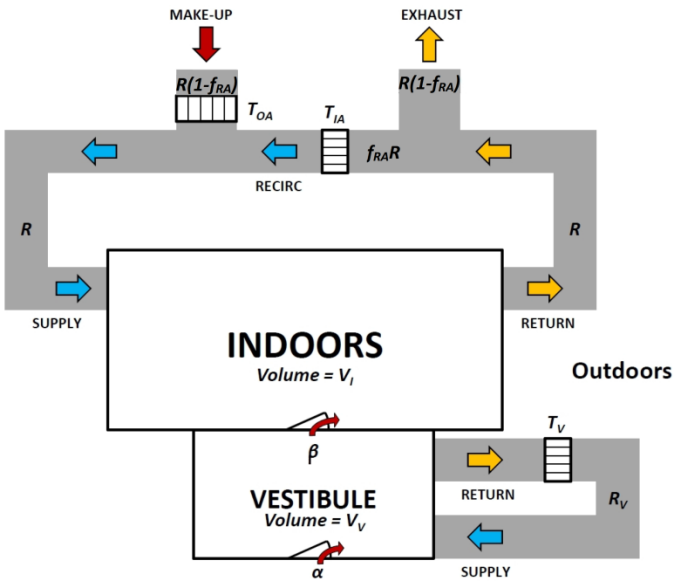

Figure 4.9 A non-pressurized room with leakage due to a vestibule

A state space equation for such a non-pressurized room with leakage due to a vestibule is,

$$\begin{pmatrix} \dot{c}_i \\ \dot{L}_i \\ \dot{c}_V \end{pmatrix} = \begin{pmatrix} a-g & 0 & g \\ \theta & 0 & 0 \\ f & 0 & c-f-h \end{pmatrix} \begin{pmatrix} c_i \\ L_i \\ c_V \end{pmatrix} + \begin{pmatrix} \gamma H(t) \\ 0 \\ hH(t) \end{pmatrix} c_{out} \tag{4.30}$$

Use the Final Value Theorem to get

$$\frac{1}{PF_i} = \lim_{t\to\infty} \frac{c_i(t)}{c_{out}} = \lim_{s\to 0} \frac{sc_i(s)}{c_{out}} = \frac{\gamma - \dfrac{gh + f\gamma + h\gamma}{c}}{\left(-a + g + \dfrac{-gh + af + ah}{c}\right)} \tag{4.31}$$

Similarly,

$$\frac{1}{PF_V} = -\frac{\gamma}{g} + \frac{g-a}{g}\frac{1}{PF_i} \tag{4.32}$$

4.2.7 Comparison of Scenarios

Some simulations were performed to compare the PFs in the above six scenarios, but two of them were exactly the same, so only five scenarios were shown in Figures 4.10-4.12. In these three figures, the simulation results for the three non-pressurization scenarios in Sections 4.2.4-4.2.6 are from Ginsberg and Bui's work (2013). Simulation input parameters are summarized in Table 4.1.

Table 4.1 Parameters for model simulation

T_{OA}	0.0038 (for HEPA) or 0.38 (for MERV 8)	OA filter transmittance for the room
T_{IA}	$= T_{OA}$	RA filter transmittance for the room
T_V	$= T_{OA}$	RA filter transmittance for the vestibule
f_{RA}	0.8	in the indoor ventilation system
α	1/30 m^3 or (1/30 m^3/s)	For Sections 4.2.1-4.2.3: air exchange volume when vestibule exterior door is opened; for Sections 4.2.4-4.2.6: constant air exchange rate
β	$= \alpha$	For Sections 4.2.1-4.2.3: air exchange volume when vestibule interior door is opened; for Sections 4.2.4-4.2.6: constant air exchange rate
R	0.472 m^3/s	Indoor ventilation rate
R_V	0.094 m^3/s	Ventilation rate in the vestibule
R_{IV}	0.009 m^3/s	Inter-zone leakage rate
T_0	30 min	Door-opening period
V_I	226.535 m^3	Volume of the room
V_V	8.155 m^3	Volume of the vestibule
Θ	0.242 L/s	Respiratory rate of an adult

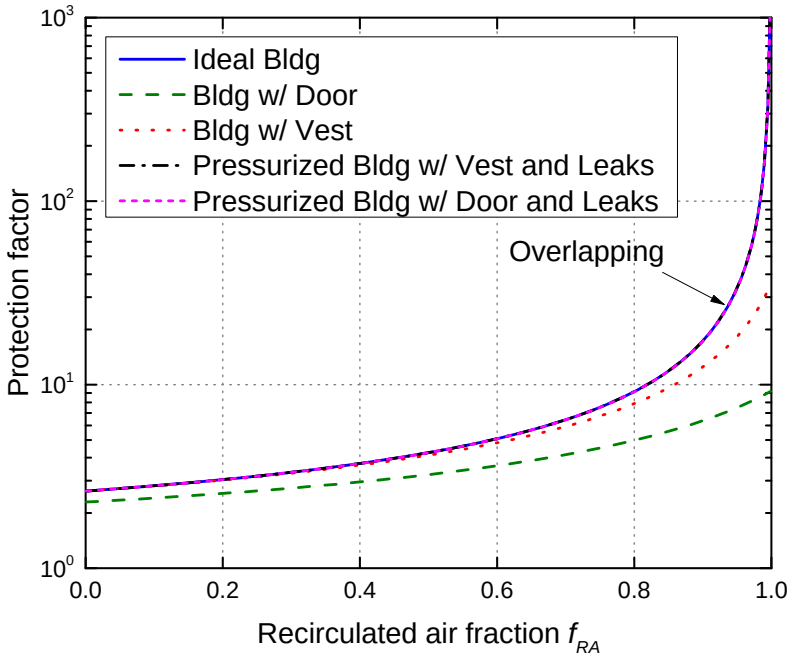

(a) MERV 8, α, α=β (Figure 4.10 (cont.))

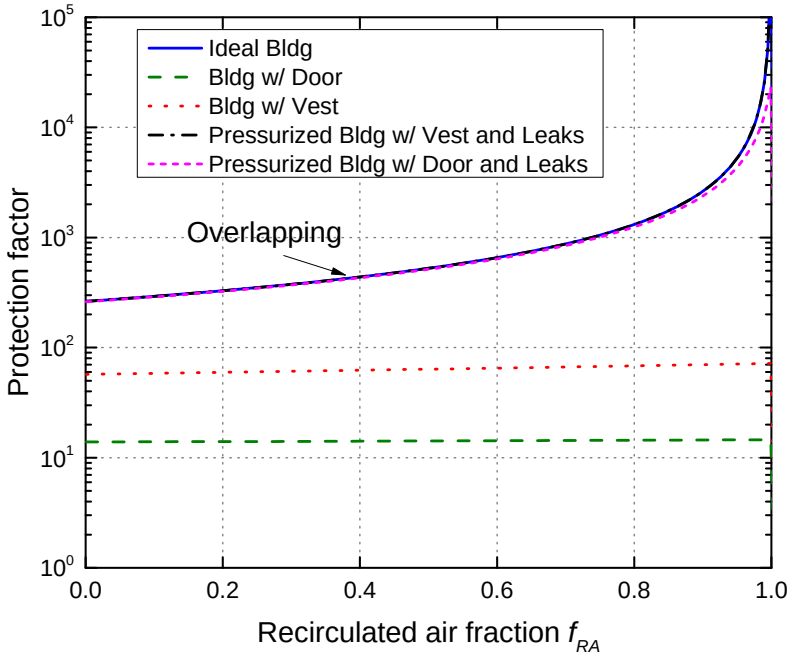

(b) HEPA, α, α=β

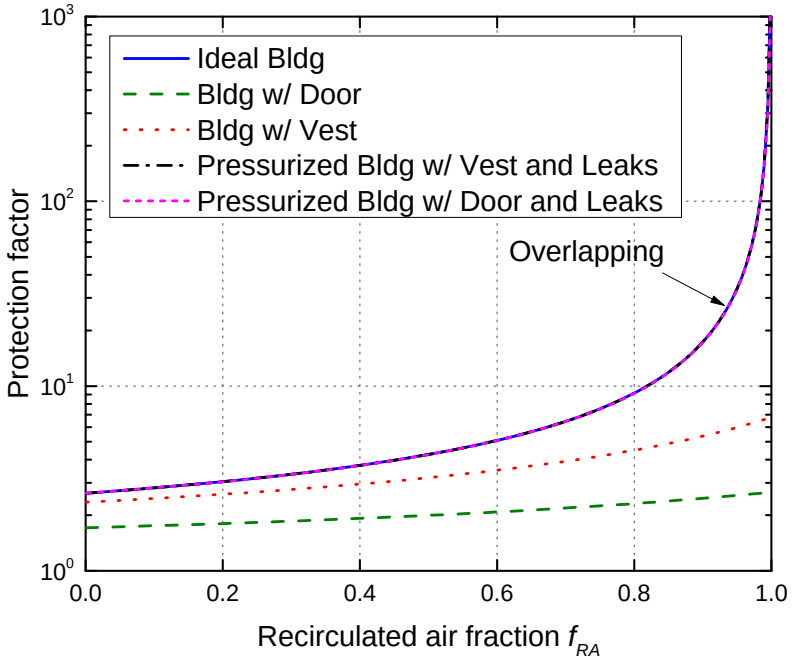

(c) MERV 8, α×4, α=β (Figure 4.10 (cont.))

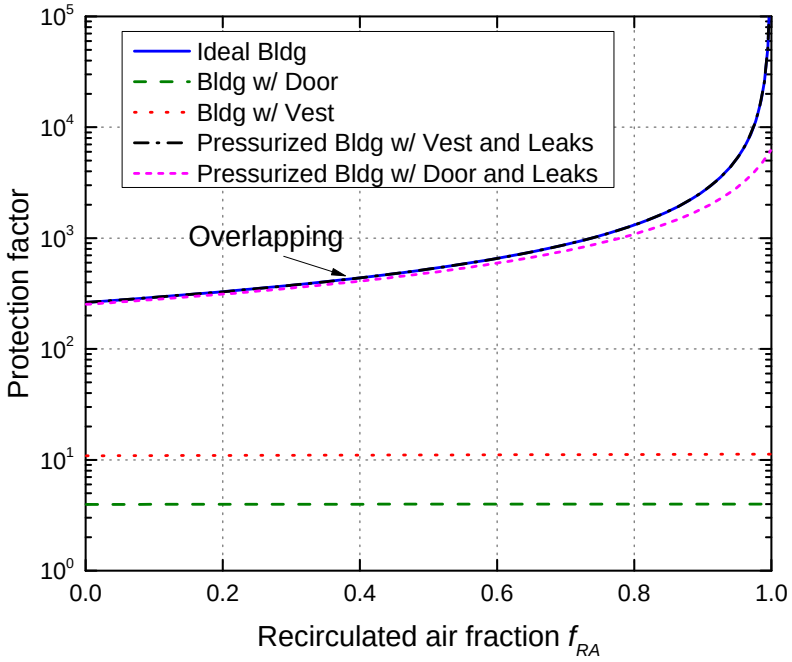

(d) HEPA, $\alpha\times4$, $\alpha=\beta$

Figure 4.10 Effect of the RA fraction on the PF at different α(s) using different filters

As shown in Figure 4.10, the pressurized building (with or without the vestibule or without the door) is effectively the same as the idealized building. The PFs in facilities protected by the HEPA filters are two orders of magnitude higher than those protected by the MERV 8 filters. As the RA fraction increases from 60% to 75% (typical range), the PF only increases by less than a factor of two for idealized buildings and pressurized facilities. For non-pressurized facilities, it is not worthwhile to enhance the PF by increasing the RA fraction. The limited effect of RA filtration is demonstrated again.

For the non-pressurized building with a door or a vestibule, if the infiltration increases by a factor of four but ventilation flow rate does not, the PF will be noticeably reduced. For instance, for the non-pressurized facility with a vestibule, the PF will drop from 60 to 10 when the facility is protected by the HEPA filters. For the non-pressurized facility with just a door, the PF will drop from 12 to 3 when the facility is protected by the HEPA filters. If the facility (pressurized or not pressurized) is protected by the MERV 8 filters, the PF is always low.

It is implied in Figure 4.10 that the existence of ventilation and filtration system is not worthwhile for non-pressurized facilities in the real world because the PF is no larger than 60 (when protected by the HEPA filters) and this number is significantly adversely affected by the

increase of infiltration flow. In other words, if vestibule doors are frequently opened, it is impossible to protect the non-pressurized facilities even by using the HEPA filters.

Pressurized buildings, on the other hand, are under relatively much better protection because the contaminant flow does not infiltrate constantly. Even for the pressurized buildings, it is still necessary to have a vestibule such that the contaminant source gets diluted before infiltrating the room.

As shown in Figure 4.11, for the non-pressurized facility with a door or a vestibule, the PF always decreases as α or β increases. For non-pressurized facility with a door, such a decrease of PF can be up to a factor of two if the MERV filters are used for filtration. If the HEPA filters are used, the decrease of PF is up to two orders of magnitude, making it not worthwhile (or impossible) to protect such a facility. For all the scenarios, the existence of the vestibule always relieves the decrease of PF as α or β increases, because the vestibule is effectively a buffer zone in which the contaminant gets diluted before infiltrating the room. For the pressurized building with a door or a vestibule, it is effectively the same as the idealized building and will not be noticeably affected by α or β.

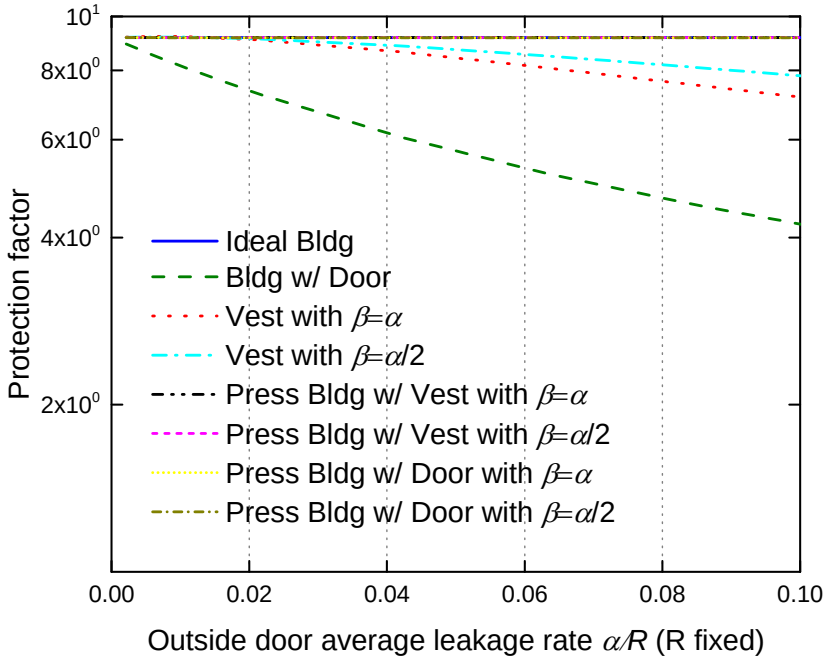

(a) MERV8, α (Figure 4.11 (cont.))

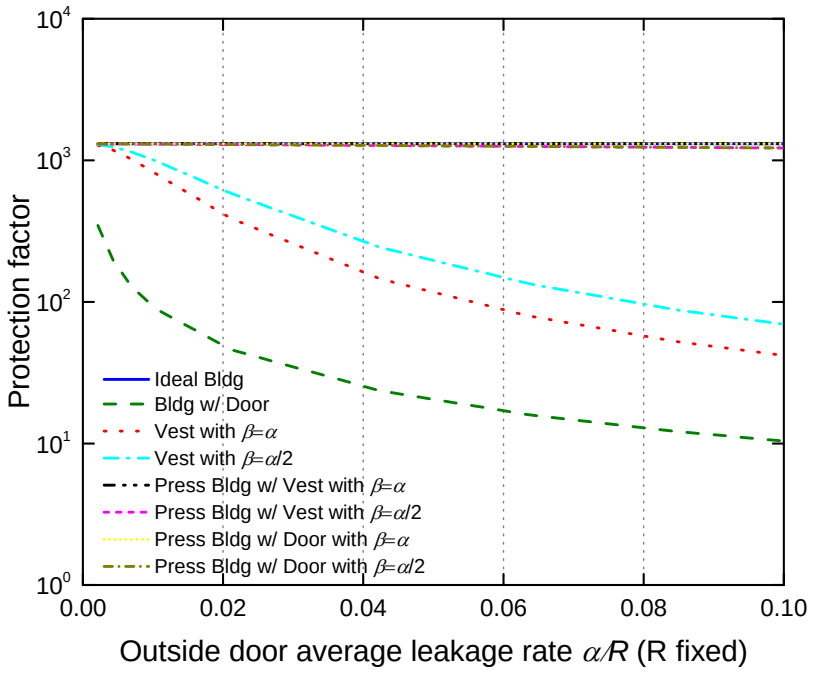

(b) HEPA, α

Figure 4.11 Effect of α and β on PF using different filters

As shown in Figure 4.12, for the non-pressurized facility with a vestibule, the PF always increases as R_V increases. This is because there is a constant flow exchange between the vestibule and the room. If the vestibule gets "cleaner," the inter-zone exchange flow will facilitate cleaning the room. It is not economical to operate the DBVS in the vestibule at a flow rate as high as indoor SA flow rate (i.e., R_V=R). The limited effect of RA flow rate on the PF is demonstrated again. For the pressurized facility, it is effectively the same as the idealized building and will not be noticeably affected by the R_V.

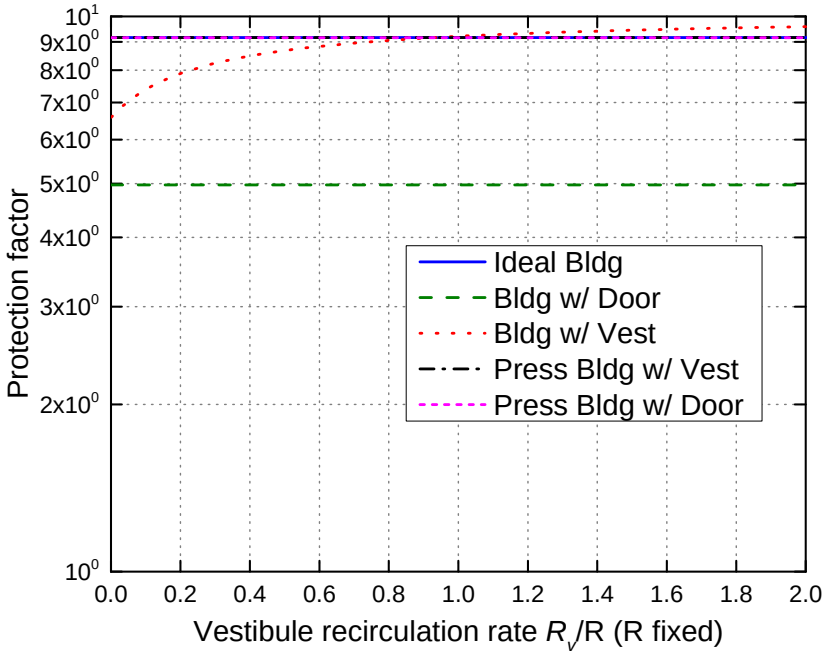

(a) MERV8, α

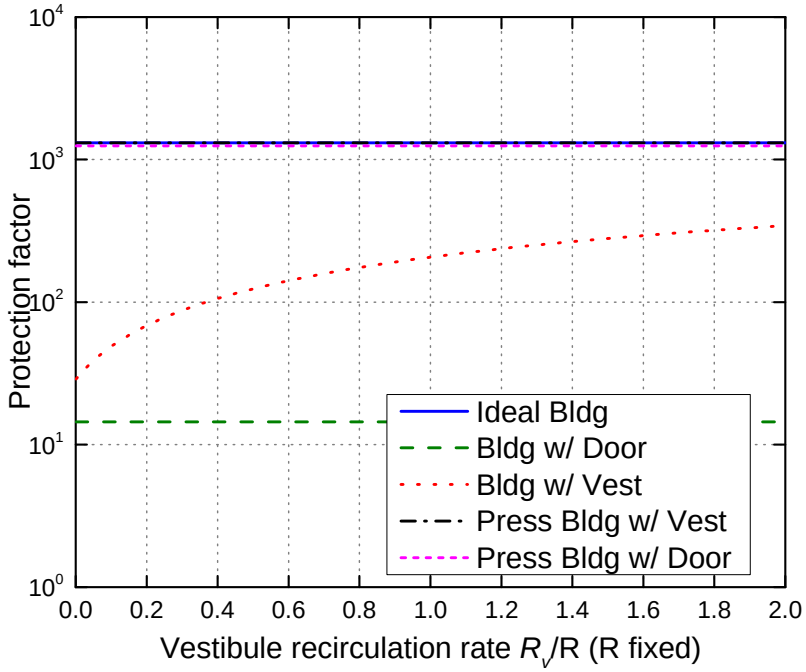

(b) HEPA, α

Figure 4.12 Effect of R_V on the PF using different filters

4.3 Characteristics of Ventilated Vestibules

In this section, the characteristics of the ventilated vestibule were investigated. A method to determine the door opening period T_0 was introduced. Small leakiness was assumed for the room and vestibule (vestibule interior door crack area: 10 $cm^2/m^2 \times 2.5$ m^2). Model simulation parameters are summarized in Table 4.2.

Table 4.2 Parameters for model simulation

T_{OA}	0.0038 (for HEPA) or 0.38 (for MERV 8)	OA filter transmittance for the room
T_{IA}	$= T_{OA}$	RA filter transmittance for the room
T_V	$= T_{OA}$	RA filter transmittance for the vestibule
f_{RA}	0.75	RA fraction in the indoor ventilation system
q	5 L/(s·m^2 of door area)	Unit air infiltration through exterior doors
Δt	3 sec (minimum)	Door opening time
A_{vd}	$1.36 \times 3 \sim 2.3 \times 3$ m^2	Vestibule door area
α	0.061~0.104 m^3	Air exchange volume when exterior door is opened
β	$\alpha/10 \sim \alpha$	Air exchange volume when interior door is opened
R	0.472 m^3/s	Indoor ventilation rate
R_V	0~0.094 m^3/s	Ventilation rate in the vestibule
R_{IV}	0.007~0.045 m^3/s	Inter-zone leakage rate
T_0	30 min	Door-opening period
V_I	226.535 m^3	Volume of the room
V_V	8.155 m^3	Volume of the vestibule
Θ	0.242 L/s	Respiratory rate of an adult

4.3.1 Door Opening Period T_0: Scenario 1

It is noteworthy that the PF derived in the above Section 4.2 involves the door opening period T_0, but the method to obtain T_0 was not discussed. In this section, such a method is developed.

The scenario in this section is exactly the same as that in Section 4.2.1. The difference is that instead of finding a steady-state PF value by using the Laplace Transform, the source deposition due to air exchange is treated as an initial condition. To be specific, once the person gets into the vestibule, the deposited source gets well mixed in the vestibule instantaneously before he can open the interior door of the vestibule. The elevated contaminant concentration is

the initial condition for the governing equation based on contaminant conservation. It is assumed that before a source deposition occurs, the contaminant concentrations in the room and in the vestibule are at steady state. After obtaining a solution for the contaminant concentration and requiring it to be the same as the steady-state concentration such that a periodic deposition of contaminant does not cause contaminant accumulation in the vestibule, a door opening period can then be obtained.

$$\frac{dc_i}{dt} = ac_i + \gamma c_{out} \tag{4.33a}$$

$$a = -R\left(1 - f_{RA}T_{IA}\right)/V_I \tag{4.33b}$$

$$\gamma = R\left(1 - f_{RA}\right)T_{OA}/V_I \tag{4.33c}$$

$$g = \beta/V_I \tag{4.33d}$$

$$IC: c_i\left(0^+\right) = \frac{-\beta c_i\left(0\right) + \beta c_V\left(0\right)}{V_I} + \frac{V_I - \beta}{V_I}c_i\left(0\right) \tag{4.33e}$$

$$\text{i.e., } c_i\left(0^+\right) = \left(-\frac{\gamma}{a}c_{out}\right)\left[1 + \left(\frac{m}{-\gamma/a} - 2\right)g\right] \tag{4.33f}$$

where $c_i\left(0\right)$ and $c_V\left(0\right)$ are assumed to be the same steady state concentrations as those in Equations 4.19 (a) and 4.19 (b):

$$c_i\left(0\right) = \frac{T_{OA}}{1 + \left(1/\left(1 - f_{RA}\right) - 1\right)\left(1 - T_{IA}\right)}c_{out} = -\frac{\gamma}{a}c_{out} \tag{4.33g}$$

$$c_V\left(0\right) = \frac{R_{IV}}{R_{IV} + R_V\left(1 - T_V\right)}c_i\left(0\right) = -\frac{\gamma}{a}\frac{R_{IV}}{R_{IV} + R_V\left(1 - T_V\right)}c_{out} = mc_{out} \tag{4.33h}$$

The solution to Equation 4.33 is:

$$c_i\left(t\right) = \left(-\frac{\gamma}{a}c_{out}\right)\left[1 + e^{at}\left(\frac{m}{-\gamma/a} - 2\right)g\right] \tag{4.34}$$

For the vestibule of the same pressurized building with leakage and a vestibule:

$$\frac{dc_V}{dt} = jc_i + \left(c - j\right)c_V \tag{4.35a}$$

$$a = -R\left(1 - f_{RA}T_{IA}\right)/V_I \tag{4.35b}$$

$$c = -R_V\left(1 - T_V\right)/V_V \tag{4.35c}$$

$$f = \beta / V_V \tag{4.35d}$$

$$g = \beta / V_I \tag{4.35e}$$

$$h = \alpha / V_V \tag{4.35f}$$

$$j = R_{IV} / V_V \tag{4.35g}$$

$$m = -\frac{\gamma}{a}\frac{R_{IV}}{R_{IV} + R_V\left(1 - T_V\right)} \tag{4.35h}$$

$$\gamma = R\left(1 - f_{RA}\right)T_{OA} / V_I \tag{4.35i}$$

$$IC: c_V\left(0^+\right) = \frac{\beta c_i\left(0\right) - \beta c_V\left(0\right) + \alpha c_{out} - \alpha c_V\left(0\right)}{V_V} + \frac{V_V - \alpha - \beta}{V_V} c_V\left(0\right) \tag{4.35j}$$

$$\text{i.e., } c_V\left(0^+\right) = \left(-\frac{\gamma}{a} c_{out}\right)\left[f + \frac{h}{-\gamma/a} + \frac{m}{-\gamma/a}\left(1 - 2f - 2h\right)\right] \tag{4.35k}$$

The solution to Equation 4.35 is:

$$c_V\left(t\right) = \left(-\frac{\gamma}{a} c_{out}\right)\left[\frac{m}{-\gamma/a} + \left(\begin{array}{c} f - h\frac{a}{\gamma} - \frac{2m}{-\gamma/a}\left(f + h\right) \\ -\frac{\left(\frac{m}{-\gamma/a} - 2\right) jg}{a + j - c} \end{array}\right) e^{(c-j)t} + \frac{\left(\frac{m}{-\gamma/a} - 2\right) jg}{a + j - c} e^{at}\right] \tag{4.36}$$

In order to obtain the period (T_0) necessary for the concentration to fall back to the steady state value, let

$$c_V\left(t\right) = c_{V\,steady} = \left(-\frac{\gamma}{a} c_{out}\right)\left(\frac{m}{-\gamma/a}\right) \tag{4.37}$$

Solve Equations 4.36 and 4.37 to get

$$e^{(a+j-c)T_0} = \frac{\left(f - h\frac{a}{\gamma} - \frac{2m}{-\gamma/a}\left(f + h\right)\right)}{-\frac{\left(\frac{m}{-\gamma/a} - 2\right) jg}{a + j - c}} + 1 \tag{4.38}$$

Finally the period T_0 is obtained by solving Equation 4.38:

$$T_0 = \frac{1}{(a+j-c)} \ln \left\{ \frac{\left(f - h\frac{a}{\gamma} - \frac{2m}{-\gamma/a}(f+h) \right)}{-\frac{\left(\frac{m}{-\gamma/a} - 2 \right) jg}{a+j-c}} + 1 \right\} \tag{4.39}$$

It is noteworthy that the T_0 is the shortest time needed to allow the contaminant concentration in the vestibule to fall back to a level no higher than the one in the previous cycle. As long as such a door opening period is maintained, the contaminant(s) in the vestibule will not accumulate.

From Equation 4.38, it can be seen that $a + j - c > 0$, because the right-hand side is positive, i.e.,

$$\frac{R_V}{R} > \frac{V_V}{V_I} \frac{(1 - \eta T_{IA})}{1 - \left(T_V - \frac{R_{IV}}{R_V} \right)} \tag{4.40}$$

The inequality in Equation 4.40 is suggested to serve as a lower-bound requirement of R_v/R ratio. It is noteworthy that this lower-bound requirement of R_V/R is normally met because V_V/V_I ratio is typically very small.

It can also be seen from Equation 4.38 that T_0 is independent of ambient spore concentration and α. It is only dependent on the ratio of β/α. As a matter of fact, the following relationship can be found, which is a rearrangement of Equation 4.38:

$$T_0 = S \cdot \ln(\beta / \alpha) + U \tag{4.41}$$

where S and U are determined by ventilation flow rates, inter-zone leakage flow rate, filter efficiencies, room and vestibule volumes.

An example simulation is shown in Figure 4.13 that demonstrates the linear relationship between T_0 and $\ln(\beta/\alpha)$. Some more simulations made to investigate the effect of filter efficiency on T_0 are shown in Figure 4.14. It can be seen that the smallest T_0 is achievable within a narrower efficiency range (for instance, $0.05 < T_{OA} < 0.2$). The ratio of β/α and the filter efficiency generally do not have significant impact on T_0.

The effect of vestibule ventilation flow rate R_V on T_0 is shown in Figure 4.15. It seems that increasing R_V is more effective than changing filter in shortening the T_0. It also can be seen

that a R_V/R ratio of around 0.45 is necessary in order to obtain a T_0 of 10 min. Assuming R=0.472 m^3/s and R_V=0.212 m^3/s, Figure 4.16 can be obtained to explore the effect of R_{IV} on T_0. It can be seen that at a R_{IV}/R ratio of 0.2, a T_0 of ~7.5 min can be obtained using HEPA filters. Normally for a building, the leakage level is a set value once the building is constructed, and the pressurization level can be adjusted by the ventilation system, but not within a wide range.

Based on simulation results in Figures 4.13-4.16, T_0 is affected most significantly by R_V, then by β/α ratio. Any attempt to decease T_0 by increasing R_{IV} or changing T_{OA} will fail, because 1) R_{IV} is usually determined by construction and a small R_{IV} (indicating a tight building) is the right choice; 2) filter efficiency is to be determined by the required PF value, not by T_0.

In summary, the only two parameters that can be controlled to shorten the door opening period T_0 are: 1) R_V; 2) β/α ratio. The β/α ratio cannot be set at zero, because the T_0 solution in this section is derived assuming both vestibule doors are opened. If β is required to be zero, some other scenario and model need to be explored.

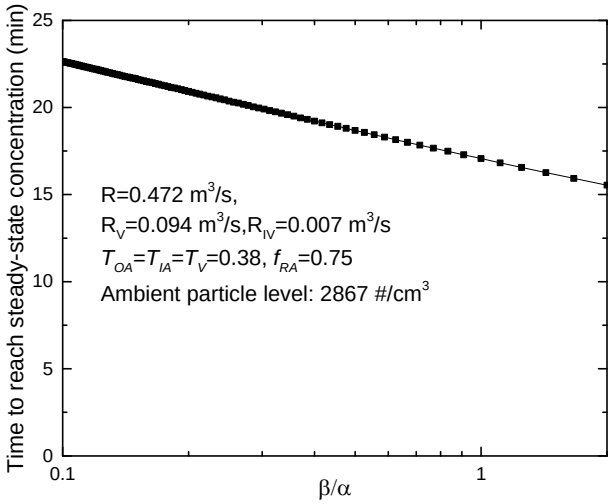

Figure 4.13 T_0 *vs*. ln(β/α)

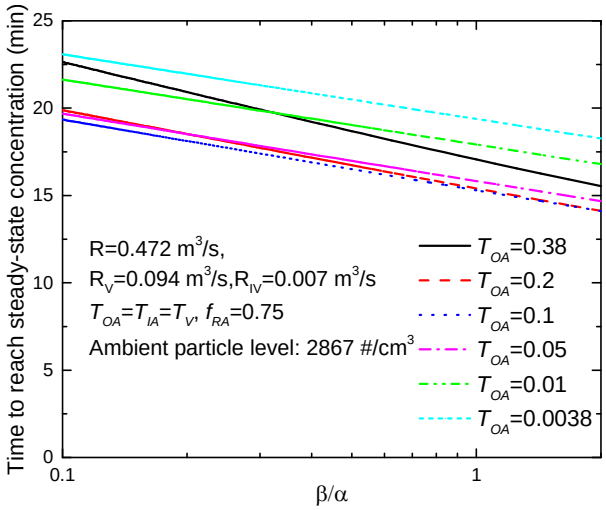

Figure 4.14 Effect of filter efficiency on T_0

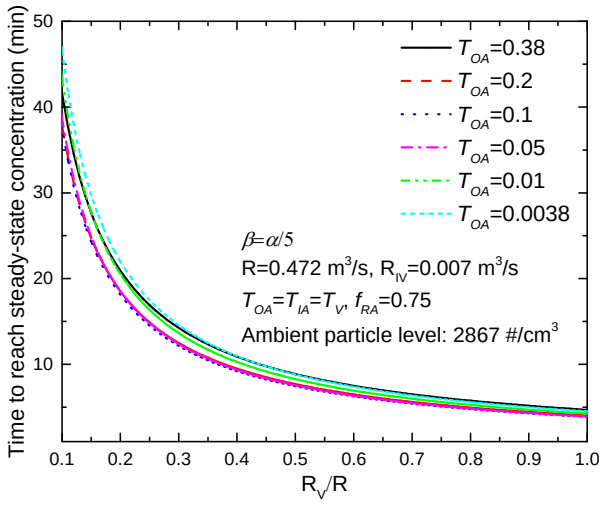

Figure 4.15 Effect of R_V on T_0

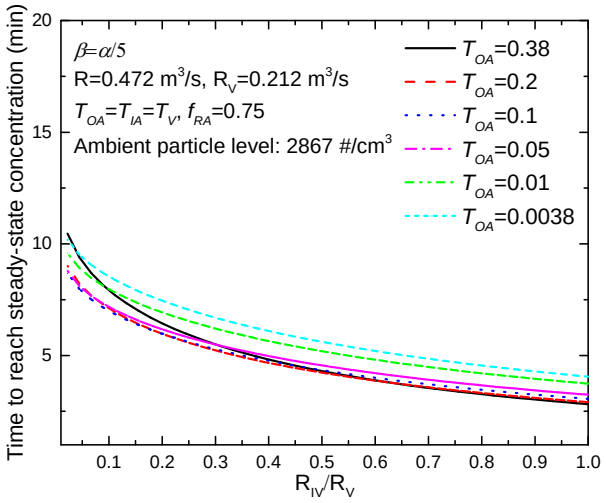

Figure 4.16 Effect of R_{IV} on T_0

4.3.2 Door Opening Period T_0: Scenario 2

To follow up Scenario 1 where $\beta \neq 0$ (no vestibule interior door control), Scenario 2 with $\beta=0$ (interior door of the vestibule closed for traffic control) is explored in this section.

Suppose that a person walks very quickly into a vestibule, incurring an air exchange of α m^3 (see Table 4.2 for meaning of α). The vestibule interior door is closed and the person is "quarantined" in the vestibule. Due to the fact that the room is protected by a positive pressure and the ambient contaminant concentration is constant, the indoor concentration remains constant. To be specific, for the indoor environment in a pressurized room with leakage and a vestibule as shown in Figure 4.4, the following equations can be obtained:

$$ac_i + \gamma c_{out} = 0 \tag{4.42a}$$

$$a = -R\left(1 - f_{RA}T_{IA}\right)/V_I \tag{4.42b}$$

$$\gamma = R\left(1 - f_{RA}\right)T_{OA}/V_I \tag{4.42c}$$

$$c_i(t) = \frac{\left(1 - f_{RA}\right)T_{OA}}{\left(1 - f_{RA}T_{IA}\right)}c_{out} = -\frac{\gamma}{a}c_{out} \tag{4.42d}$$

Assuming that the contaminant concentration in the vestibule before the source deposition has been maintained at its steady-state level:

$$c_V(0) = \frac{R_{IV}}{R_{IV} + R_V\left(1 - T_V\right)}c_i(0) = -\frac{\gamma}{a}\frac{R_{IV}}{R_{IV} + R_V\left(1 - T_V\right)}c_{out} = mc_{out} \tag{4.42e}$$

For the vestibule:

$$\frac{dc_V}{dt} = jc_i + \left(c - j\right)c_V \tag{4.44a}$$

$$a = -R\left(1 - f_{RA}T_{IA}\right)/V_I \tag{4.44b}$$

$$c = -R_V\left(1 - T_V\right)/V_V \tag{4.44c}$$

$$h = \alpha/V_V \tag{4.44d}$$

$$j = R_{IV}/V_V \tag{4.44e}$$

$$m = -\frac{\gamma}{a}\frac{R_{IV}}{R_{IV} + R_V\left(1 - T_V\right)} \tag{4.44f}$$

$$\gamma = R\left(1-f_{RA}\right)T_{OA}/V_I \tag{4.44g}$$

$$IC: c_V\left(0^+\right) = \frac{\alpha c_{out} - \alpha c_V\left(0\right)}{V_V} + \frac{\left(V_V - \alpha\right)c_V\left(0\right)}{V_V} \tag{4.44h}$$

The solution to Equation 4.44 is:

$$c_V\left(t\right) = c_{out}\left[m + h\left(1-2m\right)e^{(c-j)t}\right] \tag{4.45}$$

In order to obtain the period T_0 needed for the concentration to fall back to steady state value, let

$$c_V\left(t\right) \simeq c_V\left(0\right) = mc_{out} \tag{4.46}$$

Note that the right-hand side of Equation 4.45 is always positive, because $0 < m \ll 1/2$ and $h > 0$. The only way for the contaminant concentration to fall back to its steady-state value is through RA filtration, and the period needs to be sufficiently long such that

$$e^{(c-j)T_0} \ll \left|\frac{1}{h\left(1-2m\right)}\right| \tag{4.47}$$

i.e.,

$$T_0 \gg \left|\frac{\ln\left[h\left(1-2m\right)\right]}{j-c}\right| \tag{4.48}$$

Certain sample calculation results are shown in Figure 4.17. An increase of R_V from 0.094 m^3/s to 0.189 m^3/s reduces the door opening period T_0 from ~18 minutes to 9.2 minutes. The 18-minute time frame was obtained by letting the solution in Equation 4.45 to be 1% more than the steady-state value (i.e., $c_V\left(t\right) = 1.01 \times c_V\left(0\right)$).

Figure 4.15 was made for Scenario 1 without control for the interior door of the vestibule and a person can go through the vestibule very quickly. Figure 4.17 was made for Scenario 2 with control for the interior door of the vestibule such that a person is quarantined in the vestibule. A typical T_0 value was in the range of 5-20 minutes.

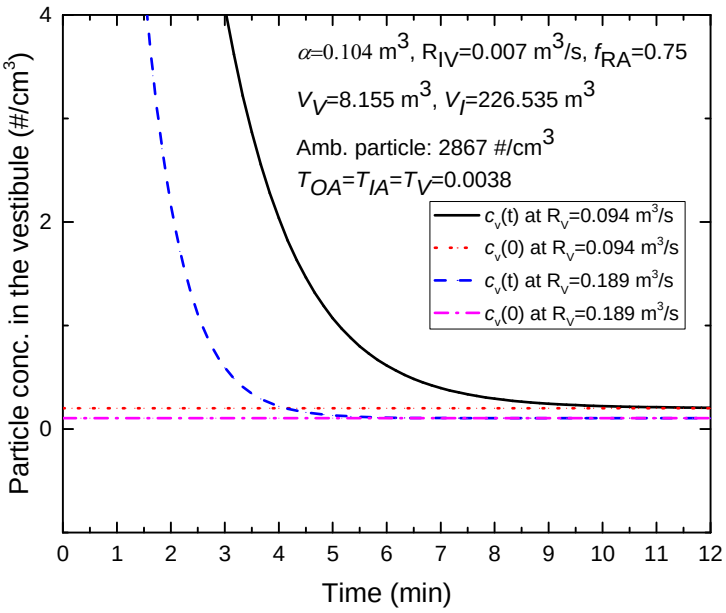

Figure 4.17 Effect of R_V on T_0 with vestibule interior door control

4.4 R_V *vs*. R at Constant PFs

With the method to determine T_0 outlined above, it is time to revisit the PF expressions in Section 4.2 and determine the indoor and vestibule ventilation flow rates necessary to maintain a specific PF level. In order to find the ventilation flow range for the ventilation systems, different PF values are set and corresponding R_V and R flow rates are plotted as shown in Figures 4.18 and 4.19. Figure 4.18 is based on Equation 4.20 in Section 4.2.1. Figure 4.19 is based on Equation 4.21 in Section 4.2.1.

In Figure 4.18, there is only one curve and the curve does not span the entire range of R (or R_V). For the pressurized facility with leakage and a vestibule, the indoor PF predicted by Equation 4.20 needs to be rearranged as follows to explain Figure 4.18.

$$PF_i = \left(-\frac{a}{\gamma}\right)\left[1+\frac{\beta\left(\dfrac{R_V\left(1-T_V\right)}{R_{IV}+R_V\left(1-T_V\right)}\right)}{R\left(1-f_{RA}T_{IA}\right)T_0}\right] \tag{4.49}$$

What this suggests is that PF_i should be very close to $-a/\gamma$ and cannot vary much from it because the second term in the square bracket in Equation 4.49 is normally much smaller than 1. What this means is that the indoor PF value is mainly determined by filter efficiency and RA

fraction f_{RA}. If R increases at conditions in which these two parameters are fixed, more contaminant is brought indoors and some of the extra contaminants can be removed by increasing R_V in the vestibule as the vestibule serves as a "cleaner" for the indoor environment. The air exchange β between the vestibule and the room helps to dilute the extra contaminant brought indoors. But this "cleaning" effect from the vestibule is limited within a small range of R_V. If the indoor contamination level surpasses the cleaning capacity of the vestibule for the room, the indoor PF will drop to a lower value (contour).

It can be seen from Figure 4.19 that as long as R_V is fixed the effect of R on the PF in the vestibule is negligible because R_{IV} is small. In practice, R_V is commonly smaller than R. If R is 1.416 m^3/s, an R_V of 0.944 m^3/s is more than likely the upper limit for the vestibule. This means that the PF value in the vestibule is just 25 even with a HEPA filter in the DBVS. A PF value higher than 25 is not a realistic goal for the vestibule in this case. The relationship between R and R_{IV} is not considered in Figure 4.19. Assuming that the crack area is uniformly distributed among only four walls of the small-leakage room (V_I =226.535 m^3) with a square floor area and a 3-meter height, because of the linear relationship between crack flow rate and crack area ($Q = C^* \Delta p^n A$), the ratio of R_{IV} to OA flow rate (1-f_{RA})R is the same as the ratio of door area to the total wall area, that is, 2.4%. From the R_V and R values in Figure 4.19, it is easy to see that R_{IV} (=0.6%×R) is trivial compared to R_V thus its impact is insignificant. What this means is that even after consideration of the linear relationship between R_{IV} and R, the effect of R_{IV} is still negligible compared to R_V in small-leakiness facilities.

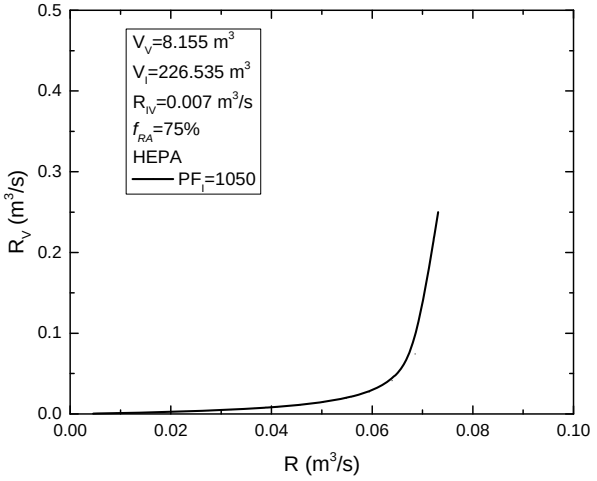

Figure 4.18 R_V *vs*. R for the indoor ventilation system

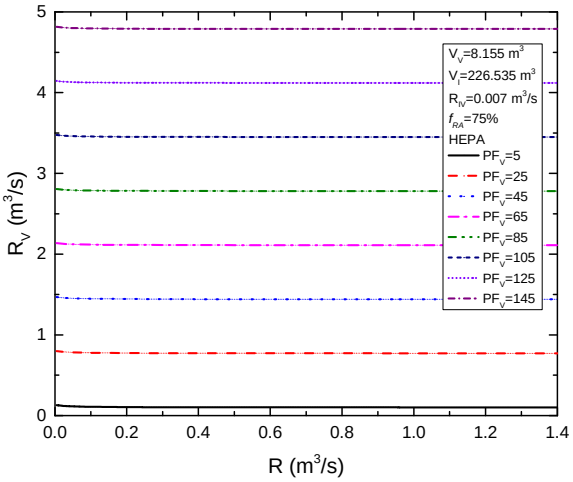

Figure 4.19 R_V *vs*. R for the vestibule ventilation system

4.5 Summary

In this chapter, a state equation for contaminant transport was derived. Through an example analytical solution, the two factors that influenced the time constants of the transient contaminant concentration were identified: 1) filtration efficiencies; 2) ventilation flow rates.

In order to better understand the essential relationship between the PF, ventilation flow rates, inter-zone leakage flow rate and room characteristics, a model (Ginsberg and Bui, 2013) was extended to explore more interested pressurization-protection scenarios. Three simplified pressurized rooms were modeled in the present study and compared to three non-pressurized rooms (Ginsberg and Bui, 2013). The pressurization protection was demonstrated to be useful because it can achieve the same protection level of an idealized room in any real-world room, which was typically much higher than that of the non-pressurized room. Facing periodic source deposition problem, a method to determine the door opening period T_0 was developed. Two scenarios were considered, one with vestibule interior door control and the other without. It was suggested that the vestibule exterior and interior doors should be closed for at least a period of T_0 in order to keep the contaminant concentration in the vestibule from accumulating to high levels. Finally, two sample simulations were made for PF contours in order to better configure the ventilation flow rates in the room and in the vestibule. It was found out that: 1) provided that sufficient positive pressure prevailed, the indoor PF level was dominantly determined by the indoor filter efficiencies and the RA fraction; 2) the vestibule PF was dominantly determined by

its RA flow rate R_V instead of indoor ventilation flow rate R (or R_{IV}), filter efficiencies and indoor RA fraction.

With the necessary information known, A PF contour plot can be made for the room and the vestibule such that the effects of R_V and R are clearly manifested. Such a plot is suitable for determining ventilation flow rate ranges in order to achieve a specific PF goal.

CHAPTER 5-CONCLUSIONS

The present study was focused on enhancing building protection against outdoor contaminant sources through pressurization. The parameters influencing the IAQ generally fell into four categories: 1) building leakage (for instance, crack areas); 2) ventilation (for instance, ventilation flow rate and OA fraction); 3) filtration (for instance, filter efficiency); and 4) room characteristics (for instance, operation schedules of the exterior and interior doors of the vestibule). The main challenges in modeling contaminant spread and mitigation in the indoor environment included but were not limited to: 1) effective and efficient estimation of building crack areas; 2) identification of an appropriate performance metric; and 3) analytical model development to understand parameter interaction and guide ventilation system selection together with vestibule door operation. The present study was performed to provide solutions targeting these challenges.

5.1 Crack Estimation

In this study, a model was developed to estimate the crack areas of a testing facility, and this model is generalizable to other multizone buildings. There were three components in the model: 1) crack area estimation using EES code; 2) pressure predication in CONTAM model using the crack areas obtained in EES code; and 3) comparison of predicted and measured overpressures using the ASTM D5157-97 standard (ASTM, 2008) to evaluate model performance. It was demonstrated that the whole-facility and the zone-by-zone approaches can provide estimation of exterior and interior crack areas simultaneously and generate good model performance (91.7% and 100% of the indicator values lie within ranges of the standard, respectively), with the latter one being preferred to use. The successful model demonstration implied that building interior and exterior crack areas can be simultaneously determined using existing unbalanced ventilation system(s) to pressurize the building. If a similar pressurization test was performed in a large multizone building but no adequate pressure difference data were available for the interior adjacent zones, the whole-facility approach then became the only option. There were two assumptions in the developed model: 1) the power-law relationship was valid between crack flow, pressure difference and crack area; 2) the flow exponent was 0.5 for large cracks and 0.65 for small cracks. If the flow exponent is treated as a variable instead of a

constant, there will be two unknown quantities (the flow exponent and the crack area) in each crack flow equation. This will increase the optimization time and elevate the difficulty level of obtaining reasonable results. Considering this, the developed model in the present study is still recommended with two possible approaches for selection.

5.2 Ventilation System and Mitigation Strategy

The PF was selected as the performance metric for the present study. Useful guidance regarding system/component comparison can be obtained by following this PF-oriented framework.

For instance, sixteen filtration schemes were compared to identify the preferred one for pressurization protection of multizone buildings in the framework. It was found that a very efficient OA filter was necessary to enhance the PF, with the HEPA filter being preferred. Filtering the RA was relatively much less effective compared to filtering the OA. This finding may lead to a significant investment and operating cost saving for the residents. It is also noteworthy that this finding regarding the RA is only applicable to situations where the contaminants are of outdoor origin.

For the vestibule protection, a stand-alone balanced system with 100% RA and a RA filter was recommended because otherwise pressurizing the vestibule may facilitate contaminant infiltration to the room. The AEI device as a new filtration technique was compared to the HEPA filter, and it can be applied as an alternative to the HEPA filter when the ambient pollution level was at low to moderate level, especially in the vestibule when it was equipped with a 100% RA balanced system.

The DUBVS was selected as a suitable ventilation system for the present study, because 1) it can provide sufficient overpressure to prevent ambient contaminant penetration and 2) some contaminated interior zone can be flexibly “isolated” from adjacent ones by adjusting pressure difference through changing ventilation flow rates.

5.3 Modeling a Protected Facility

An analytical solution of indoor contaminant concentration can show the effect of different parameters very clearly. In some rare cases, such one solution was obtainable for multizone buildings. In this study, an extension of an existing model was made for

pressurization-protection scenarios of a simplified yet representative building. Instead of solving ordinary differential equations, the PF was easily obtained through Laplace Transform to relate all the involved parameters. The effects of different parameters were obtained through parametric studies. For instance, it was found out that there was a linear relationship between door opening period T_0 and $\ln(\alpha/\beta)$. It was also shown that pressurization protection of a realistic building can achieve the same protection level as in an ideal building (one without crack areas). In order to achieve a certain PF level indoors, it was crucial to choose the OA filter efficiency and OA (or RA) fraction as the PF was mainly determined by these two factors. A typical quarantine time (or door opening period: T_0) of 15 minutes was recommended for Scenario 1 and 20 minutes for Scenario 2. Compared to the CONTAM simulation capacities in Chapter 3, the analytical PF prediction model can better determine the ventilation flow and filter efficiency at a specific PF value and guide the vestibule interior door operation.

5.4 Future Research Recommendations

The crack area estimation model was demonstrated using a few data points in this study. More experiments are needed for model validation, sensitivity analysis, and/or any extension and generalization in the future to make sure the parameters obtained by this model are reasonable.

In the present study, particle transport phenomena were simplified such that coagulation, deposition and resuspension were not considered. All of these phenomena need to be incorporated to improve the simulation. A good starting point is the incorporation of deposition and resuspension phenomena. The particle coagulation is too complicated to implement in the simulation at the current stage.

CONTAM simulation as a suitable tool for multizone simulation was used extensively in the present study. The present study was focused on contaminant of outdoor origin. It will be interesting to expand the horizon and explore the contaminant mitigation strategy for contaminants of indoor origin.

The coupling of CONTAM and CFD capabilities can provide more detail regarding contaminant concentration variation in a zone. In more and more cases, such a zonal model was desirable. NIST researchers have already developed such a coupling method and incorporated it in CONTAM. It will be worthwhile to check the “well-mixed” assumption for the present study using the coupling method.

Even though the PF was identified as the performance metric, more work is needed to 1) evaluate the range of applicability for this metric; and 2) properly incorporate the contribution of parameters such as the spore toxicity and LD_{50} on humans.

REFERENCES

ASHRAE, 2001, *ASHRAE Handbook – Fundamentals* (SI Edition), American Society of Heating, Refrigerating and Air-Conditioning Engineers, Atlanta, GA.

ASHRAE, 2007, ANSI/ASHRAE Standard 52.2-2007, Method of Testing General Ventilation Air-Cleaning Devices for Removal Efficiency by Particle Size, American Society of Heating, Refrigerating and Air-Conditioning Engineers, Atlanta, GA.

ASHRAE, 2009, *ASHRAE Handbook – Fundamentals* (SI Edition), American Society of Heating, Refrigerating and Air-Conditioning Engineers, Atlanta, GA.

ASHRAE, 2010a, ANSI/ASHRAE Standard 62.1-2010, Ventilation for Acceptable Indoor Air Quality, American Society of Heating, Refrigerating and Air-Conditioning Engineers, Atlanta, GA.

ASHRAE, 2010b, ANSI/ASHRAE Standard 90.1-2010, Energy Standard for Buildings Except Low-Rise Residential Buildings, American Society of Heating, Refrigerating and Air-Conditioning Engineers, Atlanta, GA.

ASTM, 2008, D5157-97, Standard Guide for Statistical Evaluation of IAQ Models, American Society for Testing and Materials, West Conshohocken, PA.

Baker, P., Sharples, S., Ward, I., 1987, Air Flow Through Cracks, *Bdg and Envir*, vol. 22, no. 4: pp. 293-304.

Barnes, R.A., Rogers T.R., 1989, Control of An Outbreak of Nosocomial Aspergillosis by Laminar Air-Flow Isolation, *J. Hosp.Infect*., vol. 14, no. 2: pp. 89–94.

Carrera, M., Zandomeni, R.O., Fitzgibbon, J., Sagripanti, J.L., 2007, Difference between the Spore Sizes of Bacillus Anthracis and other Bacillus Species, *Journal of Applied Microbiology*, vol. 102, no. 2: 303-312.

Carrera, M., Zandomeni, R.O. and Sagripanti, J.-L., 2008, Wet and Dry Density of Bacillus anthracis and other Bacillus Species, *Journal of Applied Microbiology*, vol. 105, no. 1: pp. 68-77.

Chen, C., Zhao, B., 2011, Review of Relationship between Indoor and Outdoor Particles: I/O Ratio, Infiltration Factor and Penetration Factor, *Atmos. Env.,* vol. 45, no. 2: pp. 275-288.

DOE, 1997, DOE-STD-3020, Specification for HEPA Filters used by DOE Contractors, U.S. Department of Energy, Washington, D.C.

Etheridge, D., 1977, Crack Flow Equations and Scale Effect, *Bdg and Envir*, vol. 12, no. 3: pp. 181-189.

Feustel, H.E., Kendon, V.M., 1985, Infiltration Models for Multicellular Structures: A Literature Review, *Energy Buildings*, vol. 8, no. 2: pp. 123-136.

Gallia, J., Meegan, D., Zadler, B., 2010, Acoustic Fractionator Air Purification System; Final Report to ERDC-CERL on Contact W9132T-10-C-0012, Applied Research Associates, Littleton, CO.

Ginsberg, M.D., Bui, A.T., 2013, Bioprotection of Facilities, *Defense and Security Analysis* (Submitted for review).

ICC, 2012, International Energy Conservation Code C402.4.7, International Code Council, Washington, DC.

Jackman, P.J., 1970, A Study of Natural Ventilation of Tall Office Buildings, *Inst Heat Vent Eng*, vol. 38: pp. 103-118.

Kowalski, W.J., Bahnfleth, W.P., Whittam, T.S., 1999, Filtration of Airborne Microorganisms: Modeling and Prediction, *ASHRAE Transactions: Research*, vol. 105, no. 2: pp. 4-17.

Kowalski W.J., Bahnfleth, W.P., 2000, UVGI Design Basics for Air and Surface Disinfection *HPAC Engineering*, vol. 72, no. 1: pp. 100-110.

Kowalski, W.J., Bahnfleth, W.P., 2002, MERV Filter Models for Aerobiological Applications, *Air Media*, summer issue: pp. 13-17.

Li, Y., 1993, Role of Multi-Zone Models in Indoor Air Flow and Air Quality Analyses, *Indoor and Built Environment*, vol. 2, no. 3: pp. 149-163.

Liddament, M.W., Allen, C., 1983, The Validation and Comparison of Mathematical Models of Air Infiltration, *TN 11*, University of Warwick Science Park, Air Infiltration Centre.

Liu, D-L, Nazaroff, W.W., 2001, Modeling Pollutant Penetration across Building Envelops, *Atmos. Env.,* vol. 35, no. 26: pp. 4451-4462.

Lorenzetti, D.M., 2002a, Assessing Multizone Airflow Simulation Software, *Proc. of 9th Intl. Conf. on Indoor Air Quality and Climate*, pp. 267-271.

Lorenzetti, D.M., 2002b, Computational Aspects of Nodal Multizone Airflow Systems, *Building and Environment*, vol. 37, no. 11: pp 1083-1090.

Meegan, G.D., Gallia, J.R, 2008, Acoustic Fractionator-Based Air Purification, *Proc. of the Chem. and Bio. Def. Phys. Sci. and Tech. Conf.*, New Orleans, LA, Nov 17-21.

Megri, A.C., Haghighat, F., 2007, Zonal Modeling for Simulating Indoor Environment of Buildings: Review, Recent Developments, and Applications, *HVAC&R Research*, vol. 13, no. 6: pp. 887-905.

Meng, L., Nawaz, K., He, J., Jacobi, A.M., Nelson A. J., Ginsberg M. D., 2012, Fast Estimation of Leakage Area in A Multizone Test Facility. *2nd Intl High Perform Bdgs Conf*, Purdue University, West Lafayette, IN., No. 3496: pp. 1-9.

Nelson, A.J., Page, M.A., Ginsberg, M.D., Rood, M.J., 2013, Bench-Scale Aerosol Filtration Test System and Evaluation of an Acoustic Bioaerosol Removal Device for Indoor Air Streams, *Aerosol Science and Technology*, vol. 47, no.12: pp. 1285-1292.

Nelson, A.J., 2011, Bench-Scale Evaluation of An Energy Efficient Acoustic Aerosol Purification Device with A Newly Designed Bioaerosol Testing and Evaluation Chamber, *MS Thesis*, *Civil & Environmental Eng. Department*, University of Illinois at Urbana-Champaign.

Novick, V.J., Monson, P.R., Ellison, P.E., 1992, The Effect of Solid Particle Mass Loading on the Pressure Drop of HEPA Filters, *Journal of Aerosol Science*, vol. 23, no. 6: pp. 657-665.

Office of Energy Efficiency & Renewable Energy, 2012, 2011 Buildings Energy Data Book, *Office of Energy Efficiency and Renewable Energy*, Washington, DC.

Persily, A., 2004, Building Ventilation and Pressurization as A Security Tool, *ASHRAE Journal*, vol. 46, no. 9: pp. 18-24.

Persily, A.K., 1998, A Modeling Study of Ventilation, IAQ and Energy Impacts of Residential Mechanical Ventilation, *NISTIR 6162*, *National Institute of Standards and Technology*, Gaithersburg, MD.

Persily, A.K., Martin, S.R., 2000, A Modeling Study of Ventilation in Manufactured Houses, *NISTIR 6455*, *National Institute of Standards and Technology*, Gaithersburg, MD.

Reponen, T.A., Gazenko, S.V., Grinshpun, S.A., Willeke, K.E., Cole, C., 1998, Characteristics of Airborne Actinomycete Spores, Appl. Environ. Microbiol., vol. 64, no. 10: pp. 3807-3812.

Riera, E., Gallego-Juarez, J.A., 1986, Ultrasonic Agglomeration of Micron Aerosols under Standing Wave Conditions, *J. Sound Vib.*, vol. 110, no. 3: pp. 413–427.

Rudnick, S.N., First, M.W., 1978, Specific Resistance (K2) of Filter Dust Cakes: Comparison of Theory and Experiments, *Third Symposium on Fabric Filters for Particulate Collection*, EPA-600/7-78-087.

Sellers, D., Friedman, H., Luskay, L., Haasl, T., 2004, Commissioning and Envelope Leakage: Using HVAC Operating Strategies to Meet Design and Construction Challenges, *Proceedings of the 2004 ACEEE Summer Study on Energy Efficiency in Building*.

Shaw, W.N., 1907, Air Currents and Laws of Ventilation, *Cambridge Univ. Press*, London.

Sherman, M., 1995, The Use of Blower-Door Data, *Indoor Air*, vol. 5, no. 3: pp. 215-224.

U.S. Energy Information Administration, 2012, Annual Energy Review 2012, United States *Energy Information Administration*, Washington, DC.

Wang, L., Chen, Q., 2008, Evaluation of Some Assumptions Used in Multizone Airflow Network Models, *Building and Environment*, vol. 43, no. 10: pp. 1671-1677.

WHO, 2005, WHO Air Quality Guidelines for Particulate Matter, Ozone, Nitrogen Dioxide and Sulfur Dioxide: Summary of Risk Assessment, *World Health Organization*, Geneva, Switzerland. 22 p.

WHO Regional Office for Europe, 2013, Health Effects of Particulate Matter: Policy Implications for Countries in Eastern Europe, Caucacus and Central Asia, *World Health Organization*, UN City, Denmark. 20p.

Withington, S., Chambers, S.T., Beard, M.E., Inder, A., Allen, J.R., Ikram, R.B., Schousboe, M.I., Heaton, D.C., Spearing, R.I., Hart, D.N., 1998, Invasive Aspergillosis in Severely Neutropenic Patients over 18 Years: Impact of Intranasal Amphotericin B and HEPA Filtration, *J. Hosp. Infect.*, vol. 28, no. 1: pp. 11-18.

Zhao, B., Wu J., 2009, Particle Pollution in Ventilated Space: Analysis of Influencing Factors, *Journal of Hazardous Materials*, vol. 163, no. 1: pp. 454-462.

APPENDIX A

A sample code using Engineering Equation Solver (EES) software package is provided to calculate the leakage areas. In this sample, trial 4 was considered.

```
c_out=194.42    "mg/m^3"
eta=0.999975
v_1=0.022507   "m^3/s"
v_2=0.132623  "m^3/s"
v_3=0.531269  "m^3/s"
v_4=0.0969836  "m^3/s"
v_5=0.201839  "m^3/s"

c_1=1
c_2=1
n=0.65

"--Wind pressure at the openings--"
p_1wa=0   "Pa"
p_2wa=0
p_3nda=0
p_3nwa=0
p_3swa=0
p_4wa=0
p_5lwa=0
p_5rwa=0
p_6sda=0

"--Wind pressure at the position of pressure transducer--"
"For zone 3, the two windward measurement positions are the same as the above openings, so the wind pressure values are the same"
```

p_1a=0

p_2a=0

p_3sa=0 "p_3sa is not the same as p_3swa, p_3sa is approximated the same as p_6sda, because the two transducers are close to each other, but a little far from south window in zone 3"

p_4a=0

p_5a=0

deltap_1a=24.17

deltap_2a=22.71

{deltap_3nda= 24.52 "23.30"

deltap_3nwa=24.52 "27.32"

deltap_3swa=24.52 "22.94"}

deltap_4a=25.41

deltap_5a=23.9

deltap_6a=14.12

"--Absolute pressure relative to 1 atm in each zone--"

p_1=deltap_1a+p_1a

p_2=deltap_2a+p_2a

p_3_ave=(p_3nda+23.30+p_3nwa+27.32+p_3sa+22.94)/3 "absolute average pressure in zone 3"

p_4=deltap_4a+p_4a

p_5=deltap_5a+p_5a

p_6=deltap_6a+p_6sda

"--Pressure difference averaged for the 3 openings in zone 3--"

deltap_3nda= p_3_ave-p_3nda

deltap_3nwa= p_3_ave-p_3nwa

deltap_3swa= p_3_ave-p_3swa

"--Pressure difference at the opening--"

deltap_1wa=p_1-p_1wa

deltap_2wa=p_2-p_2wa

deltap_4wa=p_4-p_4wa

deltap_5lwa=p_5-p_5lwa

deltap_5rwa=p_5-p_5rwa

deltap_6sda=deltap_6a

deltap_31=p_3_ave-p_1

deltap_32=p_3_ave-p_2

deltap_34=p_4-p_3_ave

deltap_35=p_3_ave-p_5

deltap_36=p_3_ave-p_6

v_1a=c_1*deltap_1wa^n*A_1a

v_2a=c_1*deltap_2wa^n*A_2a

v_3swa=c_1*deltap_3swa^n*A_3swa

v_3nda=c_1*deltap_3nda^n*A_3na

v_3nwa=c_1*deltap_3nwa^n*A_3nwa

v_4a=c_1*deltap_4wa^n*A_4a

v_5la=c_1*deltap_5lwa^n*A_5la

v_5ra=c_1*deltap_5rwa^n*A_5ra

v_6a=c_1*deltap_6a^n*A_6a

v_3sdampera=c_1*deltap_3swa^0.5*A_3sdampera

A_3na=A_6a

A_1a=A_2a

A_1a=A_3nwa

A_1a=A_3swa

A_1a=A_4a

A_1a=A_5la

A_1a=A_5ra

v_31=c_2*abs(deltap_31)^n*A_31
v_32=c_2*deltap_32^n*A_32
v_34=c_2*abs(deltap_34)^n*A_34
v_35=c_2*deltap_35^n*A_35
v_36=c_1*deltap_36^n*A_36

v_1a=v_1+v_31
v_2a=v_2+v_32
v_3=v_3swa+v_3nda+v_3nwa+v_31+v_32-v_34+v_35+v_36+v_3sdampera
v_4a=v_4-v_34
v_5la+v_5ra=v_5+v_35
v_36=v_6a

(1-eta)*c_out=c_f
v_36*c_f=v_6a*c_f

v_1+v_2+v_3+v_4+v_5=v_1a+v_2a+v_3nda+v_3nwa+v_3swa+v_4a+v_5la+v_5ra+v_6a+v_3sdampera

APPENDIX B

```
"This code is for whole-facility crack estimation approach"
"Assuming a constant leakage area for the 7 windows, d_0"
"Assuming a constant leakage area for the 2 exterior doors, d_1"
"Assuming a constant leakage area for the 5 interior doors, d_2"
"Assuming a constant leakage area for the damper, d_3"

FUNCTION Factor(d_0, d_1, d_2, d_3, NMSE, FB, FS)
IF(((NMSE<0.15) OR (NMSE=0.15)) AND ((FB<0.25) OR (FB=0.25)) AND ((FS<0.01) OR
(FS=0.01))) THEN Factor:=1 ELSE Factor:=1000
END

n=0.65          "Flow exponent is taken as a constant in this version of EES code"

M=4             "M=4 for the four trials 4,6,11 and 12"
DUPLICATE i=1,M

v_1[i]=lookup('Lookup 1',i,'v_1')  "m^3/s"    "Look up the input values in column “1” of the
Lookup Table"
v_2[i]=lookup('Lookup 1',i,'v_2')  "m^3/s"    "Look up the input values in column “2” of the
Lookup Table"
v_3[i]=lookup('Lookup 1',i,'v_3')  "m^3/s"    "Look up the input values in column “3” of the
Lookup Table"
v_4[i]=lookup('Lookup 1',i,'v_4')  "m^3/s"    "Look up the input values in column “4” of the
Lookup Table"
v_5[i]=lookup('Lookup 1',i,'v_5')  "m^3/s"    "Look up the input values in column “5” of the
Lookup Table"

"--Wind pressure at the openings--"
```

p_1wa[i]=lookup('Lookup 1',i,'p_1wa') "Look up the input values in column “n” of the Lookup Table"
p_2wa[i]=lookup('Lookup 1',i,'p_2wa')
p_3nda[i]=lookup('Lookup 1',i,'p_3nda')
p_3nwa[i]=lookup('Lookup 1',i,'p_3nwa')
p_3swa[i]=lookup('Lookup 1',i,'p_3swa')
p_4wa[i]=lookup('Lookup 1',i,'p_4wa')
p_5lwa[i]=lookup('Lookup 1',i,'p_5lwa')
p_5rwa[i]=lookup('Lookup 1',i,'p_5rwa')
p_6sda[i]=lookup('Lookup 1',i,'p_6sda')
"--Wind pressure at the position of pressure transducer--"
"For zone 3, the two windward measurement positions are the same as the above openings, so the wind pressure values are the same"
p_1a[i]=lookup('Lookup 1',i,'p_1a')
p_2a[i]=lookup('Lookup 1',i,'p_2a')
{p_3sa[i]=lookup('Lookup 1',i,'p_3sa')} "p_3sa is not the same as p_3swa, p_3sa is approximated the same as p_6sda, because the two transducers are close to each other, but a little far from south window in zone 3"
p_4a[i]=lookup('Lookup 1',i,'p_4a')
p_5a[i]=lookup('Lookup 1',i,'p_5a')

"--Pressure difference at the opening--"

"--Pressure difference measured at the position of the pressure transducer, not necessarily at the openings--"
deltap_1a[i]=lookup('Lookup 1',i,'deltap_1a')
deltap_2a[i]=lookup('Lookup 1',i,'deltap_2a')
deltap_4a[i]=lookup('Lookup 1',i,'deltap_4a')
deltap_5a[i]=lookup('Lookup 1',i,'deltap_5a')
deltap_6a[i]=lookup('Lookup 1',i,'deltap_6a') "Look up the input values in column “24” of the Lookup Table"

"Columns 25-27 of the Lookup Table are not used in this version of the code"

"-- Preszsure difference through interior door crack --"
deltap_31[i]=IF(p_3_ave[i], deltap_1a[i]+p_1a[i], deltap_1a[i]+p_1a[i]-(p_3_ave[i]), 0,
p_3_ave[i]-deltap_1a[i]-p_1a[i])
deltap_32[i]=IF(p_3_ave[i], deltap_2a[i]+p_2a[i], deltap_2a[i]+p_2a[i]-(p_3_ave[i]), 0,
p_3_ave[i]-deltap_2a[i]-p_2a[i])
deltap_34[i]=IF(p_3_ave[i], deltap_4a[i]+p_4a[i], deltap_4a[i]+p_4a[i]-(p_3_ave[i]), 0,
p_3_ave[i]-deltap_4a[i]-p_4a[i])
deltap_35[i]=IF(p_3_ave[i], deltap_5a[i]+p_5a[i], deltap_5a[i]+p_5a[i]-(p_3_ave[i]), 0,
p_3_ave[i]-deltap_5a[i]-p_5a[i])
deltap_36[i]=IF(p_3_ave[i], deltap_6a[i]+p_6sda[i], deltap_6a[i]+p_6sda[i]-(p_3_ave[i]), 0,
p_3_ave[i]-deltap_6a[i]-p_6sda[i])

"-- Tricks to guarantee the correct sign of the flow rates in the continuity equations --"
"-- Leakage function for each crack is embedded in the following equations--"
v_1a_star[i]=IF(deltap_1a[i]+p_1a[i], p_1wa[i],1*abs(deltap_1a[i]+p_1a[i]-p_1wa[i])^n*d_0, 0,
-1*abs(deltap_1a[i]+p_1a[i]-p_1wa[i])^n*d_0)
v_2a_star[i]=IF(deltap_2a[i]+p_2a[i], p_2wa[i], 1*abs(deltap_2a[i]+p_2a[i]-p_2wa[i])^n*d_0, 0,
-1*abs(deltap_2a[i]+p_2a[i]-p_2wa[i])^n*d_0)

v_3nda_star[i]=IF(p_3_ave[i], p_3nda[i], 1*abs(p_3_ave[i]-p_3nda[i])^n*d_1, 0, -
1*abs(p_3_ave[i]-p_3nda[i])^n*d_1)
v_3nwa_star[i]=IF(p_3_ave[i], p_3nwa[i], 1*abs(p_3_ave[i]-p_3nwa[i])^n*d_0, 0, -
1*abs(p_3_ave[i]-p_3nwa[i])^n*d_0)
v_3swa_star[i]=IF(p_3_ave[i], p_3swa[i], 1*abs(p_3_ave[i]-p_3swa[i])^n*d_0, 0, -
1*abs(p_3_ave[i]-p_3swa[i])^n*d_0)
v_3sdampera_star[i]=IF(p_3_ave[i], p_3swa[i], 1*abs(p_3_ave[i]-p_3swa[i])^0.5*d_3, 0, -
1*abs(p_3_ave[i]-p_3swa[i])^0.5*d_3)

v_4a_star[i]=IF(deltap_4a[i]+p_4a[i], p_4wa[i], 1*abs(deltap_4a[i]+p_4a[i]-p_4wa[i])^n*d_0, 0, -1*abs(deltap_4a[i]+p_4a[i]-p_4wa[i])^n*d_0)
v_5la_star[i]=IF(deltap_5a[i]+p_5a[i], p_5lwa[i], 1*abs(deltap_5a[i]+p_5a[i]-p_5lwa[i])^n*d_0, 0, -1*abs(deltap_5a[i]+p_5a[i]-p_5lwa[i])^n*d_0)
v_5ra_star[i]=IF(deltap_5a[i]+p_5a[i], p_5rwa[i], 1*abs(deltap_5a[i]+p_5a[i]-p_5rwa[i])^n*d_0, 0, -1*abs(deltap_5a[i]+p_5a[i]-p_5rwa[i])^n*d_0)
v_6a_star[i]=IF(deltap_6a[i]+p_6sda[i], p_6sda[i], 1*abs(deltap_6a[i])^n*d_1, 0, -1*abs(deltap_6a[i])^n*d_1)

v_31_star[i]=IF(deltap_1a[i]+p_1a[i], p_3_ave[i], 1*abs(deltap_31[i])^n*d_2, 0, -1*abs(deltap_31[i])^n*d_2)
v_32_star[i]=IF(deltap_2a[i]+p_2a[i], p_3_ave[i], 1*abs(deltap_32[i])^n*d_2, 0, -1*abs(deltap_32[i])^n*d_2)
v_34_star[i]=IF(deltap_4a[i]+p_4a[i], p_3_ave[i], 1*abs(deltap_34[i])^n*d_2, 0, -1*abs(deltap_34[i])^n*d_2)
v_35_star[i]=IF(deltap_5a[i]+p_5a[i], p_3_ave[i], 1*abs(deltap_35[i])^n*d_2, 0, -1*abs(deltap_35[i])^n*d_2)
v_36_star[i]=IF(deltap_6a[i]+p_6sda[i], p_3_ave[i], 1*abs(deltap_36[i])^n*d_2, 0, -1*abs(deltap_36[i])^n*d_2)

{These 7 equations are airflow mass conservation, for unbalanced ventilation systems in this case}
v_1a_star[i]+v_31_star[i]+v_1`[i]=0
v_2a_star[i]+v_32_star[i]+v_2`[i]=0
v_3swa_star[i]+v_3nda_star[i]+v_3nwa_star[i]+v_3sdampera_star[i]+v_3`[i]=v_31_star[i]+v_32_star[i]+v_34_star[i]+v_35_star[i]+v_36_star[i]
v_4a_star[i]+v_34_star[i]+v_4`[i]=0
v_5la_star[i]+v_5ra_star[i]+v_35_star[i]+v_5`[i]=0
v_36_star[i]+v_6a_star[i]=0

END

"-- Objective function of the least-squares minimization --"

SSRE_total=sum(((v_1`[i]-v_1[i])^2/v_1`[i]^2),i=1,M)+sum(((v_2`[i]-v_2[i])^2/v_2`[i]^2),i=1,M)+sum(((v_3`[i]-v_3[i])^2/v_3`[i]^2),i=1,M)+sum(((v_4`[i]-v_4[i])^2/v_4`[i]^2),i=1,M)+sum(((v_5`[i]-v_5[i])^2/v_5`[i]^2),i=1,M)

SSRE_total_star=SSRE_total*Factor(d_0, d_1, d_2, d_3, NMSE, FB, FS)

"-- Calculation of the statistical indices --"

NMSE=sigma/(average_vp*average_vo)/(5*M)
average_vp=sum((v_1`[i]+v_2`[i]+v_3`[i]+v_4`[i]+v_5`[i]),i=1,M)/(5*M)
average_vo=sum((v_1[i]+v_2[i]+v_3[i]+v_4[i]+v_5[i]),i=1,M)/(5*M)
FB=abs(2*(average_vp-average_vo)/(average_vp+average_vo))
theta_vp=(sum((v_1`[i]-average_vp)^2,i=1,M)+sum((v_2`[i]-average_vp)^2,i=1,M)+sum((v_3`[i]-average_vp)^2,i=1,M)+sum((v_4`[i]-average_vp)^2,i=1,M)+sum((v_5`[i]-average_vp)^2,i=1,M))/(5*M)
theta_vo=(sum((v_1[i]-average_vo)^2,i=1,M)+sum((v_2[i]-average_vo)^2,i=1,M)+sum((v_3[i]-average_vo)^2,i=1,M)+sum((v_4[i]-average_vo)^2,i=1,M)+sum((v_5[i]-average_vo)^2,i=1,M))/(5*M)
FS=abs(2*(theta_vp-theta_vo)/(theta_vp+theta_vo))

When running the optimization, press “F4” in the program interface, and a window will be displayed. In the upper left box, choose to “minimize” the “SSRE_star,” and in the upper right box, choose c, k_{z1d}, d_0, d_1, d_2 and d_3 as the four parameters, and set the “Bounds” to be: $-1 \leq d_0, d_1, d_2, d_3 \leq 1$, then choose the “Genetic method” with all the other default settings but increase the number of generations to a large enough value, for instance, 2048. After the preparation, start the optimization

APPENDIX C

Lookup Table for the Med- to High- overpressure Trials (4, 6, 11, 12)																									
1	2	3	4	5	6	7	8	9	10	11	12	13	14	15	16	17	18	19	20	21	22	23	24	25	26	27
0.023	0.133	0.531	0.097	0.202	0	0	0	0	0	0	0	0	0	0	0	0	0	0	24.2	22.7	25.4	23.9	14.1	23.3	27.3	22.9
0.000	0.087	0.275	0.092	0.185	0	0	0	0	0	0	0	0	0	0	0	0	0	0	15.3	13.7	16.3	15.0	9.4	15.8	18.6	13.3
0.252	0.368	1.446	0.347	0.677	0	0	0	0	0	0	0	0	0	0	0	0	0	0	146.4	145.1	152.1	145.3	128.1	150.8	153.8	146.1
0.334	0.361	1.276	0.326	0.116	0	0	0	0	0	0	0	0	0	0	0	0	0	0	139.3	138.7	144.6	135.3	106.0	143.5	147.1	138.8

APPENDIX D

D.1 Overview of the Case Studies

After characterization of the facility, comparisons between different ventilation systems were performed using CONTAM to select a suitable system for IAQ enhancement. The three candidate systems under investigation were: 1) a central unbalanced ventilation system (CUBVS) using which indoor overpressures were created due to the net outdoor air intake; 2) a distributed balanced ventilation system (DBVS) using which a neutral indoor pressure was maintained due to the zero net outdoor air intake; and 3) a distributed unbalanced ventilation system (DUBVS). The three configuration plans for air filters were: 1) OA filter only, 2) RA filter only, and 3) both the OA and the RA filters.

Two case studies were performed to select a suitable ventilation system:

Case 1: comparison of a CUBVS with an OA HEPA filter (η=99.9975%) to a DBVS with an AEI filtration system (AEIFS) (η=99.75%);

Case 2: comparison of three configuration plans of air filters for a DUBVS.

The above-mentioned three ventilation systems (CUBVS, DBVS and DUBVS) were compared through the two case studies in order to identify a suitable ventilation system for IAQ enhancement.

For the purpose of comparison, for all of the case studies, systems under comparison were "installed" in a similar facility to the one in Chapter 2 with different leakage areas (see Table D.1), for which the flow discharge coefficients C_D was set to be 1.0 at 4 Pa and flow exponents were set to be 0.65.

The ambient wind pressure profile was the same for the compared systems for all case studies. For Cases 1-2, there was no indoor contaminant source and the ambient environment was heavily polluted (TEP concentration was constant: 184.035 mg/m^3).

Table D.1 Assumed crack area of each opening for Cases 1-2

A_{13}	A_{1a}	A_{2a}	A_{23}	A_{43}	A_{53}	A_{63}	A_{3nda}	A_{3nwa}	A_{3swa}	A_{4a}	A_{5la}	A_{5ra}	A_{6a}
cm^2	cm^2	cm^2	cm^2	cm^2	cm^2	cm^2	cm^2	cm^2	cm^2	cm^2	cm^2	cm^2	cm^2
1659	157.4	355.7	201.4	656.5	1758	566.2	264	196.1	196.1	141	315	315	464.1

Table D.2 Contaminant properties for Cases 1-2

Species Property \ Contaminant	TEP
Molecular weight (kg/kmol)	182.155
Diffusion coefficient (m^2/s)	5.52×10^{-6}
Mean diameter (μm)	0
Effective density (kg/m^3)	7.561
Specific heat (J/kgK)	205.391

The facility with a CUBVS is shown in Figures D.1 and D.2; the one with a DBVS in Figures D.3 and D.4; and the one with a DUBVS in Figure D.5. The difference between the three systems is ventilation and filtration strategy, namely: 1) For the CUBVS, the OA is introduced into each zone to maintain an indoor overpressure and perhaps dilute some indoor contaminant sources. After some time, the OA exfiltrates the facility through cracks. There is no RA for the CUBVS. 2) For the DBVS, almost no overpressure is created. The ambient air and contaminant infiltrate the facility through cracks. Either some indoor air is drawn into and blown out of the ventilation system with much of the contaminant filtered or the OA is introduced into and out of each zone to dilute indoor contaminant source(s). In the present study, only the 100% RA scenario is considered. 3) For the DUBVS, dissimilar to the DBVS, some OA is introduced to maintain an indoor overpressure and perhaps dilute some indoor contaminant sources. Some indoor air is drawn into and blown out of the system with much of the contaminant filtered. Thus, both the OA and the RA systems are installed. For the CUBVS, an OA filter is necessary. For the DBVS, a RA filter is necessary. For the DUBVS, there could be only one OA filter, or only a RA filter, or both filters (see Case 2). The CUBVS and the DUBVS both provide positive pressure difference across the building envelope to prevent exterior contaminant infiltration from the ambient environment and the vestibule. The difference between them is that “isolation” of some contaminated indoor zones is more flexible using the DUBVS by adjusting the relative pressure differences between adjacent zones. Since the priority and focus in the present study is IAQ enhancement and building protection, the DUBVS is a more suitable system than the CUBVS in terms of indoor contaminant mitigation and control.

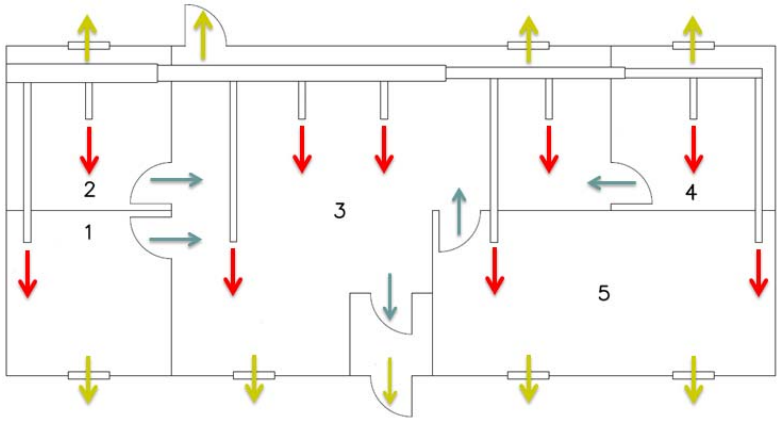

Figure D.1 A facility with a CUBVS

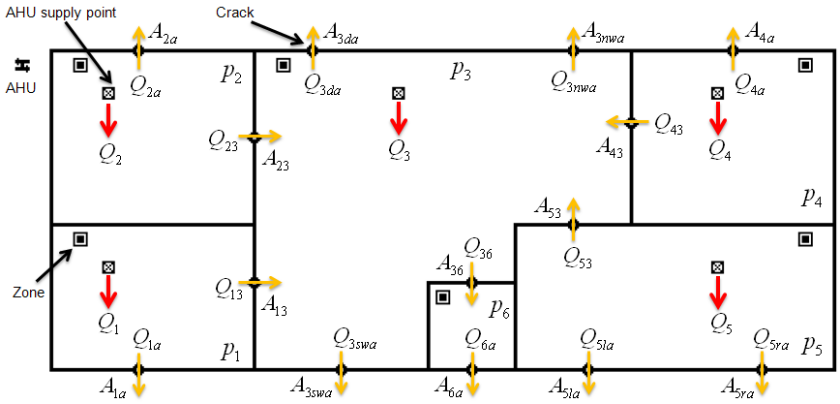

Figure D.2 Illustration of the flow network for the CUBVS

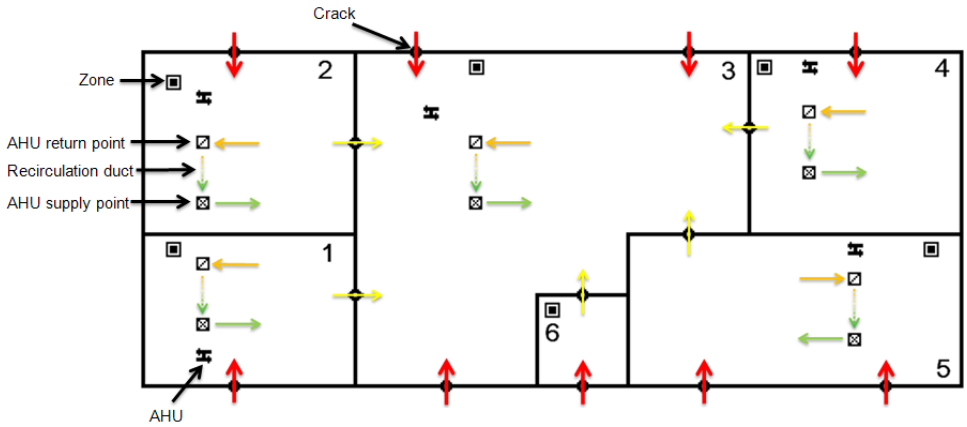

Figure D.3 A facility with a DBVS

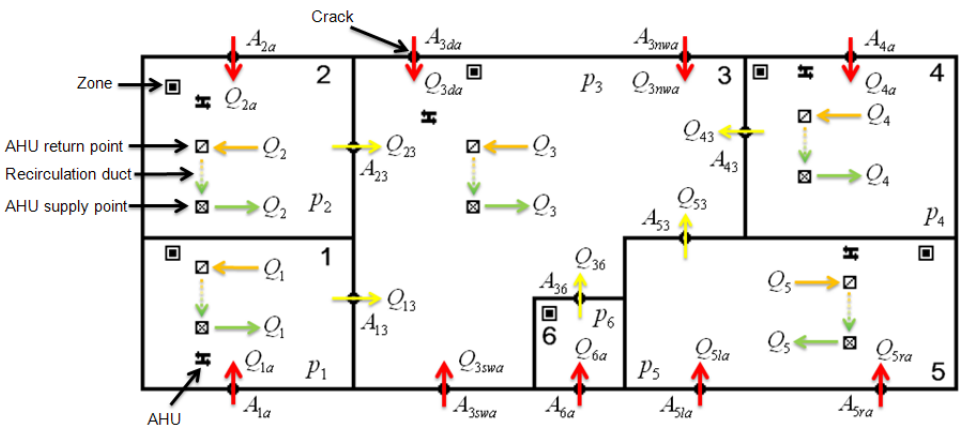

Figure D.4 Illustration of the flow network for the DBVS

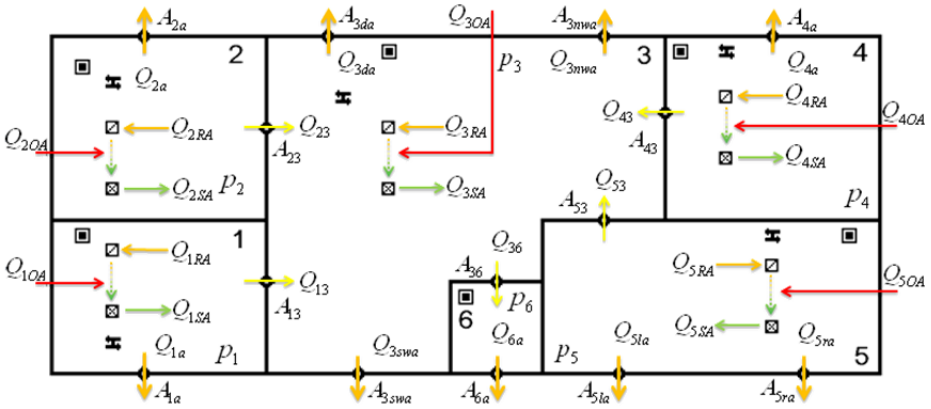

Figure D.5 Illustration of the flow network for the DUBVS

D.2 Case 1

A comparison was performed between a CUBVS with an OA HEPA filter (η_{HEPA}=99.9975%) and a DBVS with a RA AEIFS (η_{RA}=99.75%), as shown in Figures D.2 and D.4. For the CUBVS, a central air handling unit (AHU) was installed outside the facility to filter the contaminated air and supply air flow to each zone to maintain a sufficient overpressure. As a comparison, for the DBVS, a distributed AHU was installed in each zone such that contaminated air can be drawn into the AHU through recirculated air duct, filtered and then supplied back into the same zone. No other systems were used to provide any other air flow. The supply air flow rates were set the same as those listed in Figures D.6 and D.7 for both ventilation systems. There was no ambient wind speed and the ambient TEP concentration was 184.035 mg/m^3. It can be seen that the DBVS created almost no overpressure, thus the indoor contaminant (TEP)

concentration was more sensitive to ambient wind pressure due to the air/contaminant infiltration. It was quite possible that the steady-state TEP concentration was higher in the zone impacted most by the ambient wind pressure effect (zone 2) using the DBVS than the CUBVS.

As an example, the experimental TEP concentration in trial 4 is shown in Figure D.6. The simulated transient TEP concentration using the CUBVS with a HEPA filter efficiency η_{HEPA}=99.9975% at the flow rates of trial 4 in Chapter 2 is shown in Figure D.7. The simulation results and experimental data are of the same order, and the simulation results should reach steady state faster due to the "well-mixed" assumption. For the CUBVS providing a sufficient overpressure, the steady-state indoor TEP concentration is only determined by the filter efficiency and the ambient TEP concentration. Thus, the TEP concentration in each zone reaches the same value at steady state. Figure D.8 is an extension of Figure D.7, which shows that the simulation results do reach a uniform TEP concentration at the steady state. At a higher OA flow rate, the ambient contaminant intake rate is higher. Thus, the contaminant concentration in a zone with a higher OA flow rate reaches steady state faster than others, as can be seen from Figure D.7 or D.8.

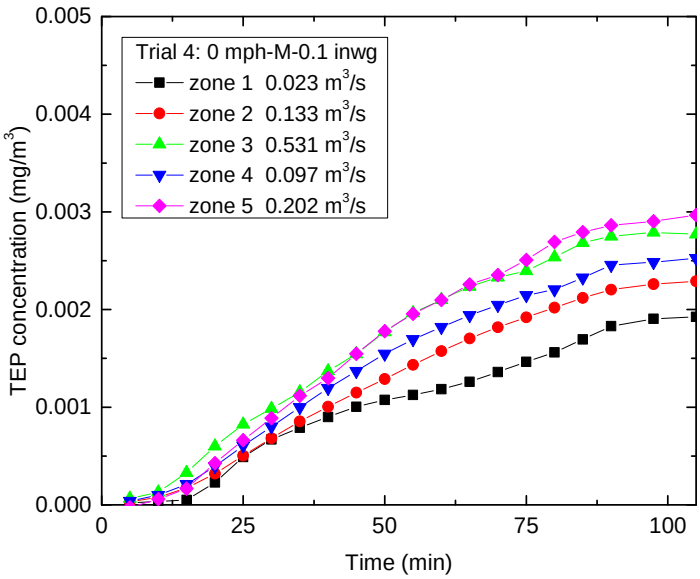

Figure D.6 Experimental TEP conc. in trial 4

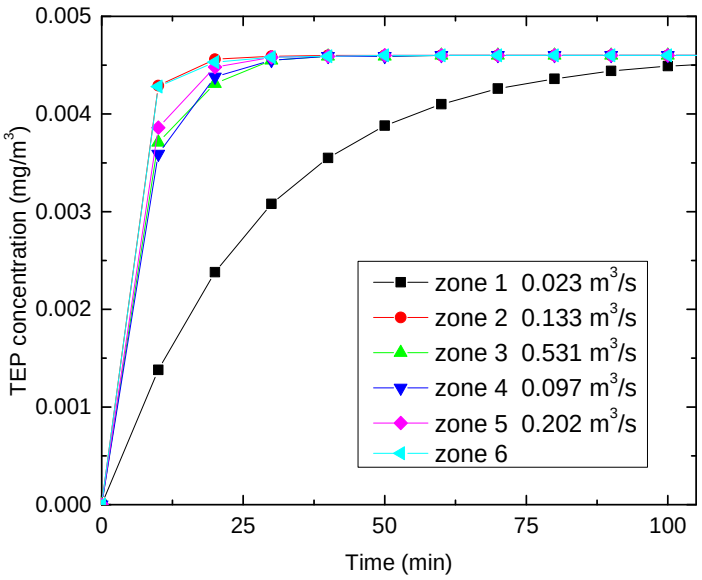

Figure D.7 Simulation results for trial 4

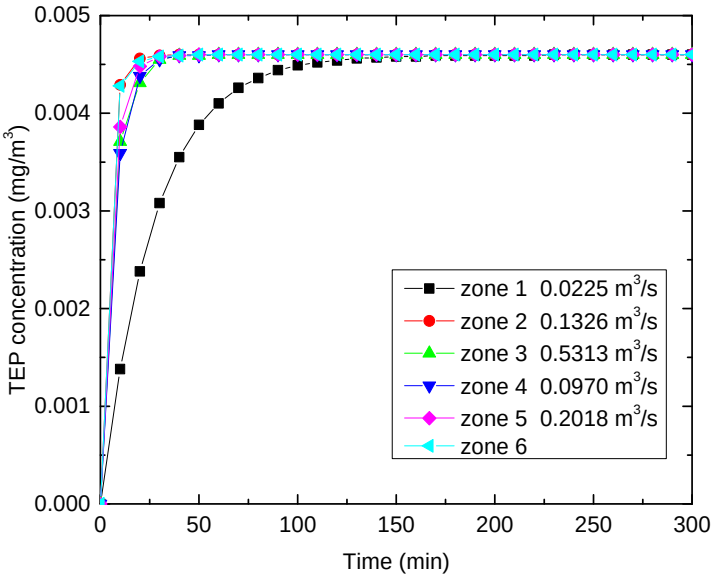

Figure D.8 Simulation results reaching steady state with the CUBVS

For the DBVS, it is of interest to investigate the wind pressure effects on the indoor TEP concentration. For the purpose of comparison, the results are shown in Figure D.9 (a) when the facility is under a uniform windward wind pressure of 2 Pa and leeward wind pressure of -1 Pa (see Figure D.9 (c)). The results are shown in Figure D.9 (b) when the facility is under a uniform windward wind pressure of 0.02 Pa and a leeward wind pressure of -0.01 Pa (see Figure D.9 (d)).

It is confirmed from Figure D.9 that the TEP concentration reaches the highest level in zone 2, which is impacted most by the wind pressure. The TEP concentrations are higher in the windward zones 2, 3 and 4 than in those leeward zones 1 and 5, because the former three zones are impacted more significantly by the ambient TEP infiltration. The TEP concentration may reach a high value in zone 6 due to lack of ventilation. In this case, it is shown that a reduction of the ambient wind pressure by two orders of magnitude can lead to a reduction of the TEP concentration by one order of magnitude in zones 2 and 4, and two orders of magnitude in zones 1, 3, 5 and 6.

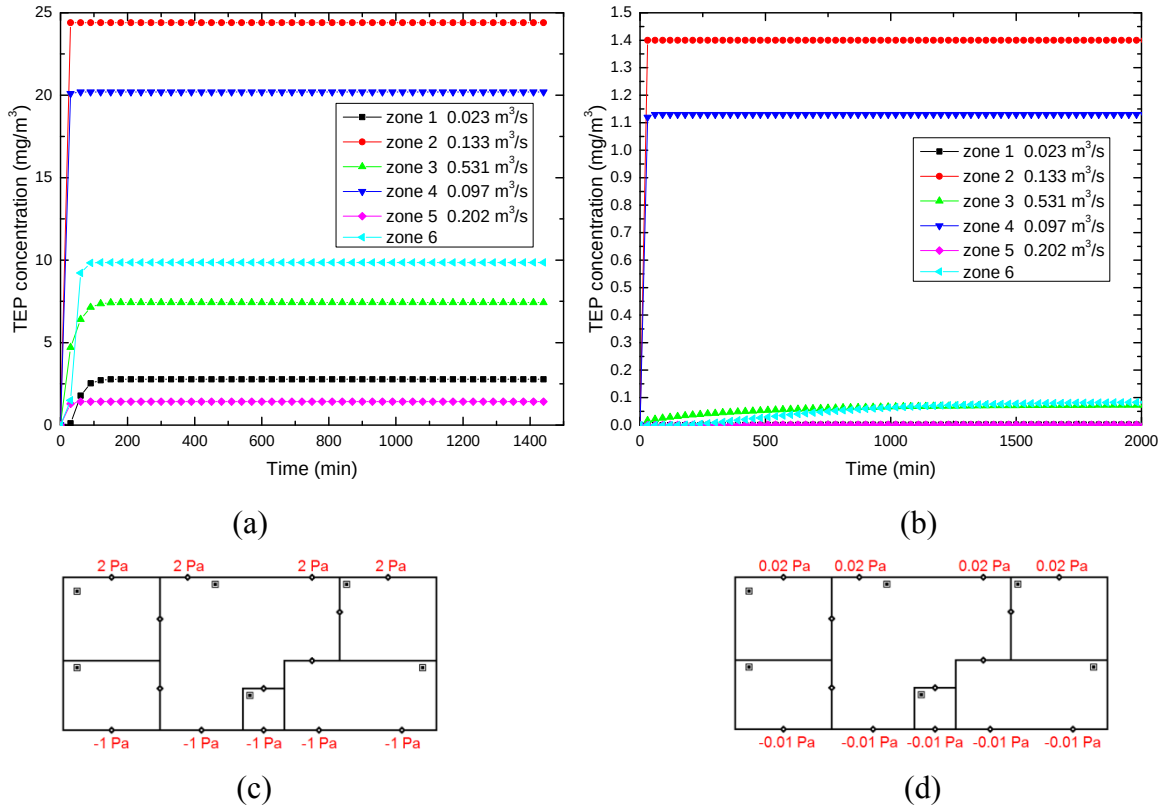

Figure D.9 Sample simulations of the wind pressure effects on the DBVS

In order to know the purifying capacity of the DBVS, some extreme flow rates (10 m^3/s for zones 2, 3 and 4, and 1 m^3/s for zones 2 and 5) were assumed in order to get a low steady-state TEP concentration. The results are shown in Figure D.10 (a) when the facility is under a uniform windward wind pressure of 2 Pa and leeward wind pressure of -1 Pa (see Figure D.10 (c)), and in Figure D.10 (b) when the facility is under a uniform windward wind pressure of 0.02

Pa and leeward wind pressure of -0.01 Pa (see Figure D.10 (d)). Comparing Figures D.9 and D.10, the DBVS operating at very high flow rates can reduce the TEP concentration by around two orders of magnitude. A comparison between Figures D.8 and D.10 (a) shows that the TEP concentration obtained using the DBVS is typically two orders of magnitude higher than that using the CUBVS. This means that even at very high flow rates, the DBVS still cannot compete with the CUBVS with a HEPA filter (η_{HEPA}=99.9975%) in terms of enhancing the indoor IAQ.

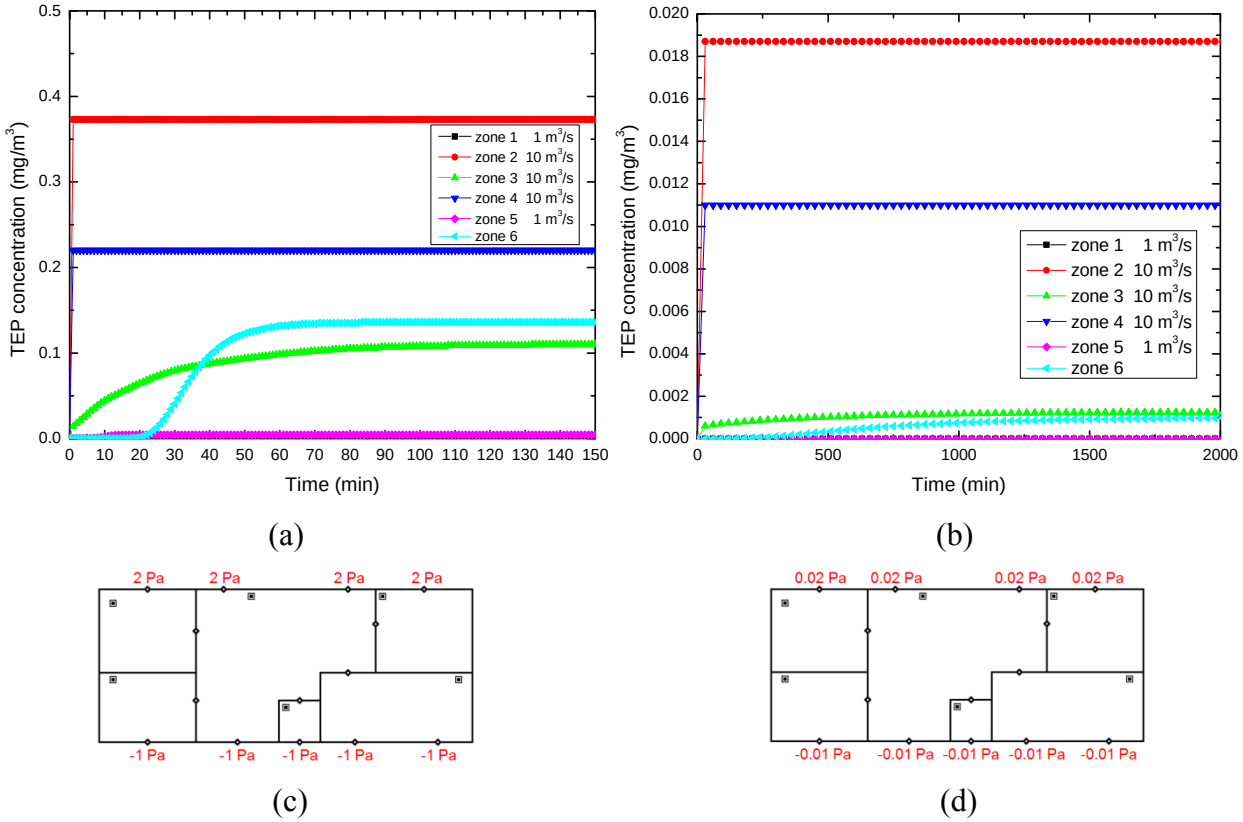

Figure D.10 Sample simulations of the wind pressure effects on the DBVS at high flow rates

In summary, the CUBVS with a HEPA filter (η_{HEPA}=99.9975%) can provide sufficient overpressure to prevent contaminant infiltration thus keeping a low contamination level. The DBVS with an AEIFS (η_{RA}=99.75%) is more sensitive to the ambient wind pressure. Moreover, the maximum steady-state TEP concentration obtained by the CUBVS is one to three orders of magnitude lower than the DBVS (compare Figures D.8 and D.9 (b)) at the same air flow rates. Thus, the CUBVS (η_{HEPA}=99.9975%) is preferred over the DBVS (η_{RA}=99.75%) in terms of IAQ enhancement.

Table D.3 Comparison of the two ventilation systems

	CUBVS with a HEPA filter	DBVS with an AEIFS
Overpressure (Pa)	25	-2~0
Filtration efficiency	99.9975%	99.75%
Supply air (m^3/s)	0.985 (total flow rate of trial 4)	0.985
Max. S.S. TEP conc. (mg/m^3)	0.0046	1.4~24.4 (varying with ambient wind pressure)

D.3 Case 2

Through Case 1, it was found out that unbalance system was a more suitable option than the balanced system in terms of maintaining a low indoor contaminant concentration. In this case study, three air filtration plans were compared for the DUBVS (shown in Figure D.5). The three plans were: 1) a DUBVS equipped with an OA filter and an RA filter in each zone (Plan 1); 2) a DUBVS with only an RA filter in each zone (Plan 2); and 3) a DUBVS with only an OA filter in each zone (Plan 3).

If the indoor overpressure is sufficient, take zone 2 for instance, three different relationships can be shown in Table D.4 for the three plans at steady state. The f_o in the table means the OA fraction, i.e., OA/SA.

It was noted that Plan 3 was not economical, because the RA system was operating but there was no RA filter to perform any filtration. Therefore, the DUBVS with Plan 3 was not of much interest for investigation, and the focuses were Plans 1 and 2. In this case study. It was assumed that the ambient wind speed was 2.24 m/s, and the ambient pressure profile (ASHRAE, 2001) was in red color in Figure D.11. All of the pressure values (unit: Pa) were gauge readings.

Table D.4 Three air filtration plans for the DUBVS

Plan 1	Plan 2	Plan 3
η_{OA}=99.9975%, η_{RA}=99.75%	η_{RA}=99.75%	η_{OA}=99.9975%
$Q_{2OA} = Q_{2a} + Q_{23}$ $Q_{2OA} \cdot (1-\eta_{OA}) \cdot c_{out} - Q_{2RA} \cdot \eta_{RA} \cdot c_{f1} = Q_{2OA} \cdot c_{f1}$ $Q_{2RA} = Q_{2SA} - Q_{2OA} = Q_{2OA}/f_o - Q_{2OA}$ $\frac{c_{f1}}{c_{out}} = \frac{1-\eta_{OA}}{1+(1/f_o-1)\eta_{RA}}$	$Q_{2OA} = Q_{2a} + Q_{23}$ $Q_{2OA} \cdot c_{out} - Q_{2RA} \cdot \eta_{RA} \cdot c_{f2} = Q_{2OA} \cdot c_{f2}$ $Q_{2RA} = Q_{2SA} - Q_{2OA} = Q_{2OA}/f_o - Q_{2OA}$ $\frac{c_{f2}}{c_{out}} = \frac{1}{1+(1/f_o-1)\eta_{RA}}$	$Q_{2OA} = Q_{2a} + Q_{23}$ $Q_{2OA} \cdot c_{out} \cdot (1-\eta_{OA}) = Q_{2OA} \cdot c_{f3}$ $\frac{c_{f3}}{c_{out}} = (1-\eta_{OA})$

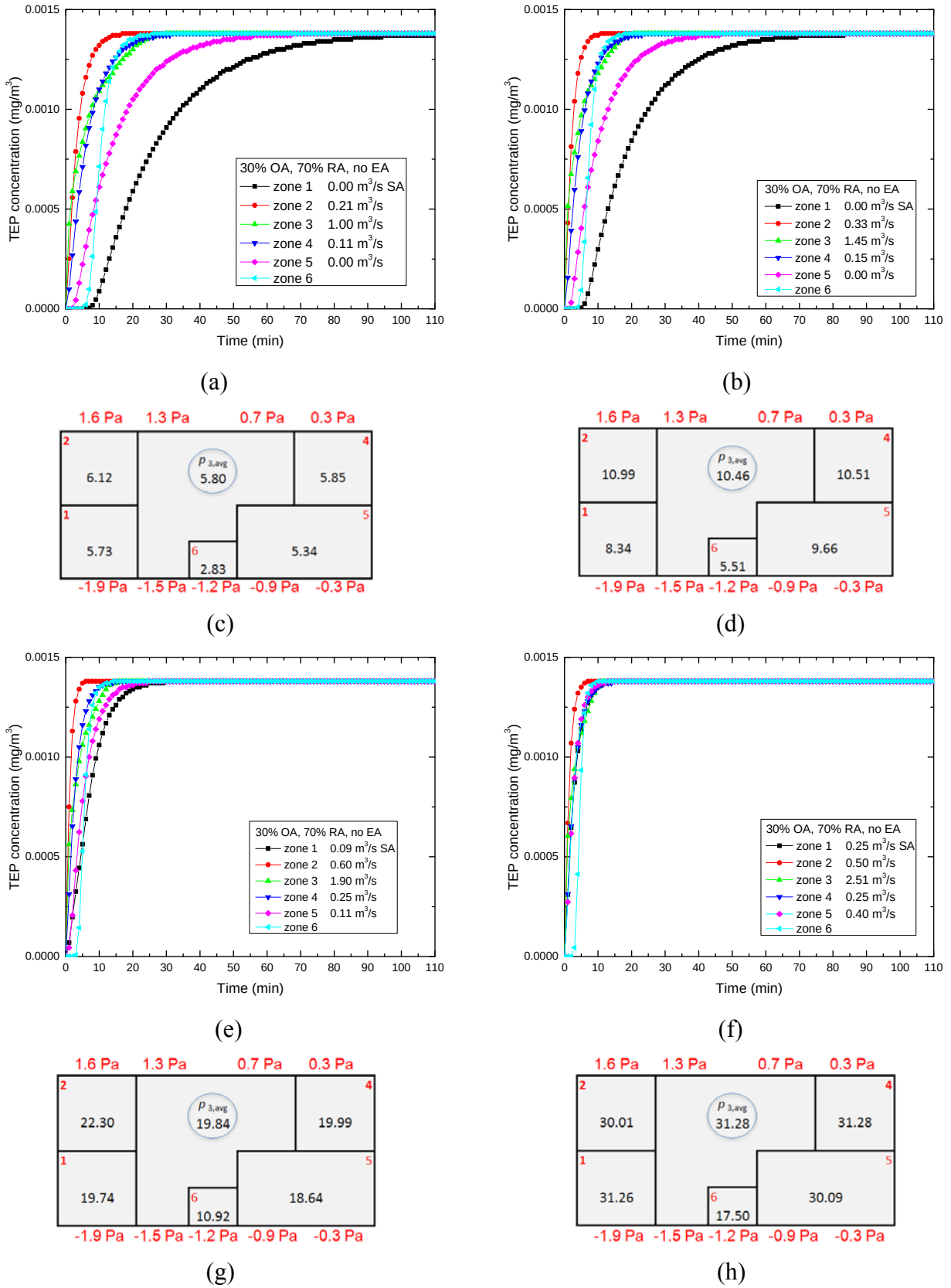

Figure D.11 TEP concentration at different flow rates for the DUBVS with Plan 1

Different overpressure levels (5 Pa, 10 Pa, 20 Pa and 30 Pa) were obtained by adjusting the SA flow rates, as shown in Figure D.11. It was also confirmed that as long as sufficient overpressure was maintained, the same steady-state TEP concentration was obtained from CONTAM simulations. What changed was the speed for the TEP concentration to reach steady state. As previously analyzed in Case 1, a higher OA flow rate meant a higher contaminant intake rate, implying a short time frame to reach the steady state. For Plan 2, there was a similar trend of TEP concentration variation with flow rate compared to that for Plan 1, as shown in Figure D.12. The difference between Figures D.11 and D.12 was that the indoor steady-state TEP concentration was much higher using Plan 2 than Plan 1, as clearly manifested in Table D.4.

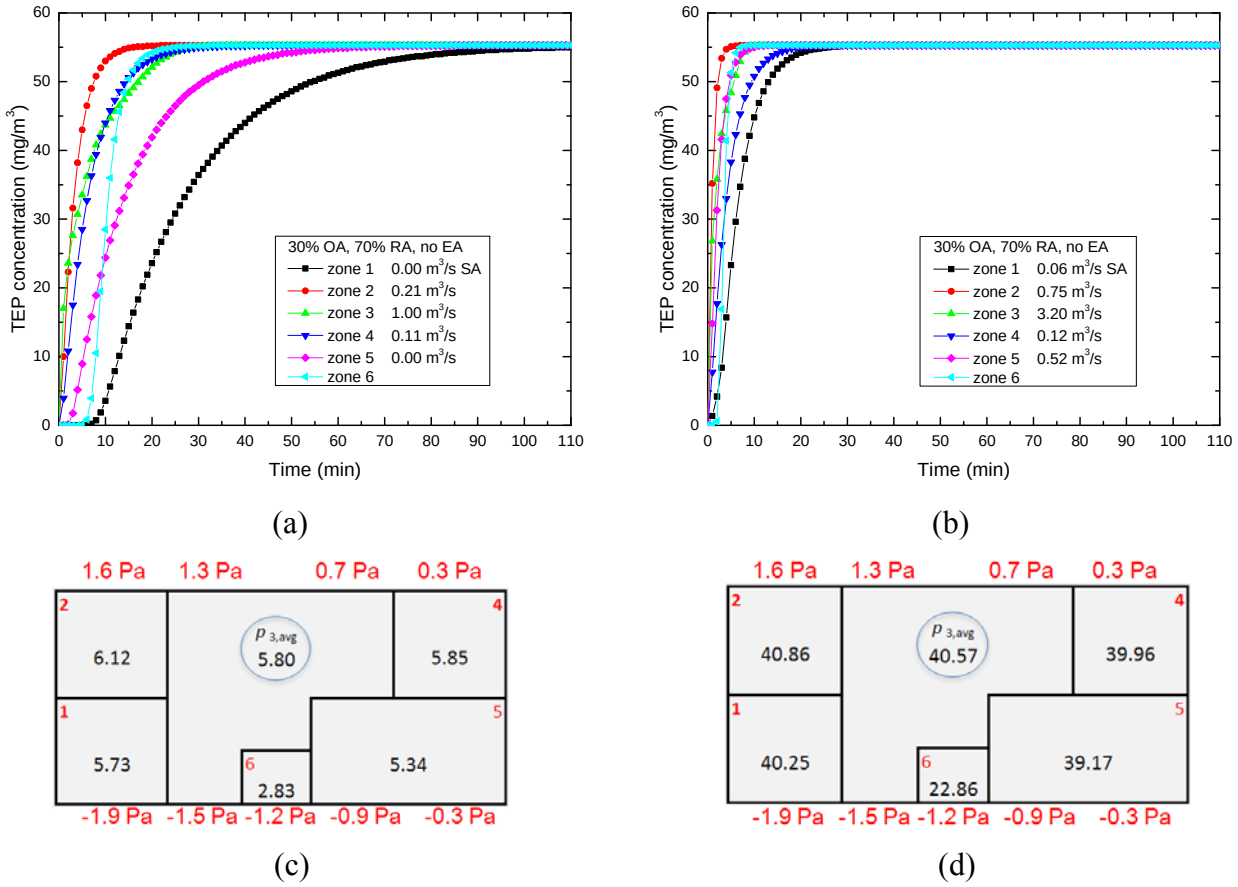

Figure D.12 TEP concentration at different flow rates for the DUBVS with Plan 2

A summary comparison of the three plans is given in Table D.5. It can be seen that when the ambient is heavily polluted, a highly efficient OA filter is very important but an RA filter I

relatively much less important. The unit energy in Table D.5 was based on product catalog data and/or estimation.

It is noteworthy that there is an excellent agreement between the three analytical relationships (listed in Table D.4) and the CONTAM simulation results, as shown in Table D.6. The excellent agreement is within expectation, because CONTAM is also based on the "well-mixed" assumption and air flow/contaminant conservation laws. The analytical relationships in Table D.4 are more user-friendly and can provide guidance in setting matrix of flow rate, filter efficiency, and OA fraction for a ventilatoin system based on requirement of the indoor contaminant level.

Table D.5 Comparison of the three plans for the DUBVS

	Ventilation strategy	Overpressure (Pa)	Supply air (m^3/s)	Unit energy consumption (J/L)	Energy consumption (W)	Max. S.S. TEP conc. (mg/m^3)
Plan 1	30% OA, 70% RA, no EA; η_{OA}=99.9975%, η_{RA}=99.75%	~5	1.32	0.25~1 for M98 HEPA filter, 0.5 for acoustic filtration system	561~858	0.00138
		~10	1.93		821~1255	
		~20	2.95		1254~1918	
		~30	3.91		1662~2542	
		~40	4.65		1977~3023	
Plan 2	30% OA, 70% RA, no EA; η_{RA}=99.75%, no OA filter	~5	1.32	0.5 for acoustic filtration system	462	55.3
		~10	1.93		676	
		~20	2.95		1033	
		~30	3.91		1369	
		~40	4.65		1628	
Plan 3	30% OA, 70% RA, no EA; η_{OA}=99.9975%, no RA filter	~5	1.32	0.25~1 for M98 HEPA filter	99~396	0.0046
		~10	1.93		145~579	
		~20	2.95		221~885	
		~30	3.91		293~1172	
		~40	4.65		349~1395	

Table D.6 Comparison of the analytical relationships and CONTAM simulations

DUBVS	Filter efficiency	Ambient TEP concentration (c_{out}) (mg/m^3)	Relationship derived based on S.S. contaminant conservation	S.S. TEP concentration predicted by the relationship (mg/m^3)	S.S. TEP concentration predicted by CONTAM (mg/m^3)
Plan 1	η_{OA} =99.9975%, η_{RA} =99.75%	184.035	$\frac{c_{f1}}{c_{out}} = \frac{1-\eta_{OA}}{1+\left(\frac{1}{f_o}-1\right)\eta_{RA}}$	c_{f1} =0.001383	0.00138
Plan 2	η_{RA} =99.75%	184.035	$\frac{c_{f2}}{c_{out}} = \frac{1}{1+\left(\frac{1}{f_o}-1\right)\eta_{RA}}$	c_{f2} =55.307	55.3
Plan 3	η_{OA} =99.9975%	184.035	$\frac{c_{f3}}{c_{out}} = \left(1-\eta_{OA}\right)$	c_{f3} =0.0046	0.0046

D.4 Summary

An OA HEPA filter is a key component for maintaining a low indoor contaminant concentration when the ambient is heavily polluted. The addition of another RA filter can further lower the indoor TEP concentration, but its effect in lowering the contaminant concentration is much less than that of the OA filter.

Three analytical relationships relating I/O ratio to filter efficiencies and OA fraction were derived based on air mass and contaminant conservation. In some cases, these relationships can be adpoted as an alternative to CONTAM simulations to save simulation time.

As an outcome of Cases 1-2, the DUBVS was found to be a suitable ventilation system for effective building protection and IAQ enhancement.